Title	Design and Applications of Highly Functional Catalysts Using Metal-Organic Frameworks
Author(s)	Toyao, Takashi
Editor(s)	
Citation	
Issue Date	2015-07
URL	http://hdl.handle.net/10466/14770
Rights	

Design and Applications of Highly Functional Catalysts Using Metal–Organic Frameworks

（金属-有機構造体を利用した高機能触媒の設計と応用）

Takashi Toyao

鳥屋尾 隆

July 2015

Doctoral Thesis at Osaka Prefecture University

Contents

Chapter 3. Developments of various one-pot reactions over bifunctional MOF catalysts

Chapter 1

General introduction

Background

Recently, nanoporous materials such as zeolites and mesoporous materials have emerged as important and interesting class of materials in the field of catalysis owing to their excellent physical characteristics including high surface area and large pore volume.[1-3] The use of nanoporous materials induces effective adsorption of the reactants and allows for exposure of the catalytically active sites to contact with the reactants during the catalytic process.[4-5] Consequently, efficient catalytic processes are realized for environmentally friendly and sustainable chemical production. Much effort has been devoted to developments heterogeneous catalysts using such nanoporous materials, especially to introduce catalytically active sites ranging from Brønsted to Lewis acids and even redox sites into the framework of zeolites and mesoporous materials.[6] Despite the many advances made in this field, however, the control and modulation of the framework properties are still limited, and in any case, it is far less controlled than for homogeneous molecular catalysts.[7]

In this line, there have been extensive interests in the development of inorganic-organic hybrid catalysts that can provide the potential of well-defined and uniform active sites.[8-10] One current definition what we understand under inorganic-organic hybrid materials is given by the International Union of Pure and Applied Chemistry (IUPAC): "*A hybrid material is composed of an intimate mixture of inorganic components, organic components, or both types of component. Note: The components usually interpenetrate on scale of less than 1 μm*".[11] More specifically, an inorganic-organic hybrid material consists of at least two components, usually an inorganic and an organic component that are molecularly dispersed in the material.[12] These combinations of inorganic and organic components integrated at the molecular level can offer a novel platform for highly designed and controlled catalytically active sites as well as the reaction fields. As a consequence, efficient catalytic

systems with separation and recyclability advantages of heterogeneous catalysts will be realized for the development of greener and more environmentally benign catalytic processes.

Metal−organic frameworks (MOFs)

Metal–organic frameworks (MOFs) also called porous coordination polymers (PCPs) are new crystalline inorganic-organic hybrid materials prepared via well-established principles of coordination chemistry using self-assembly of metal ions or metal-oxo clusters with organic linkers (**Fig. 1. 1**).[13-15] MOFs have gained recent interest because of their several attractive properties including high specific surface areas, well-ordered porous structures and structural designability.[16-19] These exceptional features of MOFs make the materials promising for applied research, addressing issues found in catalysis,[20] gas storage[21] and separation,[22] drug deliverly,[23] magnet[24] and sensing[25] (**Fig. 1. 2**).

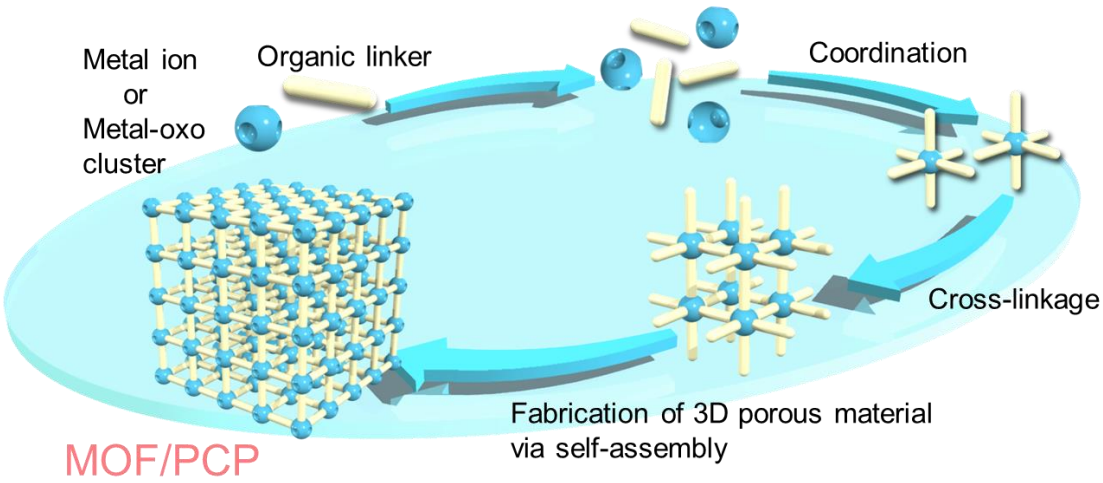

Figure 1. 1. Schematic illustration of the formation process of MOF/PCP. 3D porous structures are formed through coordination chemistry using self-assembly of metal ions or metal-oxo clusters with organic linkers.

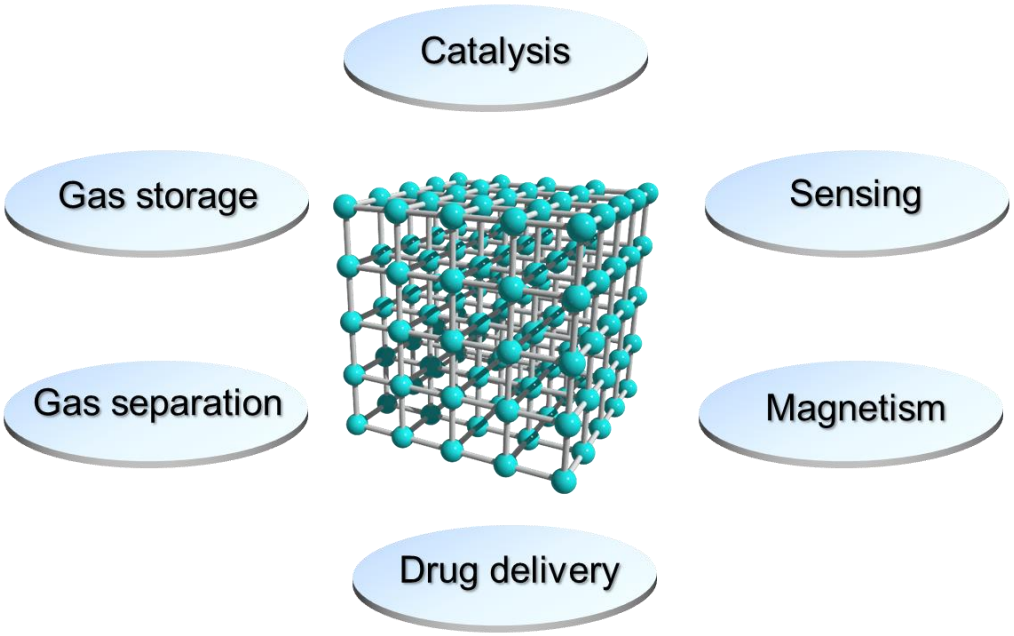

Figure 1. 2. Use of MOF/PCP for a variety of applications including catalysis, gas storage and separation, drug delivery, magnetism and sensing.

Unlike traditional inorganic nanoporous materials, unlimited possible combination of metal-oxo clusters and organic linkers enables to access the reticular structures with tunable porosity and attractive functions.[26-29] Multifunctional sites achieved through selection of appropriate metal-oxo clusters and organic linkers further enhance interest in MOF materials.[30-33] These multifunctional sites behave either cooperatively or independently to appreciate the functionality of MOFs. In this way, MOFs are able to provide a highly tunable platform for designing catalytically active sites as well as novel functions for a variety of catalytic reactions.[34] In addition, the controllable nanospace in the framework is a suitable candidate for a host of catalytically active species and will provide an accurately controlled reaction field. Furthermore, new synergetic properties have also been realized though incorporating additional catalytic species into MOFs.[35-37] Combining MOFs with a variety of

catalytic materials such as organometallic molecules,[38] enzymes,[39] metal nanoparticles,[40] heteropoly acids[41] has been shown to integrate the merits and mitigate the shortcomings of both the components. The research on MOF composites offers fabrication protocols for high-performance catalysts with sophisticated architectures. In these composite materials, the advantages of both MOFs and various kinds of catalytic materials can be combined effectively, and therefore, new physical and chemical properties and enhanced performance, which cannot be obtained by the individual components, can be accessed.[42-44] Consequently, the remarkable features of composites resulting from the synergistic combination of both MOF and other active components make them suitable for a wide range of catalytic applications.

Outline of this thesis

In this thesis, research efforts have been devoted to design and applications of novel functional catalysts using MOF materials. The catalytically active sites and reaction fields as well as electronic states of the catalysts were controlled at molecular level by taking advantages of the designability of MOFs. The MOF-based catalysts developed here have been demonstrated to exhibit superior catalytic performance to the conventional solid catalysts explored. Moreover, various characterization technique have enable to access investigation on the structures of catalytically active site and the reaction mechanisms.

This thesis consists of 5 chapters including chapter 1 as the overall introduction regarding to present research objectives, and chapter 2–5 are summarized as follows:

Chapter 2

This chapter describes development of visible-light-responsive MOF photocatalysts. This was realized by design of novel organic linkers that can act as a light harvesting unit

upon the irradiation of visible light. Efficient hydrogen production and photocatalytic reduction of nitrobenzene were achieved by employing an amino-functionalized Ti-based MOF (Ti-MOF-NH_2) under visible-light irradiation. The results from various spectroscopic measurements have revealed that the reactions proceed through light absorption by the organic linker and subsequent electron transfer to the photocatalytically active titanium-oxo cluster. In addition, the successful expansions of utilizable range of wavelength and sacrificial reagents were attained by utilizing a bis(4'-(4-carboxyphenyl)-terpyridine)Ru(II) complex ($Ru(tpy)_2$) as an organic linker.

Chapter 3

This chapter proposes approaches to one-pot sequential reactions by using MOFs having spatially isolated and multiple active sites. The MOF catalysts have been developed by modifying or varying the core metal-oxo clusters and bridging organic linkers. The role of the catalytically active sites created over MOFs have been discussed to address the reaction mechanisms. The catalytic abilities of the developed MOF catalysts were demonstrated to be superior to those of conventional heterogeneous and homogeneous catalysts.

Chapter 4

In Chapter 4, encapsulation of metal nanoparticles have been achieved in MOF-based materials. The prepared catalysts have been found to be active for hydrogenation reactions as highly efficient and reusable heterogeneous catalysts. Size-selective reactions were achieved due to uniform and microporous structure nature of zeolitic imidazolate frameworks (ZIFs) which are one of the MOF materials.[45] The reusability and stability of the catalysts have been also described as heterogeneous catalysts.

Chapter 5

In this chapter, the results and conclusions of the various investigations covered in this thesis have been summarized.

References

1. M. Choi, K. Na, J. Kim, Y. Sakamoto, O. Terasaki and R. Ryoo, *Nature*, 2009, **461**, 246.
2. M. Waki, Y. Maegawa, K. Hara, Y. Goto, S. Shirai, Y. Yamada, N. Mizoshita, T. Tani, W. J. Chun, S. Muratsugu, M. Tada, A. Fukuoka and S. Inagaki, *J. Am. Chem. Soc.*, 2014, **136**, 4003.
3. N. R. Shiju, A. H. Alberts, S. Khalid, D. R. Brown and G. Rothenberg, *Angew. Chemie Int. Ed.*, 2011, **50**, 9615.
4. A. Fukuoka, N. Higashimoto, Y. Sakamoto, M. Sasaki, N. Sugimoto, S. Inagaki, Y. Fukushima and M. Ichikawa, *Catal. Today*, 2001, **66**, 23.
5. M. Chiesa, V. Meynen, S. Van Doorslaer, P. Cool and E. F. Vansant, *J. Am. Chem. Soc.*, 2006, **128**, 8955.
6. A. Corma, H. Garcia and F. X. Liabres i Xamena, *Chem. Rev.*, 2010, **110**, 4606.
7. A. Corma, *Chem. Rev.*, 1997, **97**, 2373.
8. N. M. Muresan, J. Willkomm, D. Mersch, Y. Vaynzof and E. Reisner, *Angew. Chemie Int. Ed.*, 2012, **51**, 12749.
9. S. Inagaki, S. Guan, Y. Fukushima, T. Ohsuna and O. Terasaki, *J. Am. Chem. Soc.*, 1999, **121**, 9611.
10. A. Leyva-Pérez, P. García and A. Corma, *Angew. Chemie Int. Ed.*, 2014, **53**, 8687.
11. J. Aleman, A. V. Chadwick, J. He, M. Hess, K. Horie, R. G. Jones, P. Kratochvil, I. Meisel, I. Mita and G. Moad, *Pure Appl. Chem.*, 2007, **79**, 1801.
12. G. Kickelbick, *Hybrid Mater.*, 2014, **1**, 39.
13. O. M. Yaghi, M. O'Keeffe, N. W. Ockwig, H. K. Chae, M. Eddaoudi and J. Kim, *Nature*, 2003, **423**, 705.

14. S. Kitagawa, R. Kitaura and S. Noro, *Angew. Chemie Int. Ed.*, 2004, **43**, 2334.

15. G. Férey, *Chem. Soc. Rev*., 2008, **37**, 191.

16. M. Eddaoudi, J. Kim, N. Rosi, D. Vodak, J. Wachter, M. O'Keeffe and O. M. Yaghi, *Science*, 2002, **295**, 469.

17. N. L. Rosi, J. Eckert, M. Eddaoudi, D. T. Vodak, J. Kim, M. O'Keeffe and O. M. Yaghi, *Science*, 2003, **300**, 1127.

18. X. Zhao, B. Xiao, A. J. Fletcher, K. Thomas, D. Bradshaw and M. J. Rosseinsky, *Science*, 2004, **306**, 1012.

19. S. Shimomura, M. Higuchi, R. Matsuda, K. Yoneda, Y. Hijikata, Y. Kubota, Y. Mita, J. Kim, M. Takata and S. Kitagawa, *Nat. Chem*., 2010, **2**, 633.

20. W. Lu, Z. Wei, Z.-Y. Gu, T.-F. Liu, J. Park, J. Park, J. Tian, M. Zhang, Q. Zhang, T. Gentle Iii, M. Bosch and H.-C. Zhou, *Chem. Soc. Rev.*, 2014, **43**, 5561.

21. R. Matsuda, R. Kitaura, S. Kitagawa, Y. Kubota, R. V. Belosludov, T. C. Kobayashi, H. Sakamoto, T. Chiba, M. Takata, Y. Kawazoe and Y. Mita, *Nature*, 2005, **436**, 238.

22. T. Rodenas, I. Luz, G. Prieto, B. Seoane, H. Miro, A. Corma, F. Kapteijn, F. X. Llabrés, J. Gascon, F. X. Llabrés i Xamena and J. Gascon, *Nat. Mater.*, 2014, **14**, 48.

23. P. Horcajada, T. Chalati, C. Serre, B. Gillet, C. Sebrie, T. Baati, J. F. Eubank, D. Heurtaux, P. Clayette, C. Kreuz, J.-S. Chang, Y. K. Hwang, V. Marsaud, P.-N. Bories, L. Cynober, S. Gil, G. Férey, P. Couvreur and R. Gref, *Nat. Mater.*, 2010, **9**, 172.

24. R. Ricco, L. Malfatti, M. Takahashi, A. J. Hill and P. Falcaro, *J. Mater. Chem. A*, 2013, **1**, 13033.

25. C.-Y. Sun, X.-L. Wang, X. Zhang, C. Qin, P. Li, Z.-M. Su, D.-X. Zhu, G.-G. Shan, K.-Z. Shao, H. Wu and J. Li, *Nat. Commun.*, 2013, **4**, 2717.

26. J. D. Evans, C. J. Sumby and C. J. Doonan, *Chem. Soc. Rev.*, 2014, **43**, 5933.

27. J. R. Li, J. Sculley and H. C. Zhou, *Chem. Rev*., 2012, **112**, 869.

28. S. Horike, M. Dinca, K. Tamaki and J. R. Long, *J. Am. Chem. Soc.*, 2008, **130**, 5854.
29. J. Lee, O. K. Farha, J. Roberts, K. A. Scheidt, S. T. Nguyen and J. T. Hupp, *Chem. Soc. Rev*., 2009, **38**, 1450.
30. F. Song, C. Wang, J. M. Falkowski, L. Ma and W. Lin, *J. Am. Chem. Soc*., 2010, **132**, 15390.
31. M. Yoon, R. Srirambalaji and K. Kim, *Chem. Rev.*, 2012, **112**, 1196.
32. P. Deria, J. E. Mondloch, O. Karagiaridi, W. Bury, J. T. Hupp and O. K. Farha, *Chem. Soc. Rev.*, 2014, 41.
33. C. A. Kent, D. Liu, L. Ma, J. M. Papanikolas, T. J. Meyer and W. Lin, *J. Am. Chem. Soc*., 2011, **133**, 12940.
34. J. Liu, L. Chen, H. Cui, J. Zhang, L. Zhang and C.-Y. Su, *Chem. Soc. Rev.*, 2014, **43**, 6011.
35. D. Bradshaw, S. El-Hankari and L. Lupica-Spagnolo, *Chem. Soc. Rev.*, 2014, **43**, 5431.
36. Y. He, B. Li, M. O'Keeffe and B. Chen, *Chem. Soc. Rev.*, 2014, **43**, 5618.
37. Q.-L. Zhu and Q. Xu, *Chem. Soc. Rev.*, 2014, **43**, 5648.
38. Z. Zhang, W.-Y. Gao, L. Wojtas, S. Ma, M. Eddaoudi and M. J. Zaworotko, *Angew. Chemie Int. Ed.*, 2012, **51**, 9330.
39. Y. Chen, V. Lykourinou, C. Vetromile, T. Hoang, L.-J. Ming, R. W. Larsen and S. Ma, *J. Am. Chem. Soc*., 2012, **134**, 13188.
40. Z. Guo, C. Xiao, R. V. Maligal-Ganesh, L. Zhou, T. W. Goh, X. Li, D. Tesfagaber, A. Thiel and W. Huang, *ACS Catal.*, 2014, **4**, 1340.
41. G. Férey, C. Mellot-Draznieks, C. Serre, F. Millange, J. Dutour, S. Surblé and I. Margiolaki, *Science*, 2005, **309**, 2040.
42. Y. Liu and Z. Tang, *Adv. Mater.*, 2013, **25**, 5819.

43. M. Zhao, K. Deng, L. He, Y. Liu, G. Li, H. Zhao and Z. Tang, *J. Am. Chem. Soc.*, 2014, **136**, 1738.
44. X.-H. Liu, J.-G. Ma, Z. Niu, G.-M. Yang and P. Cheng, *Angew. Chemie Int. Ed.*, 2015, **54**, 988.

Chapter 2

Design of MOF photocatalysts by utilizing visible-light responsive organic linkers as light harvesting unit

2. 1. Hydrogen production and photocatalytic reduction of nitrobenzene over amino-functionalized metal−organic framework photocatalyst

2. 1. 1. Introduction

In recent years, various kinds of photocatalysts have been widely investigated for applications in air and water purification, hazardous waste elimination and the production of clean energy resources.[1-5] Among them, enormous attention has been paid to photocatalytic hydrogen production from water which is a promising way to produce hydrogen as a potential clean energy source. In addition, the development of new process using photocatalysts for the organic transformations has been also studied as an important way to pursue environmentally benign and green chemistry. However, most of the photocatalysts operate only under irradiation of UV-light, consequently, only 3-5% of the solar energy reaching the earth can be utilized. Because of this limitation, development of an efficient system for light energy conversion into chemical energy is one of the urgent subjects from the viewpoint of the utilization of abundant sunlight.[6-9]

Metal−organic frameworks (MOFs) also called porous coordination polymers (PCPs) have been of great interest due to their beneficial properties such as extremely high surface areas, well-ordered porous structures and structure designability.[10-12] Taking advantage of these interesting properties, MOFs are widely studied for many potential applications to gas storage,[13-18] molecular sieving[19-23] and catalysis.[24-28] Additionally, an increasing number of studies have been explored in recent years to indicate that MOFs serve as platforms for integrating different molecular functional components to achieve light harvesting[29-34]. Garcia et al.[29] and Majima et al.[30] observed that electron transfer takes place from the photo-excited organic linker to the metal-oxo cluster within MOF-5. This process occurs in photocatalytic

reactions and photoluminescence in which MOF-5 participates. Compared to other photocatalytic systems, the MOF photocatalyst-catalyzed systems have advantages that various combinations of metal-oxo clusters and bridging organic linkers allow for fine-tuning and rational design of these photocatalysts at the molecular level, and furthermore, intrinsic porosity of MOFs facilitates the diffusion of substrates and products through the open framework structures.

In this study, a visible-light-responsive Ti-based MOF photocatalyst (Ti-MOF-NH_2) was developed by employing 2-anilinedicarboxylic acid as an organic linker. Ti-MOF-NH_2 promotes photocatalytic H_2 production from water containing sacrificial electron donors under visible-light irradiation. It is also noteworthy that the reaction proceeds through the light absorption by its organic linker and the following electron transfer to the catalytically active titanium-oxo cluster as described in **Scheme 2. 1. 1**. Furthermore, the developed visible-light-responsive MOF photocatalyst system was applied to photocatalytic reduction of nitrobenzene under visible-light irradiation.

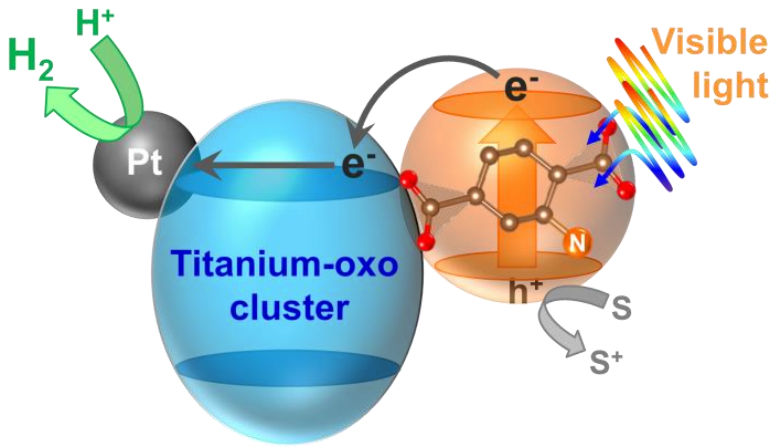

Scheme 2. 1. 1. A schematic illustration of photocatalytic hydrogen production through electron transfer from organic linker to Ti-oxo cluster over Pt-supported Ti-MOF-NH_2.

2. 1. 2. Experimental

Materials

Tetrapropyl orthotitanate (TPOT) was purchased from Tokyo Kasei Kogyo Co., Ltd. 2-Anilinedicarboxylic acid ($H_2BDC\text{-}NH_2$), 1,4-benzenedicarboxylic acid (H_2BDC), N'N-dimethylformamide (DMF), methanol, triethanolamine (TEOA), nitrobenzene and acetonitrile were purchased from Nacalai Tesque Inc. Hydrogen hexachloroplatinate(IV) hexahydrate ($H_2PtCl_6 \cdot 6H_2O$) was purchased from Kishida Chemicals Co., Ltd.

Catalysts preparation

Ti-MOF-NH_2 was synthesized on the basis of a method for the preparation of MIL-125 (Ti-MOF) previously-reported by M. Dan-Hardi *et al.*,[35] with the exception of using $H_2BDC\text{-}NH_2$ in place of H_2BDC as an organic linker. The mixture of TPOT, $H_2BDC\text{-}NH_2$, DMF and methanol was subject to react under solvothermal conditions in a Teflon-lined stainless steel autoclave for 48 h at 423 K under autogenous pressure. The precipitate was filtrated, washed repeatedly with DMF and dried at room temperature overnight. Finally, the obtained powder sample was dried under vacuum for 1 h at 423 K to remove the residual $H_2BDC\text{-}NH_2$. For comparison, the conventional Ti-MOF was also prepared by using H_2BDC as an organic linker.

Pt deposition on Ti-MOF-NH_2 as a cocatalyst were performed by employing a photodeposition method. A suspension containing Ti-MOF-NH_2 (0.4 g), 0.039 M H_2PtCl_6 methanol solution (0.55-2.2 mL), DMF (20 mL) and methanol (20 mL) was irradiated with UV light from a 100 W high-pressure Hg lamp at 5 mW cm^{-2} for 3 h with continuous stirring. The obtained precipitate was centrifuged, washed repeatedly with DMF and dried in air at room temperature overnight. Finally the obtained powder sample was dried under vacuum at

423 K for 1 h, yielding Pt(X)/Ti-MOF-NH_2, where X = 0.5, 1.0, 1.5 and 2.0 wt%.

General methods

Standard θ–2θ X-ray diffraction (XRD) data were recorded on a Shimadzu X-ray diffractometer XRD-6100 using Cu Kα radiation (λ = 1.5406 Å). Specific surface areas were estimated from the amount of N_2 adsorption at 77 K using the BET (Brunauer-Emmett-Teller) equilibrium equation. Diffuse reflectance UV–vis spectra were obtained with a Shimadzu UV–vis recording spectrophotometer 2200A. Electron spin resonance (ESR) spectra were recorded with a JEOL JES-RE-2X at 77 K. Prior to the measurements, the sample immersed in an aqueous solution containing 0.01 M TEOA (2 mL) was added an in-situ cell, evacuated at 77 K to remove dissolved oxygen and then irradiated with visible light having a wavelength of λ > 420 nm from a Xe lamp (500 W; San-Ei Electric Inc. XEF-501S) with a cut-off filter for 3 h at room temperature. FT-IR measurements were carried out in the transmission mode using a FT-IR spectrometer (JASCO FT-IR 660 Plus). Self-supporting pellets of the samples diluted with KBr were loaded in a specially constructed IR cell, which was equipped with CaF_2 windows. After the pellets were evacuated at 473 K for 30 min, the spectra were measured at room temperature.

Photocatalytic hydrogen production reaction

The photocatalyst (10 mg) and 0.01 M aqueous TEOA solution (2 mL) were added to a Pyrex reaction vessel connected to vacuum line. The resulting mixture was evacuated at 77 K to remove dissolved oxygen. Subsequently, the sample was irradiated with the 500 W Xe lamp through a cut-off filter (λ > 420 nm) with stirring at room temperature. After the reaction, the resulting gas was analyzed by using a gas chromatograph (GC) of Shimadzu GC-12A with a thermal conductivity detector equipped with a packed column (MS-5A).

Photocatalytic reduction of nitrobenzene

The photocatalyst (25 mg) and 4 mL of acetonitrile containing nitrobenzene (0.1 mmol) and TEOA (1.0 mmol) were added to a Pyrex reaction vessel. The vessel was sealed with a rubber septum, followed by 15 min of Ar bubbling. The reaction mixture was irradiated with visible light having a wavelength of $\lambda > 420$ nm from the 500 W Xe lamp with a cut-off filter ($\lambda > 420$ nm) at room temperature. The progression of the reaction was monitored by a GC (Shimadzu GC-14B with a flame ionization detector) equipped with an InertCap®1 capillary column.

Reusability of the photocatalyst was studied as follows. After the first run, the photocatalyst was washed three times with methanol, dried at 323 K in air and reused for the next run. The above procedure was repeated three times.

2. 1. 3. Results and discussion

Figure 2. 1. 1 shows XRD patterns for Ti-MOF-NH_2 and Ti-MOF, before and after the photodeposition of Pt nanoparticles. As can be seen by viewing these patterns, Ti-MOF-NH_2 exhibits the same diffraction pattern as Ti-MOF, indicating that a MIL-125 structure is produced when H_2BDC-NH_2 is utilized as an organic linker (**Figure 2. 1. 2**).[35] Additionally, no traces of characteristic peaks corresponding to bulk titanium dioxide phases, such as anatase and rutile, are observed in the diffraction pattern of Ti-MOF-NH_2. This result indicates that the framework of Ti-MOF-NH_2 consists of small titanium oxide clusters in the absence of bulky aggregated titanium oxide species. After photodeposition of Pt nanoparticles, the diffraction patterns of Ti-MOF-NH_2 and Ti-MOF remained nearly unchanged, suggesting that the photodeposition process does not influence the structures of these materials.

To evaluate the pore structures and specific surface areas of the materials, N_2 adsorption measurements were performed before and after photodeposition of Pt nanoparticles. The specific surface areas of Ti-MOF-NH_2 and Ti-MOF were determined to be 1101 and 1202 m^2 g^{-1}, respectively, by using BET method based calculations on N_2 adsorption isotherm data. These findings show that Ti-MOF-NH_2 and Ti-MOF have large specific surface areas associated with their microporous structures. Although the specific surface areas of these materials decrease slightly after Pt nanoparticle photodeposition owing to a pore blockage, Ti-MOF-NH_2 and Ti-MOF maintain their porous structures and high specific surface areas of 910 and 946 m^2 g^{-1}, respectively. **Figure 2. 1. 3** displays diffuse-reflectance UV–vis spectra of Ti-MOF-NH_2 and Ti-MOF, together with those of H_2BDC-NH_2 and H_2BDC as reference samples (inset). The spectrum of Ti-MOF shows absorption bands below 350 nm, while an observable absorption band is seen in the spectrum of Ti-MOF-NH_2 up to around 500 nm that is associated with the chromophore in H_2BDC-NH_2. The results demonstrate that Ti-MOF-NH_2, containing H_2BDC-NH_2 as the organic linker, is a visible-light absorbing MOF.

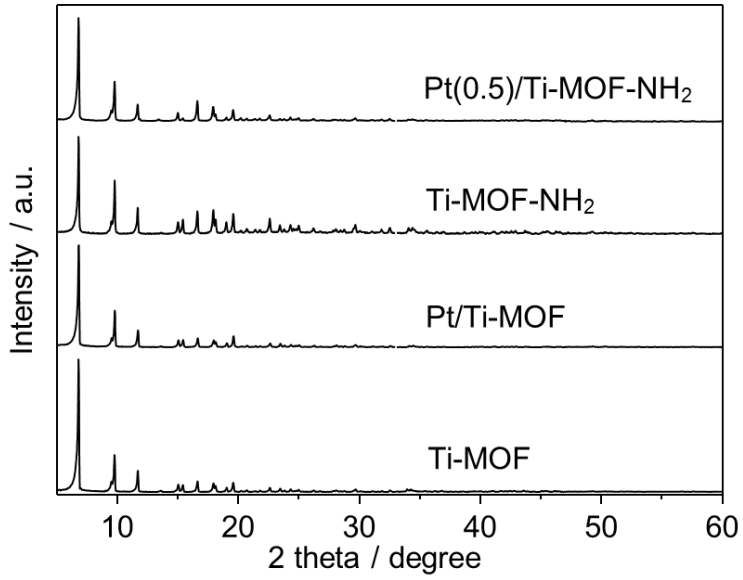

Figure 2. 1. 1. XRD patterns of Ti-MOF, Pt/Ti-MOF, Ti-MOF-NH_2 and Pt(0.5)/ Ti-MOF-NH_2.

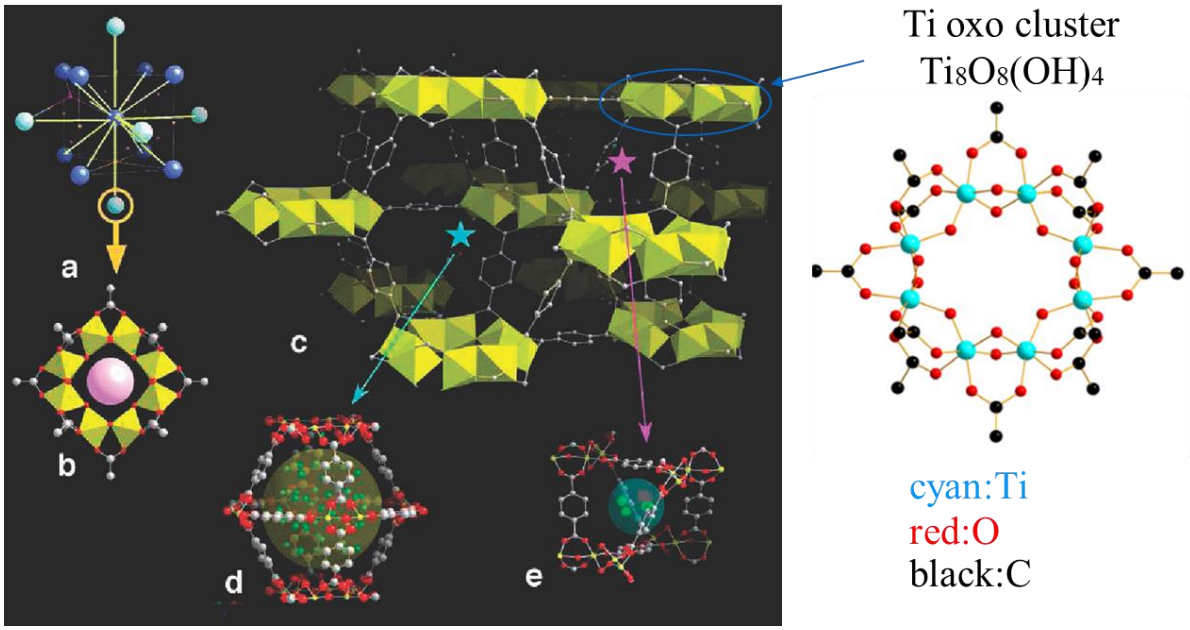

Figure 2. 1. 2. Structure of Ti-MOF (MIL-125).[35] (a) Perspective view of a centered cubic (*cc*) arrangement; the 12-fold coordination is evidenced by yellow lines. Purple and orange dots indicate the positions of the centers of the tetrahedral and octahedral vacancies. (b) View of the perforated cyclic octamer with edge- and corner-sharing Ti octahedra; it corresponds to the atom with an orange circle of the classical cc packing through the SBU augmentation. (c) Perspective view of MIL-125 with the central octamer surrounded by 12 others; the pink and blue stars indicate the centers of the tetrahedral and octahedral vacancies in MIL-125. (d) Ball and stick representation of the octahedral vacancy, filled by water molecules (in green); the large yellow sphere represents the effective accessible volume of the cage. (e) The tetrahedral vacancy; in (d) and (e) the color code is as follows: carbon, gray; oxygen, red; water, green; titanium, yellow.

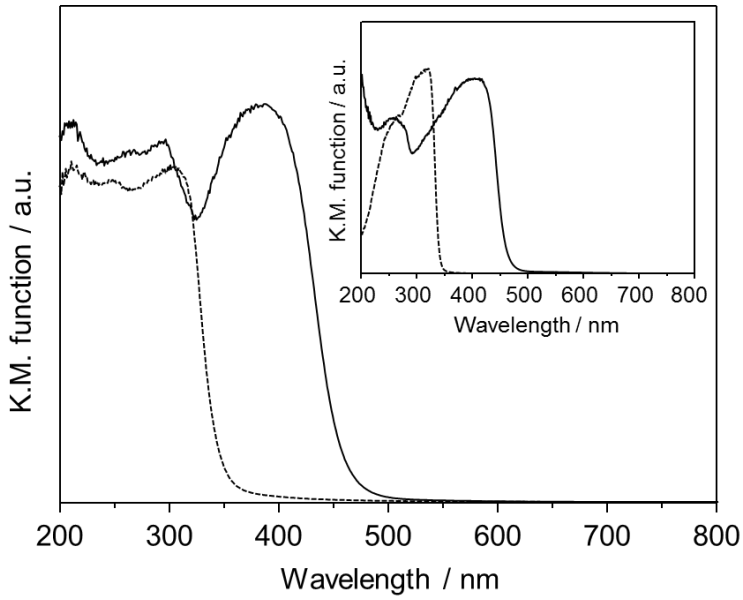

Figure 2. 1. 3. Diffuse-reflectance UV–vis spectra of Ti-MOF (dotted line) and Ti-MOF-NH_2 (solid line). Inset shows the diffuse-reflectance UV–vis spectra of H_2BDC (dotted line) and H_2BDC-NH_2 (solid line).

In an investigation exploring the potential photocatalytic activity of Pt(0.5)/Ti-MOF-NH_2, hydrogen production from an aqueous solution containing this catalyst and 0.01 M TEOA as a sacrificial electron donor was monitored while being subjected to visible light irradiation at room temperature. Optical filters were used to modulate the wavelength of the broad-band visible light source. The time course of photocatalytic hydrogen production under visible light irradiation ($\lambda > 420$ nm) over Pt(0.5)/Ti-MOF-NH_2 for 9 h, with intermittent evacuation and exposure to atmospheric conditions every 3 h, is displayed in **Fig. 2. 1. 4**. Continuous hydrogen production occurs from the beginning of the irradiation period, and the total evolution of hydrogen after 9 h irradiation reaches 33 μmol. These results clearly show that Pt(0.5)/Ti-MOF-NH_2 acts as an efficient visible-light-responsive, hydrogen production photocatalyst and that it does not lose its photocatalytic activity over at least three cycles. However, as inspection of the XRD patterns displayed in **Fig. 2. 1. 5** shows, the porous

network of Pt(0.5)/Ti-MOF-NH_2 is found to be partly deteriorated (*i.e.*, the intensities of the diffraction peaks corresponding to the MIL-125 structure decrease slightly). In contrast, Pt/Ti-MOF displays no photocatalytic activity when employed under the same reaction conditions. This finding indicates that visible-light absorption characteristics associated with the BDC-NH_2 moiety are indispensable for promoting the photocatalytic hydrogen production reaction under visible-light irradiation. Incidentally, Ti-MOF-NH_2, not containing deposited Pt nanoparticles, exhibits a lower photocatalytic activity than does Pt(0.5)/Ti-MOF-NH_2, suggesting that efficient charge separation caused by the presence of Pt nanoparticles as a co-catalyst plays a role in enhancing the efficiency of the hydrogen production reaction.

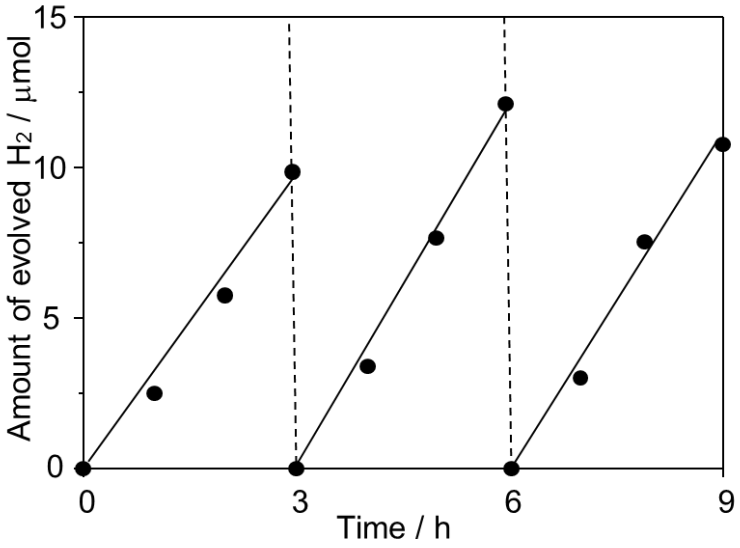

Figure 2. 1. 4. Time course of photocatalytic hydrogen production under visible-light irradiation (λ > 420 nm) over Pt(0.5)/Ti-MOF-NH_2 for a total of 9 h with intermittent evacuation and exposure to atmospheric conditions every 3 h.

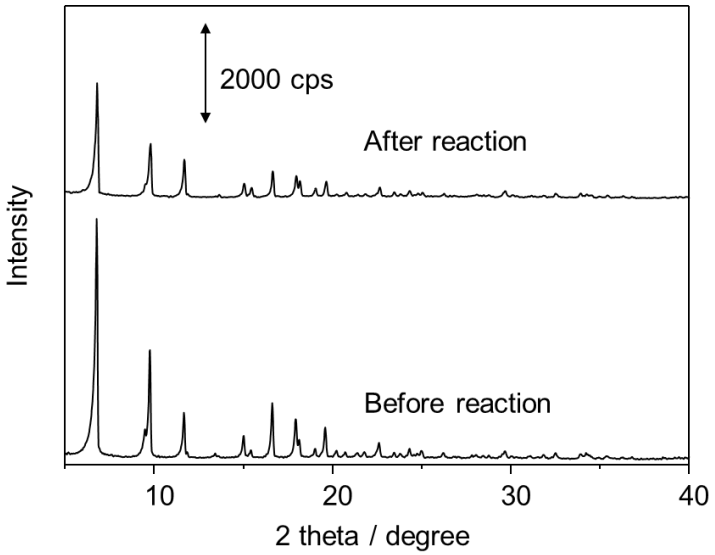

Figure 2. 1. 5. XRD patterns of Pt(0.5)/Ti-MOF-NH_2 before and after hydrogen evolution reaction.

The dependence of the hydrogen evolution rate on the wavelength of incident light employed in the Pt(0.5)/Ti-MOF-NH_2 photocatalytic system is displayed in **Fig. 2. 1. 6**. The hydrogen evolution rate is observed to depend strongly on wavelength in a manner that correlates with absorption intensities in the visible spectrum of Ti-MOF-NH_2 (**Fig. 2. 1. 6a**). The similar results were obtained by photoelectrochemical measurements. As shown in **Fig. 2. 1. 6b**, the wavelength-dependent photocurrents observed for the Ti-MOF-NH_2 electrode in an electrolyte containing TEOA under visible-light irradiation (at a constant potential of 0.5 V *vs.* SCE) demonstrated that the trend of photocurrent response shows good parallel relationship with the absorption spectrum. These findings indicate that the organic linker of BDC-NH_2 absorbs the incident visible light and that its excited state transfers electrons to the CB of titanium-oxo clusters. On the other hand, irradiation of photocatalytic system with UV-light ($\lambda > 300$ nm) from a 500 W Hg lamp (Ushio Inc.), Pt(0.5)/Ti-MOF-NH_2 leads to a much

higher hydrogen evolution rate (11.7 μmol h^{-1}) as a consequence of direct excitation of titanium-oxo clusters.

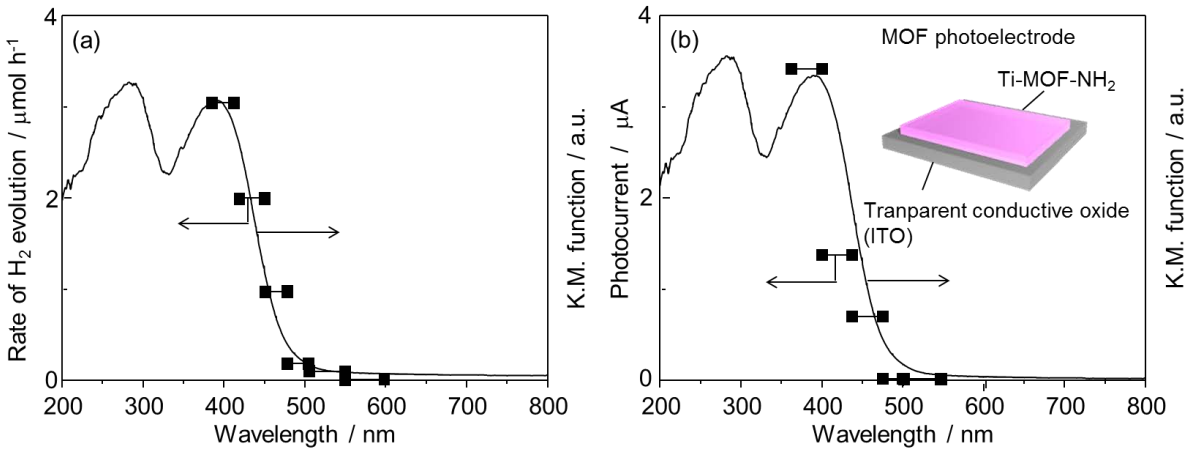

Figure 2. 1. 6. The dependence of (a) the hydrogen evolution rate for Pt(0.5)/Ti-MOF-NH_2 and (b) the photocurrent for the Ti-MOF-NH_2 electrode on the wavelength of incident light with diffuse-reflectance UV–vis spectrum of Ti-MOF-NH_2. The photocurrents were recorded in 0.25 M K_2SO_4 aqueous solution containing 0.01 M TEOA under visible-light irradiation at a constant potential of 0.5 V *vs.* SCE.

The results of *in situ* ESR measurements after visible-light irradiation also confirmed the proposed electron transfer mechanism. For this measurement, Ti-MOF-NH_2 was immersed in a solution of 0.01 M aqueous TEOA, and the suspension was evacuated at 77 K. This was followed by irradiation with visible light ($\lambda > 420$ nm) for 3 h at room temperature. After irradiation, the ESR spectrum was recorded at 77 K. As show in **Fig. 2. 1. 7**, the ESR spectrum after visible-light irradiation contains signals which have parameters that are characteristic of paramagnetic Ti^{3+} centers in a distorted rhombic oxygen ligand field (g_x =

1.980, g_y = 1.953, and g_z = 1.889).[36,37] In contrast, no signals assignable to Ti^{3+} species are observed in the ESR spectrum of Ti-MOF after visible-light irradiation. These results suggest that visible light promotes transfer of photogenerated electrons from the excited BDC-NH_2 group to the CB of titanium-oxo cluster, resulting in the formation of Ti^{3+} species. After exposure to air, the signals in the Ti-MOF-NH_2 spectrum corresponding to Ti^{3+} species disappear, indicating the reoxidation of generated Ti^{3+} species to Ti^{4+} species.

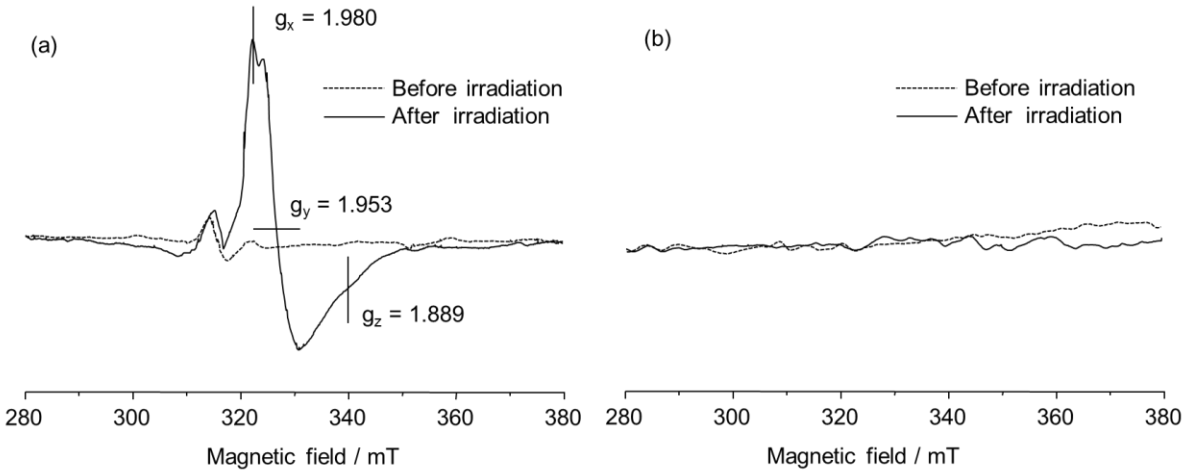

Figure 2. 1. 7. ESR spectra observed at 77 K for (a) Ti-MOF-NH_2 and (b) Ti-MOF, immersed in aqueous 0.01 M TEOA solution, before (dotted line) and after (solid line) visible-light irradiation (λ > 420 nm). The suspension was degassed under vacuum at 77 K and irradiated with visible light for 3 h at room temperature, followed by spectrum acquisition at 77 K.

To gain further evidence for the operation of the electron transfer mechanism, Pt(0.5)/Zr-MOF-NH_2, a Pt-supported UiO-66 type MOF comprised of BDC-NH_2 units and zirconium-oxo clusters whose CB potential is more negative than that of titanium-oxo cluster, was prepared (**Fig. 2. 1. 8**). Prolonged λ > 420 nm irradiation (24 h) of the

Pt(0.5)/Zr-MOF-NH_2 system did not lead to production of hydrogen, in spite of the fact that Pt(0.5)/Zr-MOF-NH_2 has excellent visible light absorption characteristics (**Fig. 2. 1. 9**). In view of the fact that Pt/Zr-MOF-NH_2 can promote the hydrogen production reaction when irradiated with UV light, it appears that electron transfer from the excited organic linker to the zirconium-oxo cluster is inefficient because the zirconium-oxo cluster has a highly negative CB edge. Additionally, *in situ* ESR measurements before and after visible-light irradiation of Zr-MOF-NH_2 system provided informative results. In particular, the absence of characteristic signals in the spectrum assignable to Zr^{3+} species after visible-light irradiation demonstrates that electron transfer does not occur in this system. The results summarized above clearly demonstrate that the photocatalytic hydrogen production reactions using Pt(0.5)/Ti-MOF-NH_2 and Ti-MOF-NH_2 proceed through a pathway involving light absorption by the BDC-NH_2 chromophore and subsequent electron transfer to the titanium-oxo cluster.

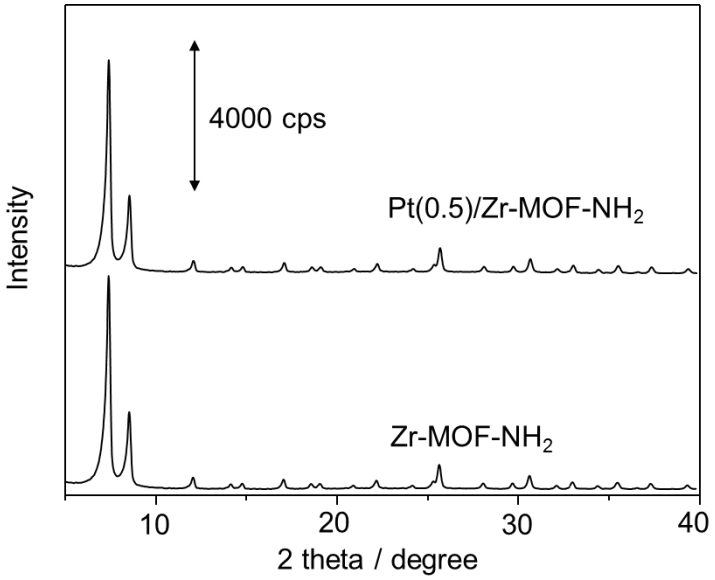

Figure 2. 1. 8. XRD patterns of Zr-MOF-NH_2 and Pt(0.5)/Zr-MOF-NH_2.

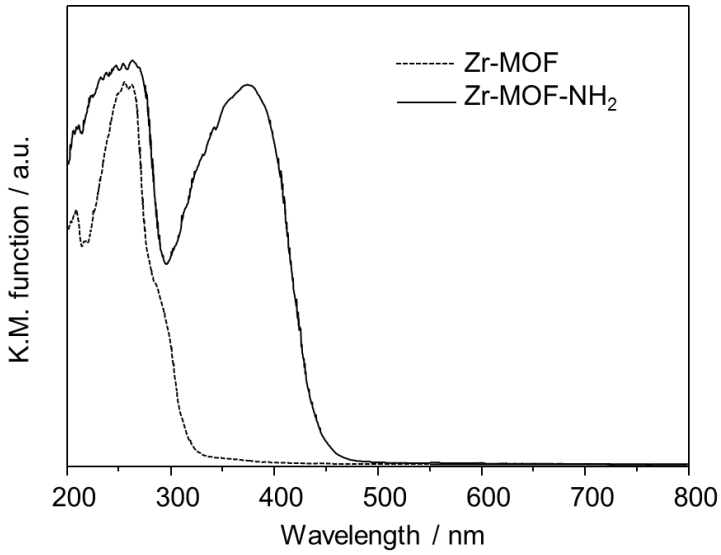

Figure 2. 1. 9. Diffuse-reflectance UV–vis spectra of Zr-MOF (dotted line) and Zr-MOF-NH_2 (solid line).

The design of effective photocatalysts for the synthesis of specialty chemicals under visible-light irradiation is one of the essential and stimulating research subjects.[38-40] Photochemical excitation can be conducted at room temperature without the use of harmful reagents, which results in environmentally benign and energy saving processes.[41,42] From this point of view, the visible-light-responsible MOF (Ti-MOF-NH_2) was applied to photocatalytic reduction of nitrobenzene under visible-light irradiation ($\lambda > 420$ nm). Prior the application for the photocatalytic reduction of nitrobenzene, the amount of Pt deposited were optimized, as shown in **Fig. 2. 1. 10**. The results show that Ti-MOF-NH_2 with 1.5 wt% of Pt as a cocatalyst (Pt(1.5)/Ti-MOF-NH_2) exhibit the highest catalytic activity. Pt(1.5)/Ti-MOF-NH_2 was then applied to photocatalytic reduction of nitrobenzene under visible-light irradiation ($\lambda > 420$ nm). **Figure 2. 1. 11** shows the time courses of the amounts of nitrobenzene, nitrosobenzene and aniline. The amounts of nitrobenzene monotonously decreased along with photoirradiation time and the amount of aniline increased. In addition,

nitrosobenzene was also obtained as an intermediate product of the reaction. For comparison of the photocatalytic activities of Pt(1.5)/Ti-MOF-NH_2, the initial reaction rates for Pt(1.5)/Ti-MOF-NH_2 and Ti-MOF-NH_2 were determined to be 3.3 and 2.3 μmol h^{-1}, respectively. Pt(1.5)/Ti-MOF-NH_2 exhibited higher photocatalytic activity than Ti-MOF-NH_2, indicating deposited Pt efficiently act as a cocatalyst in this system. It was also confirmed that selectivities of the reaction are almost the same regardless of the presence of Pt species. On the other hand, no reaction took place in the absence of visible-light irradiation, Pt(1.5)/Ti-MOF-NH_2 and TEOA as a sacrificial electron donor, that is, Pt(1.5)/Ti- MOF-NH_2 acts as a visible-light responsive photocatalyst in this system. In addition, the reaction did not proceed when using Pt(1.5)/Ti-MOF or a physical mixture of Pt(1.5)/Ti-MOF and H_2BDC-NH_2 as a photocatalyst. This fact indicates that the coordination networks of Ti-oxo cluster and BDC-NH_2 units are key factors for the progression of the reaction.

To further confirm the reaction mechanism, the wavelength dependence of apparent quantum efficiency was investigated, as shown in **Fig. 2. 1. 12**. The trend of the apparent quantum yield matches well with that of the absorption spectrum. This result suggests that the reaction proceeds through the light absorption by its organic linker and the following electron transfer to the catalytically active titanium-oxo cluster, as displayed in **Scheme 2. 1. 1**. Therefore, it can be considered that nitrobenzene was reduced over Pt deposited on Ti-oxo clusters and TEOA was sacrificially oxidized over BDC-NH_2 groups under visible-light irradiation.

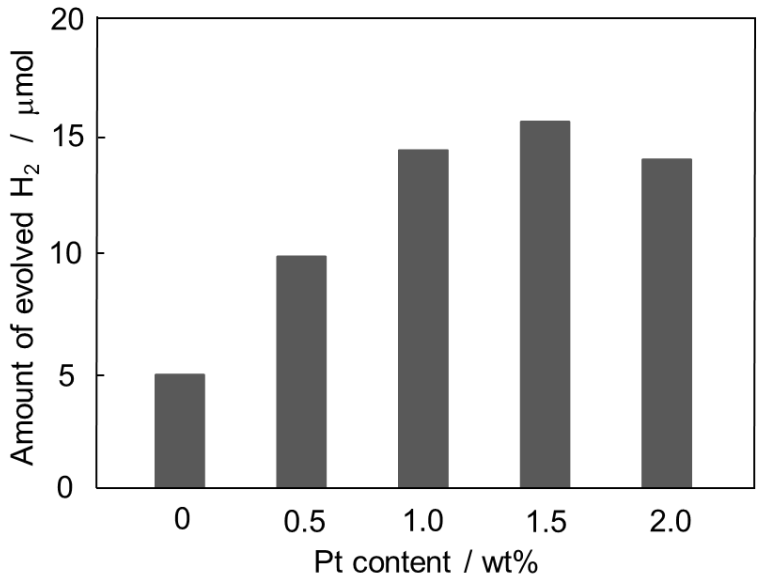

Figure 2. 1. 10. Photocatalytic hydrogen production under visible-light irradiation (λ > 420 nm) over Ti-MOF-NH_2 and Pt(X)/Ti-MOF-NH_2.

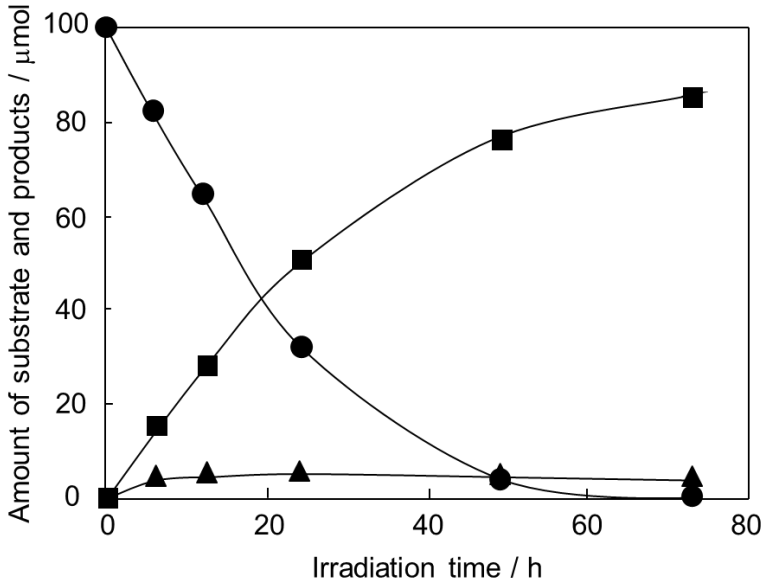

Figure 2. 1. 11. Time course of photocatalytic reduction of nitrobenzene (●) to nitrosobenzene (▲) and aniline (■) under visible-light irradiation (λ > 420 nm) in the presence of TEOA over Pt(1.5)/Ti-MOF-NH_2.

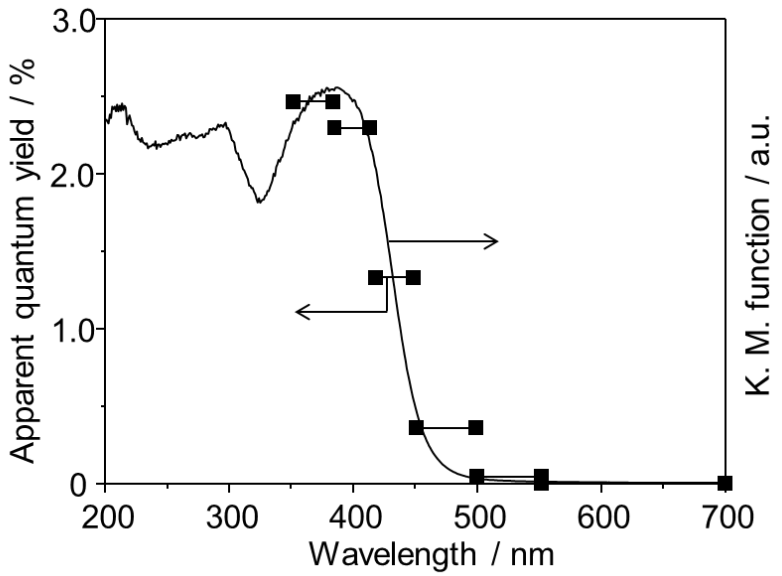

Figure 2. 1. 12. Wavelength-dependent apparent quantum yield for photocatalytic reduction of nitrobenzene over Pt(1.5)/Ti-MOF-NH_2.

Finally, the reusability of Pt(1.5)/Ti-MOF-NH_2 was investigated, as shown in **Fig. 2. 1. 13**. The catalyst after the reaction for 72 h was washed with methanol, dried under vacuum, and then reused for the next run. The results of recycling tests indicated no significant loss of photocatalytic activities even after three cycles. Moreover, XRD and FT-IR measurements were performed before and after four cycles of the reaction to investigate the stability of Pt(1.5)/Ti-MOF-NH_2 (**Fig. 2. 1. 14** and **Fig. 2. 1. 15**). The diffraction peaks corresponding to the MIL-125 structure were maintained even after the four cycles of the reaction. FT-IR spectra of Pt(1.5)/Ti-MOF-NH_2 both before and after four cycles of the reaction exhibit two absorption bands at around 3382 and 3470 cm^{-1} which are attributed to the symmetrical and asymmetrical stretching vibrations of free amino groups (–NH_2), respectively. This fact demonstrates that the organic linker with amino group stably exist during the reaction.

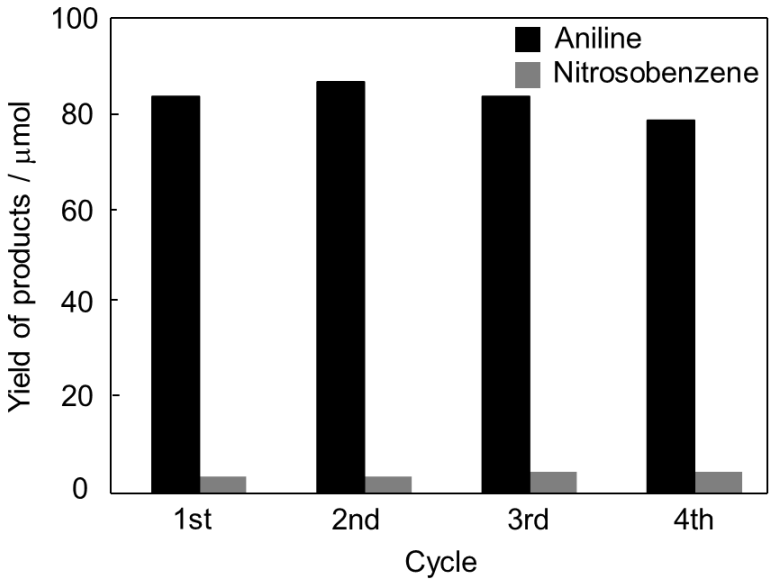

Figure 2. 1. 13. Recycling tests for photocatalytic reduction of nitrobenzene under visible-light irradiation (λ > 420 nm) over Pt(1.5)/Ti-MOF-NH_2. Reaction conditions: catalyst (25 mg), acetonitrile containing 0.1 mmol of nitrobenzene and 1.0 mmol of TEOA (4 ml), Xe lamp (500 W) light source with a cutoff filter, Pyrex reaction vessel, room temperature, 72 h.

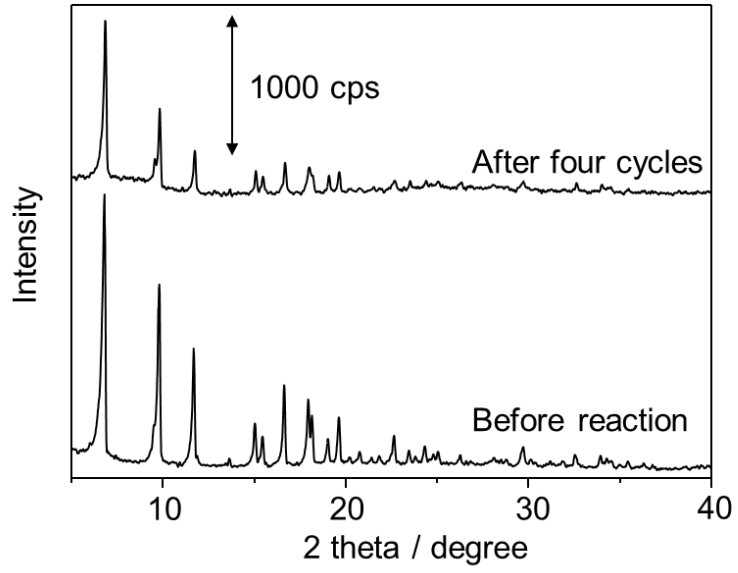

Figure 2. 1. 14. XRD patterns of Pt(1.5)/Ti-MOF-NH_2 before and after four cycles of photocatalytic reduction of nitrobenzene under visible-light irradiation (λ > 420 nm).

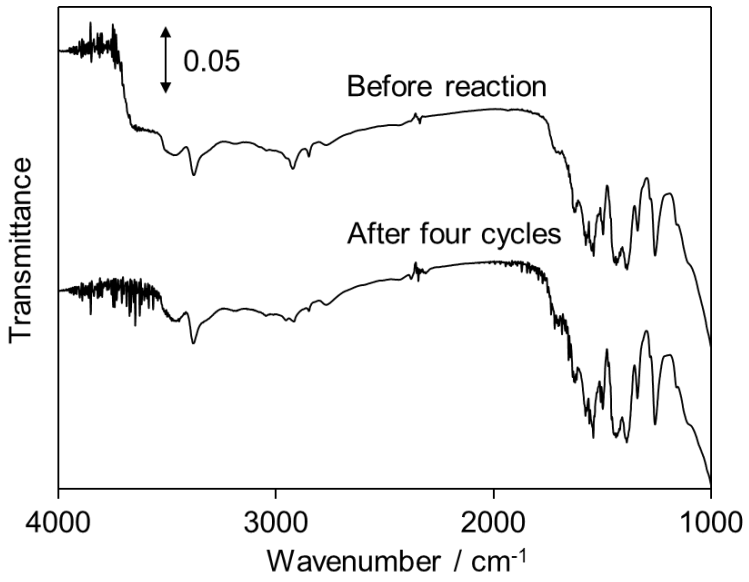

Figure 2. 1. 15. FT-IR spectra of Pt(1.5)/Ti-MOF-NH_2 before and after four cycles of photocatalytic reduction of nitrobenzene under visible-light irradiation ($\lambda > 420$ nm).

2. 1. 4. Conclusions

In the effort described above, a new visible-light-responsive metal–organic framework (MOF) photocatalyst was developed by utilizing a 2-anilinedicarboxylic acid organic linker. The amino-functionalized Ti-based MOF (Ti-MOF-NH_2) was found to efficiently photocatalyze the hydrogen production reaction in an aqueous solution containing TEOA as a sacrificial electron donor under visible-light irradiation conditions. In this process, the organic linker absorbs visible light and its excited state transfers an electron to the CB of the photocatalytically active titanium-oxo cluster. To the best of our knowledge, this is the first example of photocatalytic hydrogen production system employing MOF materials and visible-light irradiation at wavelengths up to 500 nm. Furthermore, this system was successfully extended to photocatalytic reduction of nitrobenzene under visible-light

irradiation ($\lambda > 420$ nm). The observations made in this investigation should offer new insight into the design and manipulation of specifically functioning MOFs that have applications in the fields of photo-functionalized materials, such as photocatalysts and luminescent materials.

2. 1. 5. References

1. A. Fujishima and K. Honda, *Nature*, 1972, **238**, 37.
2. M. Matsuoka, M. Kitano, M. Takeuchi, K. Tsujimaru, M. Anpo and J. M. Thomas, *Catal. Today,* 2007, **122**, 51.
3. M. Kitano, K. Funatsu, M. Matsuoka, M. Ueshima and M. Anpo, *J. Phys. Chem. B*, 2006, **110**, 25266.
4. Z. Zou, J. Ye, K. Sayama and H. Arakawa, *Nature*, 2001, **414**, 625.
5. A. Kudo and Y. Miseki, *Chem. Soc. Rev.*, 2009, **38**, 253.
6. M. Anpo and M. Takeuchi, *J. Catal*., 2003, **216**, 505.
7. K. Maeda, K. Teramura, D. Lu, T. Takata, N. Saito, Y. Inoue and K. Domen, *Nature*, 2006, **440**, 295.
8. D. Gust, T. A. Moore and A. L. Moore *Acc. Chem. Res*., 2009, **42**, 1890.
9. A. J. Nozik, M. C. Beard, J. M. Luther, M. Law, R. J. Ellingson and J. C. Johnson, *Chem. Rev.*, 2010, **110**, 6873.
10. O. M. Yaghi, M. O'Keeffe, N. W. Ockwig, H. K. Chae, M. Eddaoudi and J. Kim, *Nature*, 2003, **423**, 705.
11. S. Kitagawa, R. Kitaura and S. Noro, *Angew. Chem., Int. Ed.*, 2004, **43**, 2334.
12. G. Férey, *Chem. Soc. Rev*., 2008, **37**, 191.
13. M. Eddaoudi, J. Kim, N. Rosi, D. Vodak, J. Wachter, M. O'Keeffe and O. M. Yaghi, *Science*, 2002, **295**, 469.
14. N. L. Rosi, J. Eckert, M. Eddaoudi, D. T. Vodak, J. Kim, M. O'Keeffe and O. M. Yaghi *Science*, 2003, **300**, 1127.
15. X. Zhao, B. Xiao, A. J. Fletcher, K. Thomas, D. Bradshaw and M. J. Rosseinsky, *Science*, 2004, **306**, 1012.

16. A. R. Millward and O. M. Yaghi, *J. Am. Chem. Soc*., 2005, **127**, 17998.
17. S. Shimomura, M. Higuchi, R. Matsuda, K. Yoneda, Y. Hijikata, Y. Kubota, Y. Mita, J. Kim, M. Takata and S. Kitagawa, *Nat. Chem*., 2010, **2**, 633.
18. M. P. Suh, H. J. Park, T. K. Prasad and D. W. Lim, *Chem. Rev.*, 2012, **112**, 782.
19. D. N. Dybtsev, H. Chun, S. Yoon, D. Kim and K. J. Kim, *J. Am. Chem. Soc.*, 2003, **126**, 32.
20. R. Matsuda, R. Kitaura, S. Kitagawa, Y. Kubota, R. V. Belosludov, T. C. Kobayashi, H. Sakamoto, T. Chiba, M. Takata, Y. Kawazoe and Y. Mita, *Nature*, 2005, **436**, 238.
21. H. Bux, F. Liang, Y. Li, J. Cravillion, M. Wiebcke and J. Caro, *J. Am. Chem. Soc.*, 2009, **127**, 16000.
22. B. Chen, S. Xiang and G. Qian, *Acc. Chem. Res.*, 2010, **43**, 1115.
23. J. R. Li, J. Sculley and H. C. Zhou, *Chem. Rev*., 2012, **112**, 869.
24. A. Corma, H. Garcia and F. X. Liabres i Xamena, *Chem. Rev.*, 2010, **110**, 4606.
25. S. Horike, M. Dinca, K. Tamaki and J. R. Long, *J. Am. Chem. Soc.*, 2008, **130**, 5854.
26. J. Lee, O. K. Farha, J. Roberts, K. A. Scheidt, S. T. Nguyen and J. T. Hupp, *Chem. Soc. Rev*., 2009, **38**, 1450.
27. F. Song, C. Wang, J. M. Falkowski, L. Ma and W. Lin, *J. Am. Chem. Soc*., 2010, **132**, 15390.
28. M. Yoon, R. Srirambalaji and K. Kim, *Chem. Rev.*, 2012, **112**, 1196.
29. M. Alvaro, E. Carbonell, B. Ferrer, F. X. Liabresi Xamena and H. Garcia, *Chem. Eur. J*., 2007, **13**, 5106.
30. T. Tachikawa, J. R. Choi, M. Fujitsuka and T. Majima. *J. Phys. Chem. C*, 2008, **112**, 36.
31. J. L. Wang, C. Wang and W. Lin, *ACS catal.*, 2012, **2**, 2630.

32. C. A. Kent, D. Liu, L. Ma, J. M. Papanikolas, T. J. Meyer and W. Lin, *J. Am. Chem. Soc*., 2011, **133**, 12940.

33. C. A. Kent, D. Liu, T. J. Meyer and W. Lin, *J. Am. Chem. Soc.*, 2012, **134**, 3991.

34. K. C. Stylianou, R. Heck, S. Y. Chong, J. Bacsa, J. T. A. Jones, Y. Z. Khimyak, D. Bradshaw and M. J. Rosseinsky, *J. Am. Chem. Soc.*, 2010, **132**, 4119.

35. M. Dan-Hardi, C. Serre, T. Frot, L. Rozes, G.Maurin, C. Sanchezand and G. Ferey, *J. Am. Chem. Soc.*, 2009, **131**, 10857.

36. M. Anpo, N. Aikawa and Y. Kubokawa, *J. Phys. Chem.*, 1984, **88**, 3998.

37. T. Kamegawa, T. H. Kim, J. Morishima, M. Matsuoka and M. Anpo, *Catal. Lett*., 2009, **129**, 7.

38. B. Pal, T. Torimoto, K. Okazaki and B. Ohtani, *Chem. Commun*., 2007, 483.

39. S. Fuldner, R. Mild, H. I. Siegmund, J. A. Schroeder, M. Gruber and B. Konig, *Green Chem*., 2010, **12**, 400.

40. X. H. Li, X. Wang, M. Antonietti, *Chem. Sci.*, 2012, **3**, 2170.

41. K. Imamura, S. Iwasaki, T. Maeda, K. Hashimoto, B. Ohtani and H. Kominami, *Phys. Chem. Chem. Phys*., 2011, **13**, 5114.

42. K. Imamura, K. Hashimoto and H. Kominami, *Chem. Commun*., 2012, **48**, 4356.

2. 2. Development of Ru complex-incorporated MOF photocatalyst for hydrogen production under visible-light irradiation

2. 2. 1. Introduction

The production of chemical fuels by solar energy conversion has been considered as one of the major strategies to solve the global energy crisis. Since the pioneering work by Honda and Fujishima on photoelectrochemical water splitting using TiO_2 electrode,[1] the photocatalytic process has attracted much attention and has been extensively studied to realize clean, low-cost and environmentally friendly production of hydrogen by utilising solar energy. Recently, researchers have been focusing on the development of visible-light-responsive photocatalysts,[2–4] because the ultraviolet (UV) light only accounts for about 4% of the solar radiation energy, while the visible light contributes to about 43%.

Inorganic-organic hybrid materials have been of great interest since they not only combine the respective beneficial characteristics of inorganic and organic components, but also often exhibit unique properties that exceed what would be expected for a simple mixture of the components.[5–7] The construction of hybrid materials offers an almost infinite number of chemical and structural possibilities. Among them, metal–organic frameworks (MOFs) also called porous coordination polymers (PCPs) have also attracted much attention because of their attractive properties including high specific surface areas, well-ordered porous structures and structural designability.[8–11] The topology and surface functionality of MOFs can be readily tuned by varying the constituent metal-oxo clusters and bridging organic linkers. Taking advantages of these features, numerous efforts have been made in recent years to indicate that MOFs serve as platforms for integrating different molecular functional components to achieve light harvesting and to promote various photocatalytic reactions such

as hydrogen production, oxygen production, carbon dioxide reduction and organic transformations.[12–16] These MOF photocatalyst-catalyzed systems are advantageous that various combinations of metal-oxo clusters and bridging organic linkers enable fine-tuning and rational design of the photocatalysts at the molecular level. Previous study described the synthesis of a visible-light-responsive Ti-based MOF photocatalyst (Ti-MOF-NH_2) by employing 2-anilinedicarboxylic acid (H_2BDC-NH_2) as an organic linker and its application for photocatalytic hydrogen production and reduction of nitrobenzene under visible-light irradiation.[17–19] The reactions proceed through the light absorption by its organic linker and the following electron transfer to the catalytically active titanium-oxo cluster. Although the visible-light-responsive MOF photocatalysts were successfully developed, the longest wavelength available was only 500 nm and triethanolamine (TEOA) as a sacrificial electron donor is required for the progression of the reaction.[18,20] These are due to the limited visible-light responsivity and low oxidation power of the organic linker (BDC-NH_2). Therefore, it is highly desired that utilisable range of wavelength and sacrificial reagents are expanded by employing other organic linkers that has wide absorption and low highest occupied molecular orbital (HOMO) level (namely, high oxidation power).

This study describes synthesis of Ru complex-incorporated Ti-based MOF (Ti-MOF-$Ru(tpy)_2$) by using a bis(4'-(4-carboxyphenyl)-terpyridine)Ru(II) complex ($Ru(tpy)_2$) as an organic linker and its application for photocatalytic hydrogen production under visible-light irradiation. $Ru(tpy)_2$ possesses wider absorption band in the visible-light region and lower HOMO level than those of BDC-NH_2, as confirmed by diffuse-reflectance UV-vis spectroscopy (**Fig. 2. 2. 1**) and cyclic voltammetry (CV) (**Fig. 2. 2. 2**). Thus, it can be expected that the reaction proceeds under long-wavelength visible-light irradiation and not only when using TEOA as a sacrificial electron donor but also when using other sacrificial reagents such as ethylenediaminetetraacetic acid (EDTA) and methanol.

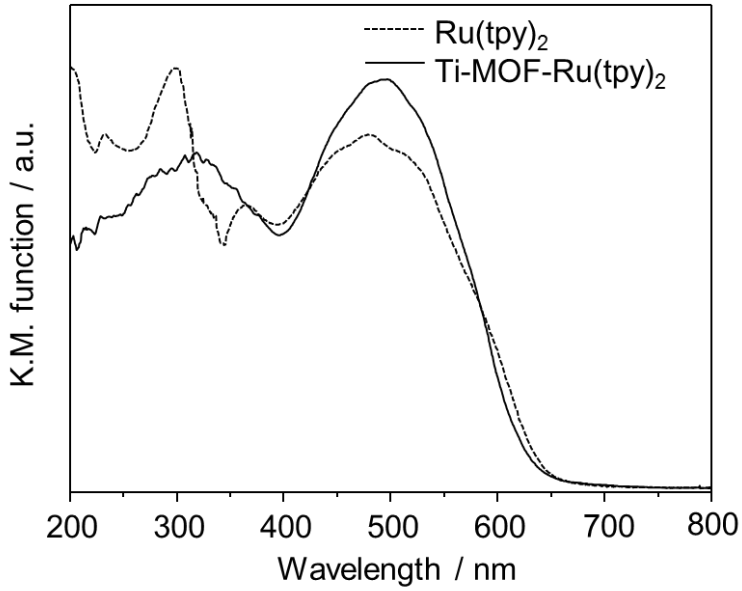

Figure 2. 2. 1. Diffuse reflectance UV-vis spectra of Ti-MOF-$Ru(tpy)_2$ (solid line) and $Ru(tpy)_2$ (dotted line).

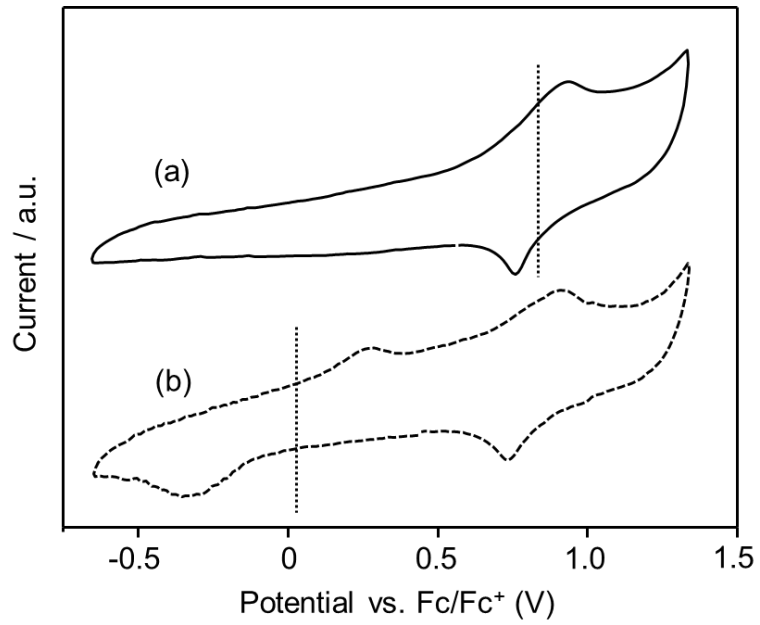

Figure 2. 2. 2. Cyclic voltammograms of (a) $Ru(tpy)_2$ and (b) 2-anilinedicarboxylic acid in CH_2Cl_2 with 0.1 M tetrabutylammonium perchlorate as supporting electrolytes. A Pt working electrode, a Pt counter electrode and a nonaqueous $Ag/AgNO_3$ reference electrode were used.

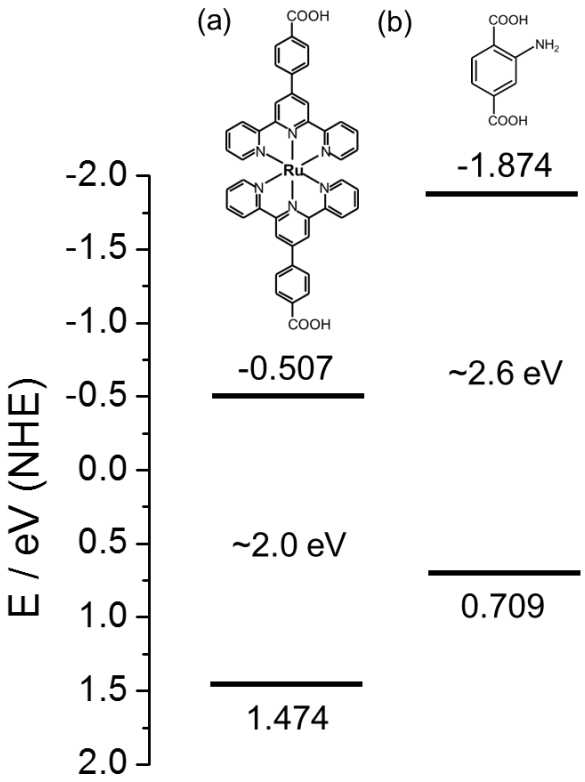

Figure 2. 2. 3. Energy diagram of HOMO-LUMO levels of (a) $Ru(tpy)_2$ and (b) $H_2BDC\text{-}NH_2$. HOMO level was determined on the basis of cyclic voltammograms, and HOMO-LUMO gaps were estimated from the onset of the diffuse reflectance UV-vis spectra.

2. 2. 2. Experimental

Materials

Tetrapropyl orthotitanate (TPOT), tetrabutylammonium perchlorate and $RuCl_3$ were purchased from Tokyo Kasei Kogyo Co., Ltd. 2-Anilinedicarboxylic acid ($H_2BDC\text{-}NH_2$), N'N-dimethylformamide (DMF), methanol, triethanolamine (TEOA), were purchased from Nacalai Tesque Inc. Hydrogen hexachloroplatinate(IV) hexahydrate ($H_2PtCl_6 \cdot 6H_2O$) was purchased from Kishida Chemicals Co., Ltd. Dichloromethane was purchased from Wako Pure Chemical Industries. Ethylenediaminetetraacetic acid disodium salt dihydrate ($EDTA\text{-}Na_2 \cdot 2H_2O$) was purchased from IBI Scientific.

Catalysts preparation

Bis(4'-(4-carboxyphenyl)-terpyridine)Ru(II) complex ($Ru(tpy)_2$) as an organic linker was prepared according to the literature.[21] Ru complex-incorporated Ti-based MOF (Ti-MOF-$Ru(tpy)_2$) was synthesized on the basis of a method for the preparation of MIL-125 (Ti-MOF) previously-reported by Dan-Hardi *et al.*,.[22] The mixture of TPOT, $Ru(tpy)_2$, DMF and methanol was subject to react under solvothermal conditions in a Teflon-lined stainless steel autoclave for 48 h at 453 K under autogenous pressure. The precipitate was filtrated, washed repeatedly with DMF and dried at room temperature overnight. Finally, the obtained powder sample was dried under vacuum for 1 h at 423 K.

General methods

Cyclic voltammograms were obtained with Hokuto Denko HZ-5000 electrochemical measurement system at a scanning rate of 100 mV s^{-1}, equipped with a normal one-compartment cell with a Pt working electrode, a Pt counter electrode, and a nonaqueous $Ag/AgNO_3$ reference electrode. The measurements were performed in a CH_2Cl_2 solution including 0.1 M tetrabutylammonium perchlorate as a supporting electrolyte. Diffuse reflectance UV–vis spectra were obtained with a Shimadzu UV–vis recording spectrophotometer 2200A. Standard θ–2θ X-ray diffraction (XRD) data were recorded on a Shimadzu X-ray diffractometer XRD-6100 using Cu Kα radiation (λ = 1.5406 Å). Nitrogen adsorption-desorption isotherms were collected by using a BEL-SORP mini (BEL Japan, Inc.) at 77 K. XAFS (XANES and EXAFS) spectra were recorded at the BL-01B1 facility of SPring-8 at the Japan Synchrotron Radiation Research Institute (JASRI). The Ru K-edge XAFS spectra were measured in the fluorescence mode, with a Si(111) double-crystal monochromator at room temperature. Curve fitting analyses of the EXAFS spectra were conducted on $k^3\chi$ (k) in k-space (k range = 3–12 $Å^{-1}$) using a REX2000J program (Rigaku). The photoluminescence spectra were recorded at room temperature by utilizing a SPEX

Fluorolog-3 spectrofluorometer with a quartz cell directly connected to a vacuum line containing stopcocks to allow gas addition and degassing. Inductively coupled plasma mass spectrometry (ICP-MS) was performed on X Series II (Thermo Fisher Scientific Inc.) to normalise the intensity of the photoluminescence spectra on the basis of Ru amount.

Photocatalytic hydrogen production reaction

The photocatalyst (10 mg) and water containing 0.01 M TEOA and 0.05 mM H_2PtCl_6 (2 mL) were added to a Pyrex reaction vessel connected to vacuum line. The resulting mixture was evacuated at 77 K to remove dissolved oxygen. Subsequently, the sample was irradiated with the 500 W Xe lamp through a cut-off filter with stirring at room temperature. After the reaction, the resulting gas was analyzed by using a gas chromatograph (GC) of Shimadzu GC-12A with a thermal conductivity detector equipped with a packed column (MS-5A). For the investigations of sacrificial reagents dependence, water containing 0.01 M EDTA and 0.05 mM H_2PtCl_6 or water containing 10 vol.% methanol and 0.05 mM H_2PtCl_6 was used as a reaction solution.

2. 2. 3. Results and discussion

Ti-MOF-Ru(tpy)$_2$ is synthesised by utilizing a solvothermal method from the mixture of tetrapropyl orthotitanate (TPOT), Ru(tpy)$_2$, DMF and methanol. XRD measurements reveal that Ti-MOF-Ru(tpy)$_2$ has a characteristic peak around 6° (2θ) owing to a framework formation although the organic linker, Ru(tpy)$_2$, has no peak such a low angle region (**Fig. 2. 2. 4**). N_2 adsorption-desorption isotherm is shown in **Fig. 2. 2. 5**. Ti-MOF-Ru(tpy)$_2$ exhibits a type III isotherm and the BET surface area was determined to be 20 $m^2\ g^{-1}$, indicating there is no porosity in the sample. Although further study using single-crystal X-ray diffraction is

needed to obtain full structural information, the result can be attributable to the interpenetration of the framework. It is well-known that the interpenetration drastically decreases the specific surface area and pore sizes within the MOFs.[21–22] Thermogravimetric (TG) analysis was also carried out to investigate the stability of Ti-MOF-Ru(tpy)$_2$ (**Fig. 2. 2. 6**). Ti-MOF-Ru(tpy)$_2$ releases water followed by desorption of some DMF and decomposes at temperatures above 650 K.

The local structure of the organic linker was investigated by Ru K-edge XAFS measurements (**Fig. 2. 2. 7**). The edge position as well as the shape of the XANES spectrum of Ti-MOF-Ru(tpy)$_2$ corresponds well to those of Ru(tpy)$_2$ as a reference. Fourier transform of EXAFS spectra (without phase-shift correction) of Ti-MOF-Ru(tpy)$_2$ and Ru(tpy)$_2$ exhibit one peak due to the neighboring nitrogen atoms at 1.5–2.0 Å, while other peaks due to the neighboring Ru atom are hardly observed in the ranges of 2.0–3.0 Å. Furthermore, the curve fitting analysis of the Ru–N peak for Ru(tpy)$_2$ reveals the existence of a shorter Ru–N bond between Ru atom and the central pyridine ring (Ru–$N_{central}$) along the main axis at 1.99 Å (coordination number (CN)= 1.9) and the other longer Ru–N bonds between Ru atom and the terminal pyridine rings (Ru–$N_{terminal}$) at 2.08 Å (CN = 4.2). These values are in good agreement with the previous studies[23] and those obtained by the curve fitting analysis of Ti-MOF-Ru(tpy)$_2$ (Ru–$N_{central}$ = 1.98 Å (CN =1.9), Ru–$N_{terminal}$ = 2.05 Å (CN = 4.0)). These results suggest that the local structure of Ru complex is maintained even after the formation of Ti-MOF-Ru(tpy)$_2$.

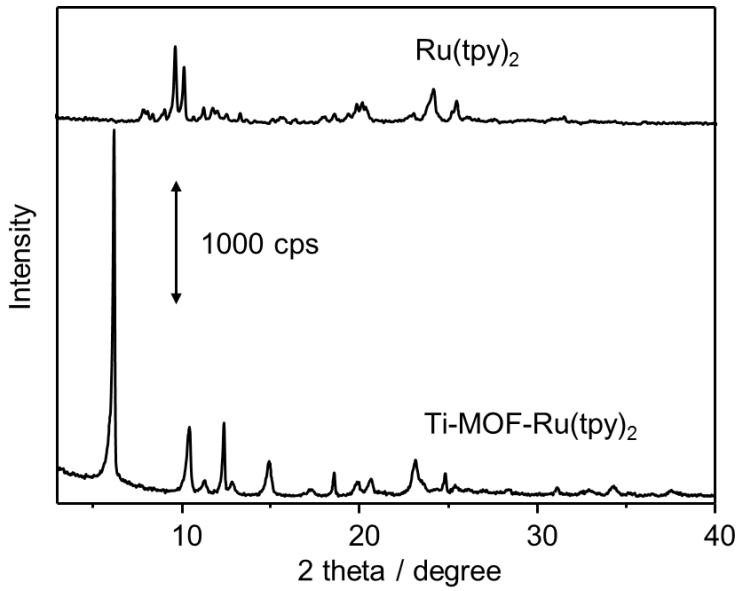

Figure 2. 2. 4. XRD patterns of Ti-MOF-Ru(tpy)$_2$ and Ru(tpy).

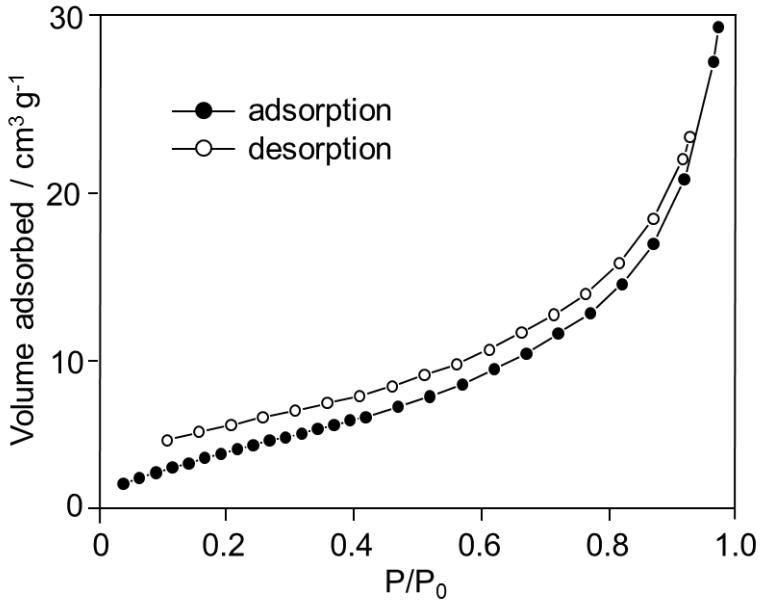

Figure 2. 2. 5. N_2 adsorption-desorption isotherm of Ti-MOF-Ru(tpy)$_2$.

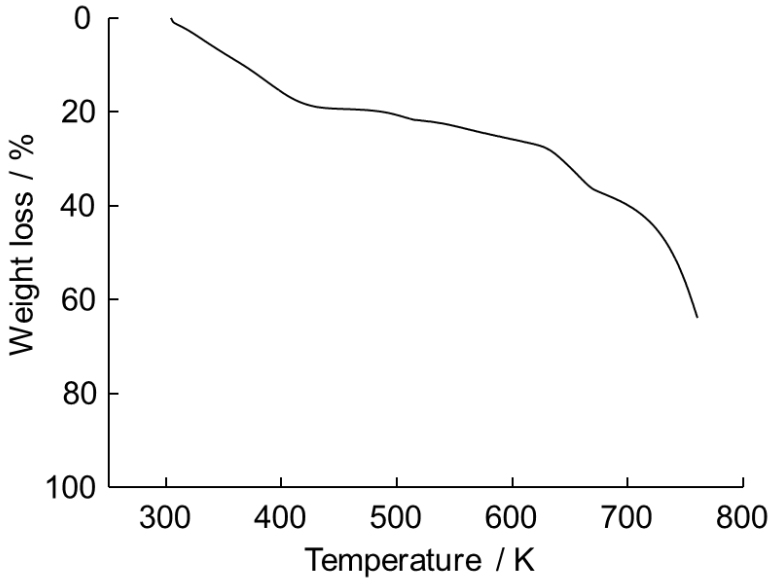

Figure 2. 2. 6. TGA curve of Ti-MOF-Ru(tpy)$_2$.

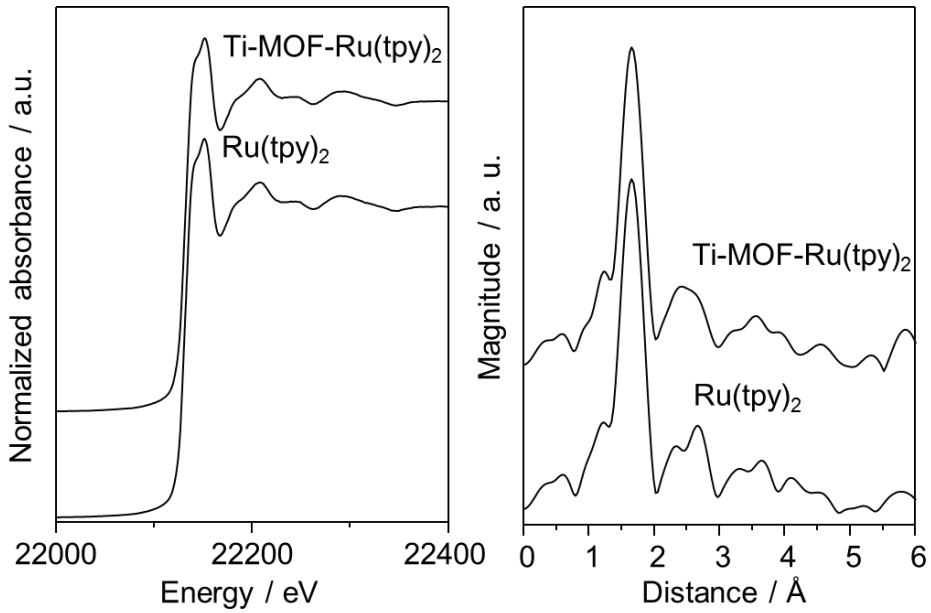

Figure 2. 2. 7. XANES and EXAFS spectra of Ti-MOF-Ru(tpy)$_2$ and Ru(tpy).

In order to investigate the potential photocatalytic activity of Ti-MOF-Ru(tpy)$_2$, hydrogen production reactions from aqueous solution containing TEOA as a sacrificial electron donor were carried out under visible-light irradiation (λ > 420 nm) at room temperature. For the reaction, Pt nanoparticles as a cocatalyst (Pt content: 1 wt%) were

deposited in-situ onto Ti-MOF-Ru(tpy)$_2$ from H_2PtCl_6 during the reaction. **Figure 2. 2. 8** shows the time course of the hydrogen production with intermittent evacuation and exposure to atmospheric conditions every 3 h. Ti-MOF-Ru(tpy)$_2$ achieves steady hydrogen production under visible-light irradiation without significant loss of photocatlytic activity over at least three cycles. It should be noted that 2.1 μmol of hydrogen is produced without H_2PtCl_6 as a precursor of the Pt nanoparticle cocatalyst (**Table 2. 2. 1**). On the contrary, the organic linker itself (Ru(tpy)$_2$) shows no photocatalytic activity under the same condition. Furthermore, the hydrogen production reaction was performed over a photocatalyst prepared by the adsorption of Ru(tpy)$_2$ on Degussa P25 TiO_2 (Ru(tpy)$_2$/TiO_2). However, hydrogen is not evolved over Ru(tpy)$_2$/TiO_2. This would be because of the Ru(tpy)$_2$ dye desorption from the TiO_2 surfaces under the reaction conditions, which makes it difficult to transfer the photogenerated electrons from Ru(tpy)$_2$ to TiO_2. This fact indicates an advantage of this photocatalytic system, in which titanium-oxo clusters and Ru(tpy)$_2$ are strongly connected, compared to the conventional dye-sensitized photocatalytic systems. The results obtained from several control reactions reveal that the light irradiation as well as the presence of Ti-MOF-Ru(tpy)$_2$ and a sacrificial electron donor are essential for the progression of the reaction (**Table 2. 2. 1**). It was also investigated by XRD that the structure of Ti-MOF-Ru(tpy)$_2$ is maintained even after the reaction (**Fig. 2. 2. 9**).

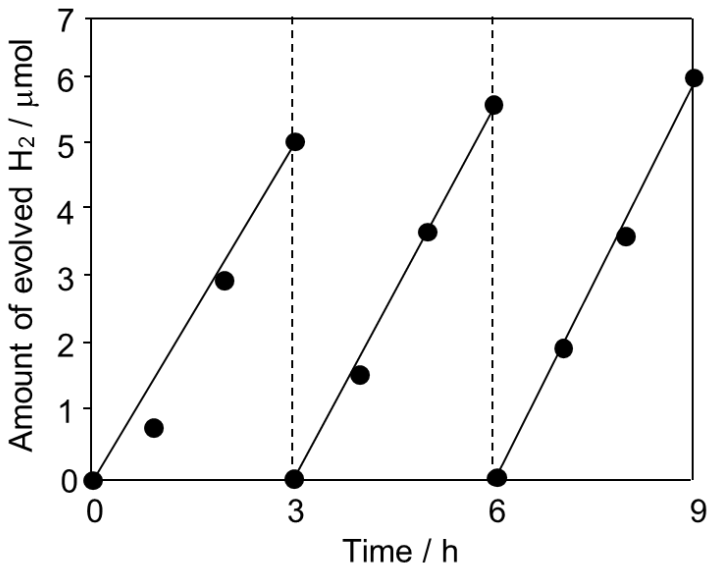

Figure 2. 2. 8. Time course of photocatalytic hydrogen production under visible-light irradiation ($\lambda > 420$ nm) from water containing 0.01 M TEOA and 0.05 mM H_2PtCl_6 using Ti-MOF-Ru(tpy)$_2$ for a total of 9 h with intermittent evacuation and exposure to atmospheric conditions every 3 h.

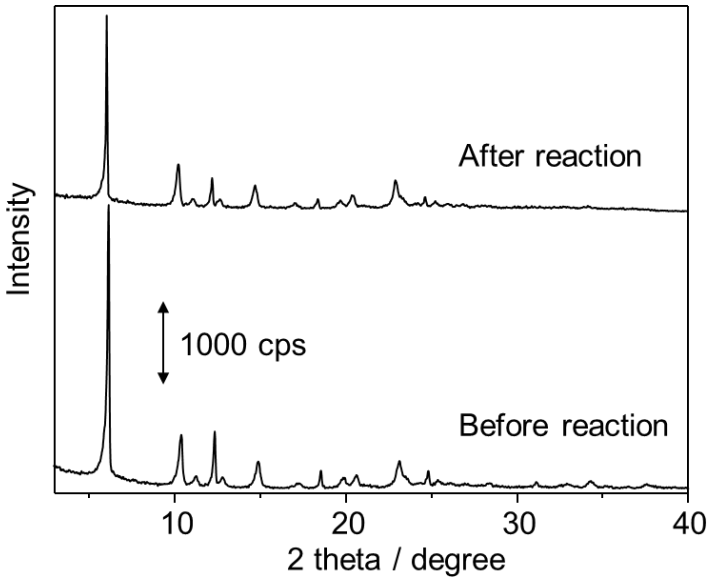

Figure 2. 2. 9. XRD patterns of Ti-MOF-Ru(tpy)$_2$ before and after the photocatalytic hydrogen production from water containing 0.01 M TEOA and 0.05 mM H_2PtCl_6 for 6 h.

As shown in **Fig. 2. 2. 10**, the wavelength dependence of apparent quantum efficiency was investigated next in order to confirm the reaction mechanism. The trend of the apparent quantum efficiency matches well with that of the absorption spectrum. This result suggests that the reaction proceeds through the light absorption by its organic linker and the following electron transfer to the catalytically active titanium-oxo cluster as is the case with the previously reported system.[17–19] In this Ti-MOF-Ru(tpy)$_2$-catalyzed system, the longest wavelength available is 620 nm. As expected, utilizable range of wavelength has been successfully expanded by employing Ru(tpy)$_2$ as an organic linker. Luminescence spectroscopy was also employed to investigate the electron transfer process as shown in **Fig. 2. 2. 11**. The metal-to-ligand charge transfer (MLCT) state luminescence of Ru^{2+}-based complex is observed for both Ti-MOF-Ru(tpy)$_2$ and Ru(tpy)$_2$. However, the luminescence intensity decreases by the formation of the MOF structure. Similar results have been observed with conventional dye-sensitized photocatalytic systems (i.e., combination between Ru^{2+}-based dyes and semiconducting materials) as a result of the efficient electron injection from the dyes to the semiconducting materials.[24–25] These facts indicate that the efficient electron transfer occurs from the organic linker to the Ti-oxo cluster in Ti-MOF-Ru(tpy)$_2$ under visible-light irradiation, resulting in the decrease of the luminescence intensity. The combined results emanating from the action spectrum and the luminescence spectroscopy clearly indicate the photocatalytic hydrogen production reaction proceed through the light absorption by its organic linker and the following electron transfer to the catalytically active titanium-oxo cluster.

In addition, the dependence of the sacrificial reagents were investigated, as described in **Fig. 2. 2. 12**. Ti-MOF-Ru(tpy)$_2$ achieves hydrogen production when using EDTA or methanol as an sacrificial reagent although hydrogen is not evolved over Ti-MOF-NH_2 as a photocatalyst under the same conditions. These results can be attributable to the higher

oxidation power of $Ru(tpy)_2$ than that of $H_2BDC\text{-}NH_2$.

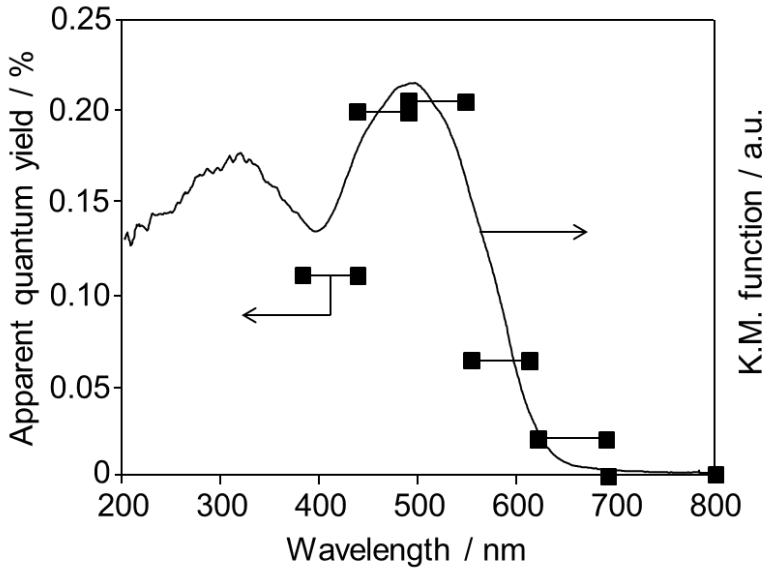

Figure 2. 2. 10. Wavelength-dependent apparent quantum efficiency for the hydrogen evolution reaction from water containing 0.01 M TEOA and 0.05 mM H_2PtCl_6 using Ti-MOF-$Ru(tpy)_2$.

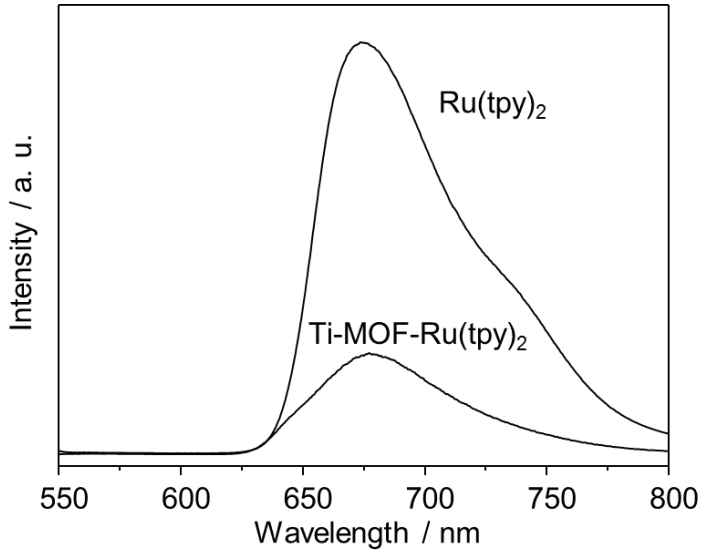

Figure 2. 2. 11. Photoluminescence spectra of Ti-MOF-$Ru(tpy)_2$ and $Ru(tpy)_2$ measured in vacuum at 77 K (Excitation: λ_{ex} = 520 nm).

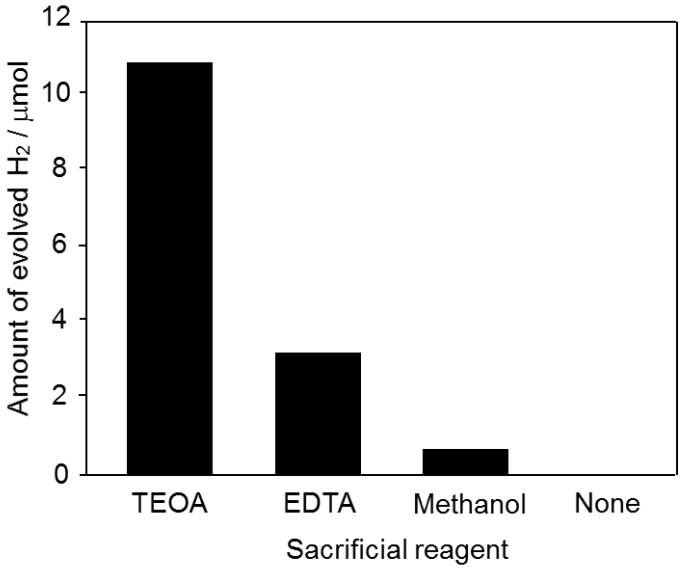

Figure 2. 2. 12. Sacrificial reagents dependence of photocatalytic hydrogen production under visible-light irradiation ($\lambda > 420$ nm) over Ti-MOF-Ru(tpy)$_2$ for the reaction time of 6 h.

2. 2. 4. Conclusions

In summary, utilizable range of wavelength and sacrificial reagents of MOF photocatalyst-catalyzed systems have been successfully expanded by employing a bis(4'-(4-carboxyphenyl)-terpyridine)Ru(II) complex (Ru(tpy)$_2$) as an organic linker. The synthesised Ru complex-incorporated Ti-based MOF (Ti-MOF-Ru(tpy)$_2$) exhibits photocatalytic activity for hydrogen production from water containing a sacrificial electron donor under visible-light irradiation up to 620 nm. This is the first example of photocatalytic hydrogen production system employing MOF materials under visible-light irradiation at wavelengths up to 620 nm.

2. 2. 5. References

1. A. Fujishima and K. Honda, *Nature*, 1972, **238**, 37.
2. A. Kudo and Y. Miseki, *Chem. Soc. Rev.*, 2009, **38**, 253.
3. K. Maeda, K. Teramura, D. Lu, T. Takata, N. Saito, Y. Inoue and K. Domen, *Nature*, 2006, **440**, 295.
4. Y. Horiuchi, T. Toyao, M. Takeuchi, M. Matsuoka and M. Anpo, *Phys. Chem. Chem. Phys.*, 2013, 15, 13243.
5. K. Ariga, A. Vinu, Y. Yamauchi, Q. Ji and J. P. Hill, *Bull. Chem. Soc. Jpn*., 2012, **85**, 1.
6. N. Mizoshita, T. Tani and S. Inagaki, *Chem. Soc. Rev*., 2011, **40**, 789.
7. T. Kamegawa, T. Sakai, M. Matsuoka and M. Anpo, *J. Am. Chem. Soc*., 2005, **127**, 16784.
8. H. Furukawa, K. E. Cordova, M. O'Keeffe and O. M. Yaghi, *Science*, 2013, **341**, 974.
9. Y. Sakata, S. Furukawa, M. Kondo, K. Hirai, N. Horike, Y. Takashima, H. Uehara, N. Louvain, M. Meilikhov, T. Tsuruoka, S. Isoda, W. Kosaka, O. Sakata and S. Kitagawa, *Science*, 2013, **339**, 193.
10. G. Férey, *Chem. Soc. Rev*., 2008, **37**, 191.
11. Y. Inokuma, S. Yoshioka, J. Ariyoshi, T. Arai, Y. Hitora, K. Takada, S. Matsunaga, K. Rissanen and M. Fujita, *Nature*, 2013, **495**, 461.
12. C. G. Silva, I. L uz, F. X. Liabres i Xamena, A. Corma and H. Garcia, *Chem. Eur. J*., 2010, **16**, 11133
13. J. L. Wang, C. Wang and W. Lin, *ACS catal.*, 2012, **2**, 2630
14. A. Fateeva, P. A. Chater, C. P. Ireland, A. A. Tahir, Y. Z. Khimyak, P. V. Wiper, J. R. Darwent and M. J. Rosseinsky, *Angew. Chem., Int. Ed*., 2012, **51**, 7440

15. Y. Fu, D. Sun, Y. Chen, R. Huang, Z. Ding, X. Fu and Z. Li, *Angew. Chem., Int. Ed.*, 2012, **51**, 3364.
16. T. Tachikawa, J. R. Choi, M. Fujitsuka and T. Majima. *J. Phys. Chem. C*, 2008, **112**, 36.
17. M. Matsuoka, Y. Horiuchi, T. Toyao, M. Saito, K. Mochizuki, M. Iwata and H. Higashimura, *JP Patent*, Appl. No., 2012−170362.
18. Y. Horiuchi, T. Toyao, M. Saito, K. Mochizuki, M. Iwata, H. Higashimura, M. Anpo and M. Matsuoka, *J. Phys. Chem. C*, 2012, **116**, 20848.
19. T. Toyao, M. Saito, Y. Horiuchi, K. Mochizuki, M. Iwata, H. Higashimura, M. Anpo and M. Matsuoka, *Catal. Sci. Technol.,* 2013, **3**, 2092.
20. Hydrogen is not evolved even in the presence of methanol or EDTA as a sacrificial electron donor.
21. E. C. Constable, E. L. Dunphy, C. E. Housecroft, M. Neuburger, S. Schaffner, F. Schaper and S. R. Batten, *Dalton Trans.*, 2007, **14**, 4323.
22. M. Dan-Hardi, C. Serre, T. Frot, L. Rozes, G.Maurin, C. Sanchezand and G. Ferey, *J. Am. Chem. Soc.*, 2009, **131**, 10857.
23. O. Shekhah, H. Wang, M. Paradinas, C. Ocal, B. Schüpbach, A. Terfort, D. Zacher, R. A. Fischer and C. Wöll, *Nat. Mater.*, 2009, **8**, 481.
24. O. M. Yaghi, *Nat. Mater.*, 2007, **6**, 92.
25. I. Ciofini, P. P. Lainé, F. Bedioui and C. Adamo, *J. Am. Chem. Soc.*, 2004, **126**, 10763.
26. K. Maeda, M. Eguchi, S.-H. A. Lee, W. J. Youngblood, H. Hata, T. E. Mallouk, *J. Phys. Chem. C*, 2009, **113**, 7962.
27. K. Hashimoto, M. Hiramoto, A. B. P. Lever, T. Sakata, *J. Phys. Chem.* 1988, **92**, 1016.

Chapter 3

Developments of various one-pot reactions over bifunctional MOF catalysts

3.1. Application of amino-functionalized metal–organic frameworks for a one-pot acid-base reaction

3. 1. 1. Introduction

Recently, synthetic organic chemists have given great attention to the development of one-pot, sequential organic reactions owing to their comparably higher efficiencies, increased cost effectiveness and reduced formation of waste materials.[1–3] An important goal in this area, is the development of new catalysts having spatially isolated, multiple active sites so that they can promote multi-step reaction cascades. Among the various systems designed to possess this capability, many of these are homogeneous catalysts and, as a result, they generally suffer from product contamination and limited recyclability.[4–6] Furthermore, catalytic acid-base one-pot reaction systems are hardly developed in the homogeneous phase because the acid and base sites are easily deactivated by each other. Therefore, the development of multifunctional heterogeneous catalysts that promote one-pot reactions is currently receiving much attention.[7–9]

Metal–organic frameworks (MOFs), also called porous coordination polymers (PCPs), have gained recent interest because of their several attractive properties, including high specific surface areas, well-ordered porous structures and structural designability. [10–15] Because of these advantageous features, MOFs have been widely investigated as solid catalysts or catalyst supports for several organic transformations, such as epoxidations, [16] cycloadditions of CO_2 with epoxides,[17] aldol condensations, [18] Knoevenagel condensations[19] and Paal-Knorr reactions. [20] In addition, because their topology and surface functionalities can be readily tuned by modifying or varying the core metal-oxo clusters and bridging organic linkers, MOFs have emerged as interesting platforms for engineering molecular solids to

create multifunctional catalysts. Several multifunctional MOF based catalytic systems have been devised[21] so that reactions are promoted by functionality in organic linkers or by coordinatively unsaturated metal sites of MOFs. Moreover, catalytic sites in these substances can be incorporated by using postsynthetic modification of organic struts.

The coordinatively unsaturated metal sites within MOFs, which can serve as catalytic centers, have been actively investigated in recent years.[22–25] These studies have shown that the sites are capable of acting as Lewis acid catalysts for various organic reactions. Because structural defects are thought to be responsible for catalysis by these MOFs, efforts have been made to enhance activities by deliberately introducing defects.[26] Although many reports exist describing the Lewis acidity of MOFs, the Brønsted acidity of these substances has not been studied greatly. However, very recently, Ameloot et al. reported that Brønsted acid sites are present in MOFs and that they are responsible for catalysis of the oligomerization of furfuryl alcohol.[27] The Brønsted acidities of MOFs are attributed to the presence of carboxylic acid moieties (–COOH groups) in the organic linker existing on the outer surface of the particles and in structural defects within the framework. Consequently, new reactions and multi-step processes that can be catalyzed by Brønsted acid sites present in MOFs would have great utility in organic synthesis.

In the study described below, the acid and base properties of the amino-functionalized MOF, MIL-101(Al)-NH_2, were examined in the context of catalysis of deacetalization and Knoevenagel condensation reactions. It is well-known that deacetalization reactions are catalyzed by Brønsted acidic sites[28] and Knoevenagel condensation reactions are catalyzed by Brønsted and Lewis base sites.[29] The results show that the respective reactions are successfully promoted by MIL-101(Al)-NH_2. The possibility that the amino-functionalized MOF can serve as a bifunctional acid-base catalyst has been demonstrated using a one-pot reaction producing benzylidenemalononitrile via sequential

deacetalization and Knoevenagel condensation (**Scheme 3. 1. 1**). Finally, observations made in this effort show that activity of MIL-101(Al)-NH_2 as acid-base bifunctional catalysts is superior to those of conventional heterogeneous, homogeneous as well as other MOF catalysts.

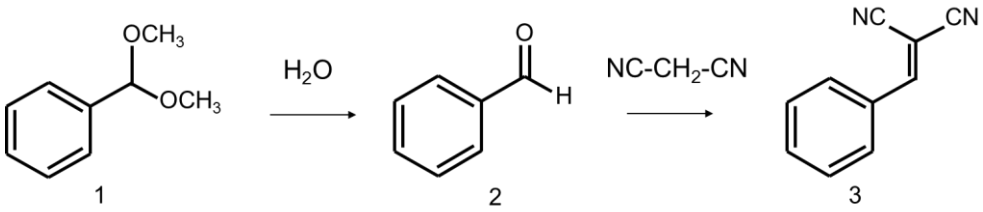

Scheme 3. 1. 1. One-pot deacetalization-Knoevenagel condensation reaction.

3. 1. 2. Experimental

Materials

2-Anilinedicarboxylic acid (H_2BDC-NH_2), 1,4-benzenedicarboxylic acid (H_2BDC), N'N-dimethylformamide (DMF), $ZrCl_4$, $Cr(NO_3)_3 \cdot 9H_2O$, NaOH, HCl, methanol, acetone, triethylamine and 1, 4-dioxane were purchased from Nacalai Tesque Inc. 1,3,5-Benzenetricarboxylic acid (H_3BTC), malononitrile, benzaldehyde and benzaldehyde dimethylacetal were purchased from Tokyo Chemical Industry Co., Ltd. $AlCl_3 \cdot 6H_2O$, $Al(NO_3)_3 \cdot 9H_2O$, $Cu(NO_3)_3 \cdot 3H_2O$ and MgO were purchased from Kishida Chemical Co., Ltd. Al_2O_3 was purchased from Evonik. HY zeolite (SiO_2/Al_2O_3 = 30) was purchased from ZEOLYST. All materials were used as received without purification.

Catalysts preparation

MIL-101(Al)-NH_2 was synthesized using the previously-reported method.[30] The mixture of $AlCl_3 \cdot 6H_2O$ (0.51 g), H_2BDC-NH_2 (0.56 g) and DMF (40 ml) was subjected to solvothermal reaction conditions in a Teflon-lined stainless steel autoclave for 40 h at 403 K

under autogenous pressure. The generated precipitate was separated by filtration, washed repeatedly with acetone and dried under vacuum for 3 h at room temperature.

General methods

Standard θ–2θ X-ray diffraction (XRD) data were recorded on a Shimadzu X-ray diffractometer XRD-6100 using Cu Kα radiation (λ = 1.5406 Å). Nitrogen adsorption-desorption isotherms were collected by using a BEL-SORP mini (BEL Japan, Inc.) at 77 K. FT-IR spectra were recorded in transmittance mode by a FT-IR spectrophotometer equipped with a DTGS detector (JASCO FT/IR 660Plus, resolution 4 cm^{-1}). Self-supporting pellets of the samples were loaded in a specially constructed IR cell, which was equipped with CaF_2 windows. Thermogravimetric (TG) analysis was carried out using a thermal analyser (Rigaku Termoplus 8120), with a heating rate of 10 K min^{-1} in air. Scanning electron microscope (SEM) images were obtained with a Hitachi S-4500.

Catalytic reactions

Deacetalization reaction: The reactions were carried out in liquid phase in a 35 ml glass reactor. A solution of benzaldehyde dimethylacetal (1 mmol) and 1, 4-dioxane (4 ml) was stirred at 363 K with 100 mg of the catalysts in powder form. The progression of the reaction was monitored by using gas chromatography (Shimadzu GC-14B with a flame ionization detector) equipped with an InertCap®1 capillary column.

Knoevenagel condensation reaction: The reactions were carried out in liquid phase in a 35 ml glass reactor. A solution of benzaldehyde (1 mmol), malononitrile (5 mmol) and 1, 4-dioxane (4 ml) was stirred at 363 K with 100 mg of the catalysts in powder form. The progression of the reaction was monitored by using gas chromatography (see above).

One-pot deacetalization-Knoevenagel condensation reaction: The reactions were carried out in liquid phase in a 35 ml glass reactor. A solution of benzaldehyde dimethylacetal (1 mmol), malononitrile (5 mmol) and 1, 4-dioxane (4 ml) were stirred at 363 K with 100 mg of the catalysts in powder form. The progression of the reaction was monitored by using gas chromatography (see above).

Reusability of the catalyst was studied as follows. After the first run, the catalyst was washed three times with 1, 4-dioxane, dried at 313 K in air and reused for the next run. The above procedure was repeated three times.

3. 1. 3. Results and discussion

The amino-functionalized MOF catalyst, MIL-101(Al)-NH_2, was prepared from $AlCl_3 \cdot 6H_2O$ and $H_2BDC\text{-}NH_2$ by using the previously described solvothermal method.[30] XRD and N_2 adsorption-desorption measurements were performed to confirm the formation of the MOF structure. **Figure 3. 1. 1** shows an XRD pattern of MIL-101(Al)-NH_2. Although the diffraction pattern does not perfectly match the diffraction pattern previously reported, the pattern can be attributable to a MIL-101 type structure.[31] In addition, because no diffraction patterns corresponding to the bulk Al_2O_3 are observed, it is confirmed that crystalline Al_2O_3 are not formed in MIL-101(Al)-NH_2. **Figure 3. 1. 2** represents N_2 adsorption-desorption isotherm of MIL-101(Al)-NH_2. This isotherm shows the well-known characteristic steps of the MIL-101 type structure. The changes present in isotherm correspond to filling only the superoctahedra at low relative pressures ($P/P_0 < 0.05$) and, as the pressure increases, medium ($P/P_0 = 0.15$) and large cavities of the MOF become filled. By using the BET (Brunauer-Emmett-Teller) method to treat the N_2 adsorption data, the specific surface area of MIL-101(Al)-NH_2 was calculated to be 800 m^2g^{-1}. This value is lower than the one previously

reported,[30] indicating that some structural defects exist in the sample of MIL-101(Al)-NH_2 prepared in this study. Despite leading to a low specific surface area of this material, the structural defects can be key features required to develop catalysts which exhibit better performances, as suggested by Corma et al.[32]

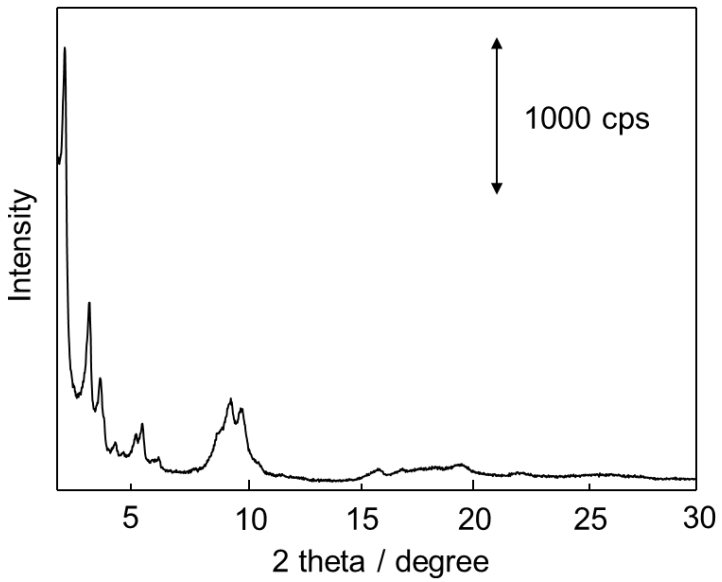

Figure 3. 1. 1. XRD pattern of MIL-101(Al)-NH_2.

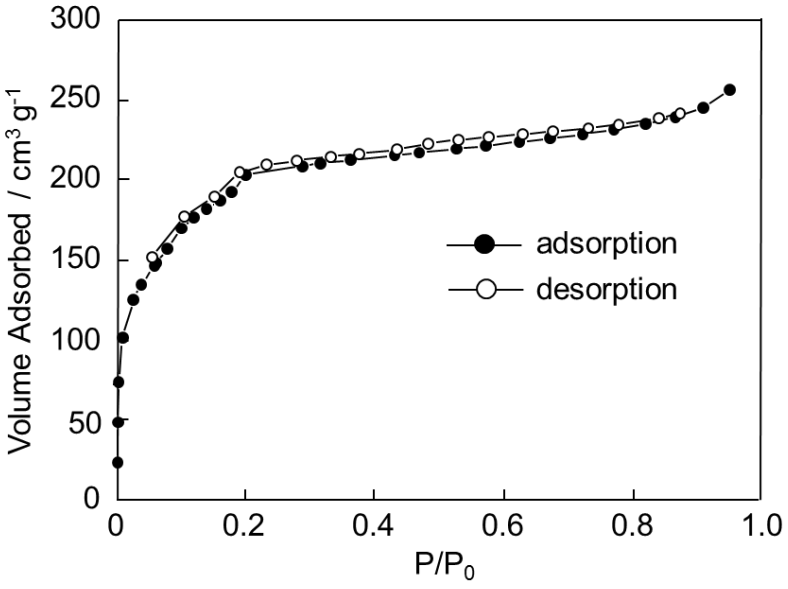

Figure 3. 1. 2. N_2 adsorption-desorption isotherm of MIL-101(Al)-NH_2.

In order to further confirm the structural features, FT-IR and TG analyses were performed (**Figures 3. 1. 3 and 3. 1. 4**). The FT-IR spectrum of MIL-101(Al)-NH_2 shows bands corresponding to the symmetric and asymmetric stretching of primary amines (3408 and 3521 cm^{-1}), indicating that the $–NH_2$ groups are free without coordination. As shown in **Fig. 3. 1. 3**, MIL-101(Al)-NH_2 releases water followed by desorption of some DMF and decomposes at temperatures above 650 K. This result indicates high thermal stability of MIL-101(Al)-NH_2 prepared in this study.

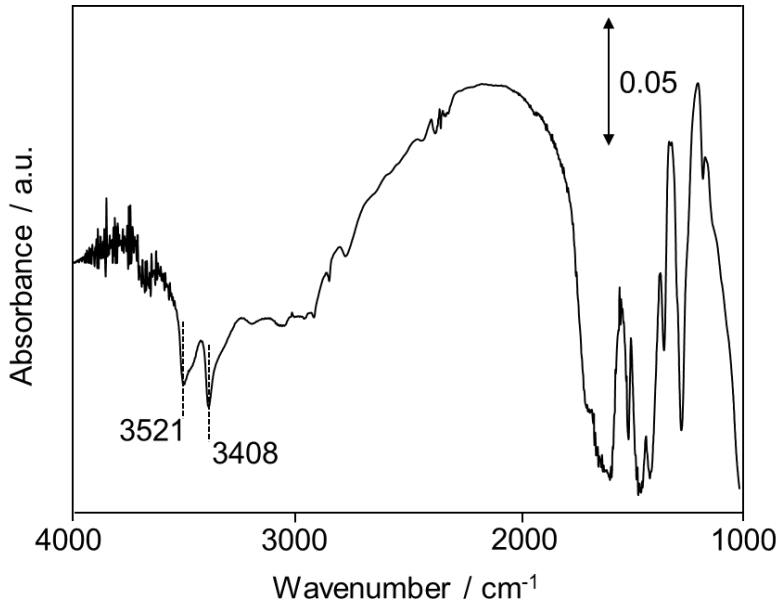

Figure 3. 1. 3. FT-IR spectrum of MIL-101(Al)-NH_2.

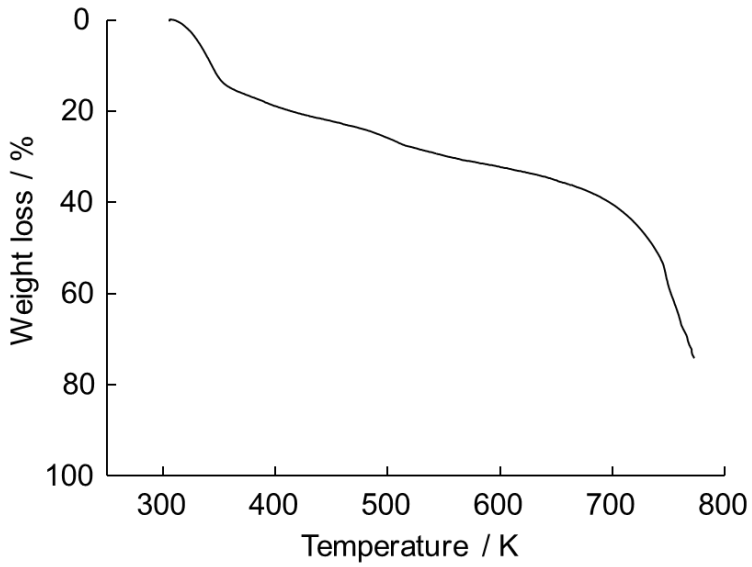

Figure 3. 1. 4. TG curve of MIL-101(Al)-NH_2 measured with a heating rate of 10 K min^{-1} in air.

Prior to exploring applications to one-pot reactions, separate deacetalization of benzaldehyde dimethylacetal and Knoevenagel condensation of benzaldehyde with malononitrile were performed over MIL-101(Al)-NH_2 as test reactions. Both reactions are widely used in organic chemistry.[33] In general, deacetalization reactions are well-known to be catalyzed over Brønsted acidic sites.[28] On the other hand, Knoevenagel condensation reactions are catalyzed over Brønsted and Lewis base sites.[29] Therefore, this study was conducted to investigate the activities of the respective Brønsted acid and base sites in MIL-101(Al)-NH_2. For comparison purposes, the activities of MIL-101(Al)-NH_2 in these reactions were compared to those of HY zeolite (SiO_2/Al_2O_3 = 30) and MgO, which are conventional acid and base catalysts, respectively. As shown in **Fig. 3. 1. 5**, inspection of the time courses for the production of benzaldehyde in deacetalization reactions of benzaldehyde dimethylacetal shows that MIL-101(Al)-NH_2 and HY zeolite serve as efficient catalysts for this process while benzaldehyde is not generated when MgO is used. The results suggest that

carboxylic acid groups (–COOH) present on outer surfaces or at defect sites in MIL-101(Al)-NH_2 act as effective Brønsted acids. Subsequently, Knoevenagel condensation reactions of benzaldehyde with malononitrile were carried out using MIL-101(Al)-NH_2, HY zeolite and MgO. The time courses displayed in **Fig. 3. 1. 6** demonstrate that MIL-101(Al)-NH_2 is an effective catalyst of this reaction, whereas MgO has a lower activity and the reaction does not proceed when HY zeolite is employed. These findings suggest that the –NH_2 groups in MIL-101(Al)-NH_2 act as base sites to promote the Knoevenagel condensation reaction. Furthermore, it is noteworthy that the reaction rate for MIL-101(Al)-NH_2 is much higher than that for MgO. This result is attributable to the presence of –NH_2 groups in MIL-101(Al)-NH_2. It is well-known that the Knoevenagel condensation reaction undergoes through the formation of imine intermediate on the catalysts containing organic amines, followed by the addition of active methylene group.[34–37] Therefore, it can be considered that the reaction is promoted more efficiently over MIL-101(Al)-NH_2 with –NH_2 groups than over MgO. As explored above, the results emanating from the above effort show that MIL-101(Al)-NH_2 possesses both Brønsted acid and base sites that serve as catalysts for respective deacetalization and Knoevenagel condensation reactions.

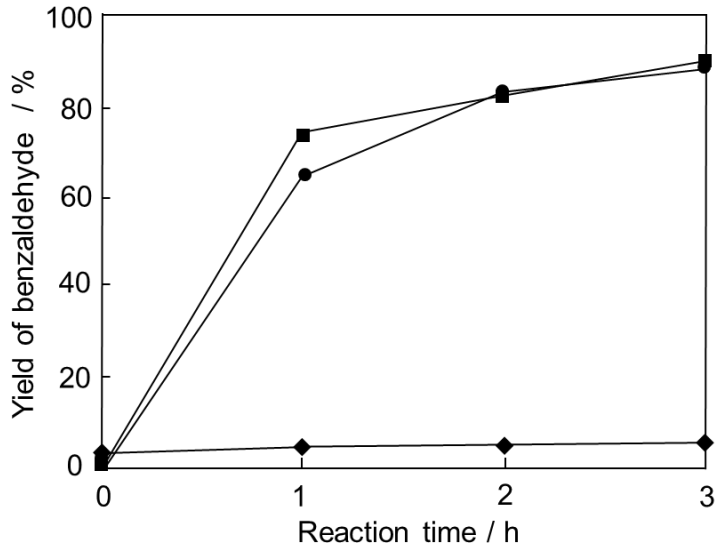

Figure 3. 1. 5. Time course of the deacetalization reaction over MIL-101(Al)-NH_2 (●), HY zeolite (■) and MgO (◆).

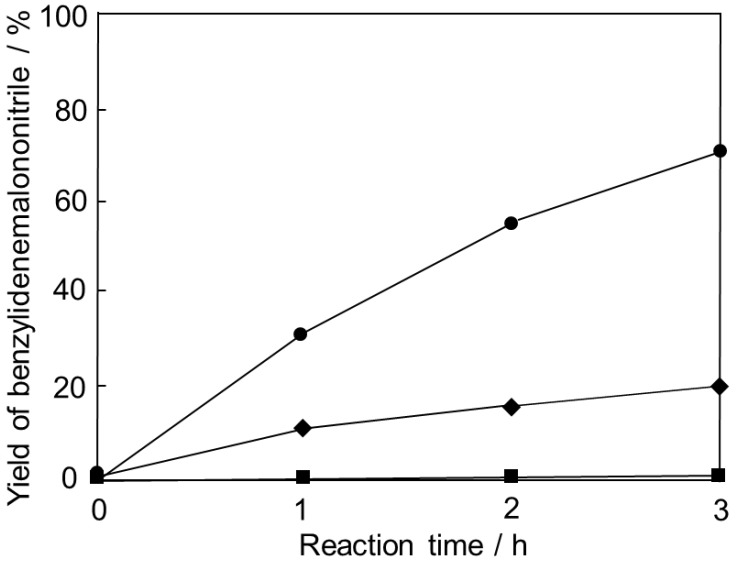

Figure 3. 1. 6. Time course of the Knoevenagel condensation reaction over MIL-101(Al)-NH_2 (●), HY zeolite (■) and MgO (◆).

The potential use of MIL-101(Al)-NH_2 as a bifunctional acid-base catalyst for one-pot reactions was investigated next. For this purpose, MIL-101(Al)-NH_2 was employed to

promote the benzylidenemalononitrile (3) forming reaction between benzaldehyde dimethylacetal and malononitrile that takes place through sequential deacetalization and Knoevenagel condensation processes. Inspection of the time course of the process displayed in **Fig. 3. 1. 7** shows that benzylidenemalononitrile is efficiently generated from benzaldehyde dimethylacetal (1) via a pathway involving initial formation of benzaldehyde (2), and that the yield of 3 reaches 94% after a 3 h reaction time. It is also shown that the reaction does not take place in the absence of a catalyst (entry 17 in **Table 3. 1. 1**). These observations clearly demonstrate that MIL-101(Al)-NH_2 serves as an effective bifunctional acid-base catalyst for the sequential deacetalization and Knoevenagel condensation reaction.

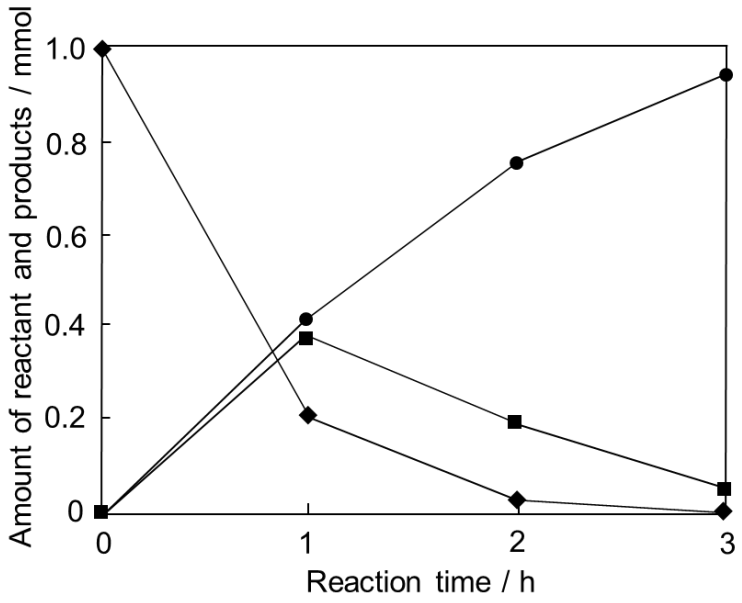

Figure 3. 1. 7. Time course of the one-pot deacetalization-Knoevenagel condensation reaction over MIL-101(Al)-NH_2; benzaldehyde dimethylacetal (◆), benzaldehyde (■), benzylidenemalononitrile (●).

For comparison purposes, conventional solid and homogeneous as well as other MOF catalysts were applied for this one-pot acid-base reaction with the results summarized in

Table 3. 1. 1. When HY zeolite is used as the catalyst (entry 2), the second step, involving Knoevenagel condensation of benzaldehyde with malononitrile, does not take place efficiently. As a result, only benzaldehyde is produced because HY zeolite only serves as an acid catalyst for the deacetalization step. In addition, when MgO is employed (entry 3), the reaction between the acetal and malononitrile does not occur because the first step in the pathway does not take place. These results clearly demonstrate that the existence of both acid and base sites, like those found in MIL-101(Al)-NH_2, are necessary for promotion of the one-pot benzylidenemalononitrile forming process. Observation made in additional studies show that Al_2O_3 does not promote this reaction, suggesting that possible impurities in MIL-101(Al)-NH_2 comprised of aluminum oxide are not responsible for the observed catalytic activity (entry 4). Also, the one-pot reaction takes place when a mixture of HY zeolite and MgO is utilized (entry 5), but the reaction rate is much lower than that of the MIL-101(Al)-NH_2 catalyzed process. These facts suggest that MIL-101(Al)-NH_2 behaves as an efficient bifunctional acid-base catalyst compared to conventional solid catalysts.

In addition, homogeneous catalysts such as HCl and triethylamine were used for the one-pot reaction. The presence of the acid catalyst (HCl) leads to quantitative deprotonation of dimethylacetal to benzaldehyde but does not lead to the formation of 3 (entry 6). On the other hand, the starting substrate remains unchanged when using triethylamine as a catalyst even after 3 h (entry 7). Furthermore, the reaction hardly occurs even the first step of the reaction when the mixture of HCl and triethylamine is employed as the catalyst (entry 8). In the homogeneous systems, acid and base catalysts are easily neutralised, resulting in the deactivation of the catalysts. Various MOF catalysts such as MIL-53(Al)-NH_2, MIL-53(Al), MIL-101(Cr)-NH_2, MIL-101(Cr), Zr-MOF-NH_2, Zr-MOF, Cu-MOF and Ca-MOF[38] were also employed for the one-pot reaction (entry 9–16).[39] Among the catalysts explored in this study, MIL-101(Al)-NH_2 was found to exhibit the highest catalytic activity for the one-pot reaction.

This result is attributable to the presence of $–NH_2$ groups and its large pore size (window size = 1.2 × 1.6Å).[30] Specifically, the $–NH_2$ groups promote the second condensation step of the reaction, and the large pore sizes enable facile diffusion of the substrates and products. Although MIL-101(Cr)-NH_2 has both $–NH_2$ groups and the same pore size as MIL-101(Al)-NH_2, its catalytic activity is lower than that of MIL-101(Al)-NH_2 (entry 11). To clarify the origin of the difference in the activity, SEM observations were conducted, as displayed in **Fig. 3. 1. 8**. The large particle size ranging from 200 nm to 400 nm is observed for MIL-101(Al)-NH_2 compared to the particle size of MIL-101(Cr)-NH_2 (50–100 nm). Since the Brønsted acidities are attributed to –COOH groups in the organic linker existing on the outer surface of the particles and in structural defects within the framework, the small particles are expected to be favorable for the reaction. On the other hand, however, these SEM images also reveal that MIL-101(Al)-NH_2 has lower crystallinity than MIL-101(Cr)-NH_2, suggesting that larger amounts of structural defects exist in MIL-101(Al)-NH_2. Therefore, the results of the one-pot reaction can be rationalized by the amount of structural defects. As a consequence, MIL-101(Al)-NH_2 exhibits better performance in the one-pot reaction. Interestingly, MOF catalysts possessing $–NH_2$ groups not only promote the Knoevenagel condensation reaction but also catalyze the first deacetalization step more efficiently than those without primary amine moieties (entry 9, 11, 13). This outcome is associated with the cooperative effect of acid and base groups that lead to acceleration of the aldehyde forming process. In addition, it should be noted that the condensation step of the reaction is catalyzed by some MOF catalysts that do not contain $–NH_2$ groups (entry 12, 14). In general, Knoevenagel condensation reactions are promoted by not only base catalysts but also Lewis acid catalysts.[40] As mentioned in the introduction, it has been widely studied that coordinatively unsaturated metal sites of MOFs can act as Lewis acid catalysts. These facts suggest that coordinatively unsaturated metal sites of MOFs catalyze the second step of the

reaction, resulting in the catalysts.

Finally, recycling experiments were carried out for the evaluation of the reusability of MIL-101(Al)-NH_2. The catalyst after the reaction for 3 h was washed with 1, 4-dioxane, dried at 313 K and then reused for the next run. As shown in **Fig. 3. 1. 9**, MIL-101(Al)-NH_2 can be reused at least three times with the retention of high catalytic activity and selectivity.

Table 3. 1. 1. One-pot deacetalization-Knoevenagel condensation reaction using various catalysts[a].

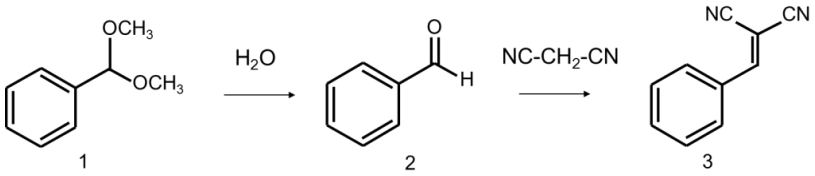

Entry	Catalyst	Conv. (%)	Yield (%)	
			2	**3**
1	MIL-101(Al)-NH_2	100	6	94
2	HY zeolite	88	79	9
3	MgO	7	6	1
4	Al_2O_3	14	1	3
5	HY zeolite + MgO[b]	67	39	20
6	HCl[c]	100	95	5
7	Triethylamine[c]	3	1	2
8	HCl + Triethylamine[d]	15	5	8
9	MIL-53(Al)-NH_2	100	81	18
10	MIL-53(Al)	14	9	5
11	MIL-101(Cr)-NH_2	86	2	84
12	MIL-101(Cr)	60	19	38
13	Zr-MOF-NH_2	99	75	23
14	Zr-MOF	85	57	26
15	Cu-MOF	79	69	7
16	Ca-MOF	38	34	2
17	No catalyst	2	0	2

[a] Reaction conditions: Benzaldehyde dimethylacetal (1 mmol), malononitrile (5 mmol), 1, 4-dioxane (4 mL), catalyst (100 mg), 363 K, 3 h. [b] The mixture of HY zeolite (50 mg) and MgO (50 mg) was employed as the catalyst. [c] 0.1 mmol of the catalyst was used. [d] The mixture of HCl (0.1 mmol) and triethylamine (0.1 mmol) was employed as the catalyst.

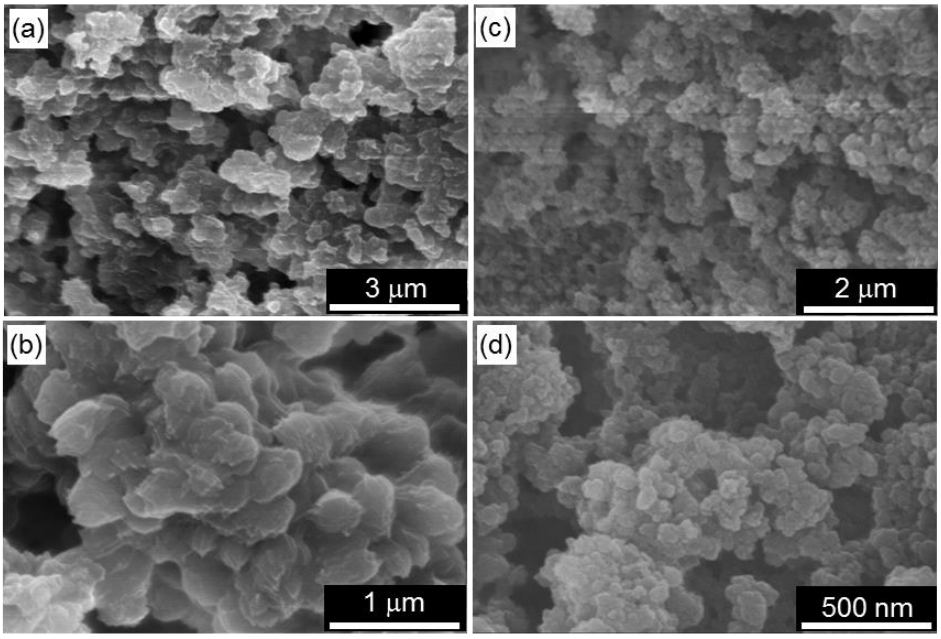

Figure 3. 1. 8. SEM images of MIL-101(Al)-NH_2 (a–b) and MIL-101(Cr)-NH_2 (c–d).

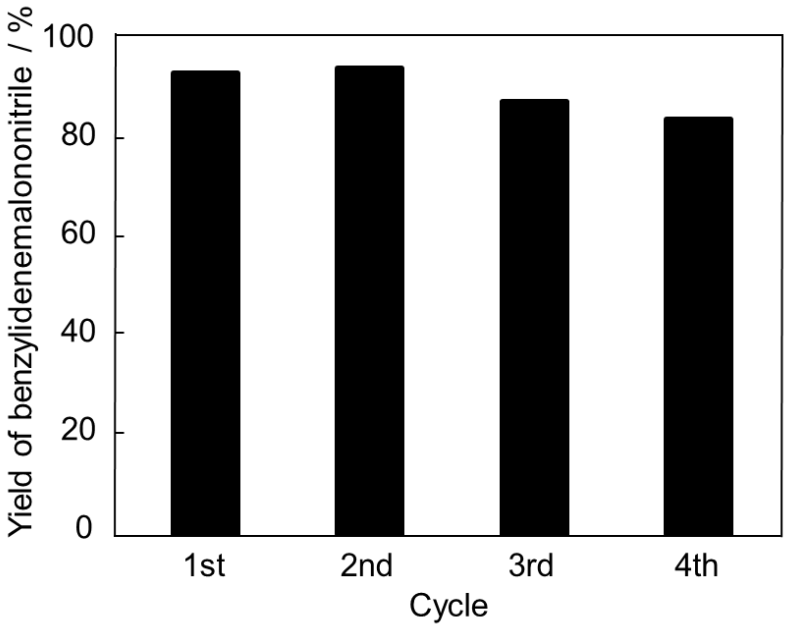

Figure 3. 1. 9. Recycling tests for the one-pot deacetalization-Knoevenagel condensation reaction over MIL-101(Al)-NH_2. Reaction conditions: Benzaldehyde dimethylacetal (1 mmol), malononitrile (5 mmol), 1, 4-dioxane (4 mL), catalyst (100 mg), 363 K, 3 h.

3. 1. 4. Conclusions

The results of the investigation described above show that the amino-functionalized MOF, MIL-101(Al)-NH_2, serves as a bifunctional acid-base catalyst. The initial studies reveal that MIL-101(Al)-NH_2 promotes both the deacetalization of benzaldehyde dimethylacetal and Knoevenagel condensation of benzaldehyde with malononitrile. Moreover, owing to the presence of Brønsted acid and base sites, MIL-101(Al)-NH_2 promotes the one-pot reaction of benzaldehyde dimethylacetal and malononitrile to produce benzylidenemalononitrile. In addition, the results show that MIL-101(Al)-NH_2 exhibits higher catalytic activities than conventional heterogeneous acid and base as well as various MOF catalysts for the one-pot acid-base reaction. Lastly, MIL-101(Al)-NH_2 can be recycled at least three times without significant loss of its catalytic activity. The observations made in this effort suggest new possibilities to design catalysts for one-pot reactions utilizing MOF materials.

3. 1. 5. References

1. J. M. Lee, Y. Na, H. Han and S. Chang, *Chem. Soc. Rev.,* 2004, **33**, 302.
2. H. C. Kolb, M. S. VanNieuwenhze and K. B. Sharpless, *Chem. Rev*., 1994, **94**, 2483.
3. J. C. Wasilke, S. J. Obrey, R. T. Baker and G. C. Bazan, *Chem. Rev*., 2005, **105**, 1001.
4. C. Gunanathan, Y. Ben-David and D. Milstein, *Science*, 2007, **317**, 790.
5. V. Cadierno, J. Francos, J. Gimeno and N. Nebra, *Chem. Commun.*, 2007, **24**, 2536.
6. T. Zweifel, J.-V. Naubron and H. Grutzmacher, *Angew. Chem., Int. Ed.*, 2009, **48**, 559.
7. K. Motokura, M. Tada and Y. Iwasawa, *J. Am. Chem. Soc.*, 2009, **131**, 7944.
8. S. Shylesh, A. Wagener, A. Seifert, S. Ernst and W. R. Tiel, *Angew. Chem., Int. Ed.*, 2010, **49**, 184.
9. A. Corma, T. Rodenas and M. J. Sabater, *Chem. Eur. J.* 2010, **16**, 254.
10. O. M. Yaghi, M. O'Keeffe, N. W. Ockwig, H. K. Chae, M. Eddaoudi and J. Kim, *Nature*, 2003, **423**, 705.
11. S. Kitagawa, R. Kitaura and S. Noro, *Angew. Chem., Int. Ed.*, 2004, **43**, 2334.
12. G. Férey, *Chem. Soc. Rev.*, 2008, **37**, 191.
13. X. Zhao, B. Xiao, A. J. Fletcher, K. Thomas, D. Bradshaw and M. J. Rosseinsky, *Science*, 2004, **306**, 1012.
14. A. Corma, H. Garcia and F. X. Liabres i Xamena, *Chem. Rev*., 2010, **110**, 4606.
15. J. Lee, O. K. Farha, J. Roberts, K. A. Scheidt, S. T. Nguyen and J. T. Hupp, *Chem. Soc. Rev*., 2009, **38**, 1450.
16. F. Song, C. Wang, J. M. Falkowski, L. Ma and W. Lin, *J. Am. Chem. Soc.*, 2010, **132**, 15390.
17. J. Song, Z. Zhang, S. Hu, T. Xu, T. Jiang and B. Han, *Green Chem*., 2009, **11**, 1031.

18. F. Vermoortele, R. Ameloot, A. Vimont, C. Serre and D. D. Vos, *Chem. Commum*., 2011, **47**, 1521.
19. J. Gascon, U. Aktay, M. D. Hernandez-Alonso, G. P. M. van Klink and F. Kapteijn, *J. Catal*., 2009, **261**, 75.
20. N. T. S. Phan, T. T. Nguyen, Q. H. Luu and L. T. L. Nguyen, *J. Mol. Catal. A: Chem.*, 2012, **362**, 178.
21. B. Li, Y. Zhang, D. Ma, L. Li, G. Li, G. Li, Z. Shi and S. Feng, *Chem. Commun*., 2012, **48**, 6151.
22. R. Srirambalaji, S. Hong , R. Natarajan, M. Yoon, R. Hota, Y. Kim, Y. H. Ko and K. Kim, *Chem. Commun*., 2012, **48**, 11650.
23. J. Park, J. R. Li, Y. P. Chen, J. Yu, A. A. Yakovenko, Z. U. Wang, L. B. Sun, P. B. Balbuena and H. C. Zhou, *Chem. Commun.*, 2012, **48**, 9995.
24. F. G. Cirujano, F. X. Llabrés i Xamena and A. Corma, *Dalton Trans*., 2012, **41**, 4249.
25. F. Vermoortele, R. Ameloot, A. Vimont, C. Serre and D. D. Vos, *Chem. Commun*., 2011, **47**, 1521.
26. (a) M. Opanasenko, A. Dhakshinamoorthy, M. Shamzhy, P. Nachtigall, M. Horáček, H. Garcia and J. Čejka, *Catal. Sci. Technol*., 2013, **3**, 500.
27. U. Ravon, M. Savonnet, S. Aguado, M. E. Domine, E. Janneau and D. Farrusseng, *Micropor. Mesopor. Mater.*, 2010, **129**, 319.
28. R. Ameloot, F. Vermoortele, J. Hofkens, F. C. D. Schryver, D. E. D. Vos and M. B. J. Roeffraers, *Angew. Chem., Int. Ed*., 2013, **52**, 401.
29. (a) R. A. Duval, R. L. Allmon and L. R. Lever, *J. Med. Chem*., 2007, **50**, 2144; (b) F. Douelle, A. S. Capes and M. F. Greaney, *Org. Lett*., 2007, **9**, 931.
30. S. Hasegawa, S. Horike, R. Matsuda, S. Furukawa, K. Mochizuki, Y. Kinoshita and S. Kitagawa, *J. Am. Chem. Soc.*, 2007, **129**, 2607.

31. P. S. Crespo, E. V. R. Fernandez, J. Gascon and F. Kapteijin, *Chem. Mater.*, 2011, **23**, 2565.
32. D. Y. Hong, Y. K. Hwang, C. Serre, G. Ferey and J. S. Chang, *Adv. Funct. Mater.*, 2009, **19**, 1537.
33. F. X. Liabres i Xamena, F. G. Cirujano and A. Corma, *Micropor. Mesopor. Mater.*, 2012, **157**, 112.
34. W. Li, J. Li, Y. Wu, N. Fuller and M. A. Markus, *J. Org. Chem.*, 2010, **75**, 1077.
35. Y. Zhang, Q. Dou, L. Dai, X. Wang and Y. Chen, *RSC Adv.*, 2012, **2**, 8979.
36. F. Bigi, M. L. R. Maggi, A. Piccinno, G. Sartori, *Green Chem.*, 2000, **2**, 101.
37. Y.-Q. Yu, Z.-L. Wang, *J. Chin. Chem. Soc.*, 2013, **60**, 288.
38. M. Hartmann and M. Fischer, *Micropor. Mesopor. Mater.*, 2012, **164**, 38.
39. Various MOF catalysts were synthesized by the recently reported methods; see ref. 30 for MIL-53(Al)-NH_2 and MIL-53(Al), Y. Lin, C. Kong and L. Chen, *RSC Adv.*, 2012, **2**, 6417 for MIL-101(Cr)-NH_2 and MIL-101(Cr), J. H. Cavka, S. Jakobsen, U. Olsbye, N. Guillou, C. Lamberti, S. Bordiga and K. P. Lillerud, *J. Am. Chem. Soc.*, 2008, **130**, 13850 for Zr-MOF-NH_2 and Zr-MOF, S. Loera-Serna, M. A. Oliver-Tolentino, M. D. Lopez-Nunez, A. Santana-Cruz, A. Guzman-Vargas, R. Cabrera-Sierra, H. I. Beltran and J. Flores, *J. Alloys Compd.*, 2012, **540**, 113 for Cu-MOF and M. Mazaj, G. Mali, M. Rangus, E. Zunkovic, V. Kaucic and N. Z. Logar, *J. Phys. Chem. C*, 2013, **117**, 7552 for Ca-MOF.
40. In this study, many attempts have been done to synthesize MIL-101(Al) without –NH_2 groups. However, all attempts failed to make MIL-101(Al) as is the case with the previous report; see ref. 30.

3. 2. Development of a novel one-pot reaction system utilizing a bifunctional metal–organic framework photocatalyst under light irradiation

3. 2. 1. Introduction

Much attention has been paid to one-pot reactions as an attractive synthetic concept for improving overall process efficiency and reducing production wastes.[1–3] Design of new catalysts with spatially isolated multiple active sites is required to progress multi-step reaction cascades. Various catalytic systems have been proposed for the realization of the one-pot reaction, but many of these employ homogeneous catalysts, which generally suffer from product contamination and limited recyclability.[4–6] Therefore, development of heterogeneous catalysts that promote one-pot reactions is currently the focus of intensive research. [7–9]

Inorganic-organic hybrid materials have also attracted considerable attentions since they not only combine the respective beneficial characteristics of inorganic and organic components, but also often exhibit unique properties that exceed what would be expected for a simple mixture of the components.[10–12] The construction of hybrid materials offers an almost infinite number of chemical and structural possibilities, namely, the structural diversity of inorganic-organic hybrid materials allows for accurate material design. Among them, metal–organic frameworks (MOFs) also called porous coordination polymers (PCPs) have been of great interest because of their attractive properties including high specific surface areas, well-ordered porous structures and structural designability.[13–15] Taking advantages of these features, MOFs have been actively studied for many applications to gas storage, gas separation, sensing and catalysis.[16–20] In addition, since the topology and surface functionality of MOFs can be readily tuned by modifying or varying the constituent metal-oxo clusters and bridging organic linkers, MOFs have emerged as an interesting platform to engineer

molecular solids for multifunctional catalysts.[21–24] Although several reaction systems have been proposed so far based on multifunctionality in organic linkers or coordinatively unsaturated metal sites of the MOF catalysts, there is no report describing multifunctionality combined with photocatalytic and catalytic activities utilizing MOF materials.

In this study, a novel one-pot reaction system is developed by utilizing photocatalytic and base properties of amino-functionalized Zr-based MOF (UiO-66-NH_2) here denoted as Zr-MOF-NH_2. Zr-MOF-NH_2 promotes sequential photocatalytic oxidation and Knoevenagel condensation reaction: the conversion of benzylalcohol into benzaldehyde through photocatalytic oxidation over Zr-oxo clusters and Knoevenagel condensation of benzaldehyde with malononitrile over –NH_2 groups, as shown in **Scheme 3. 2. 1**.

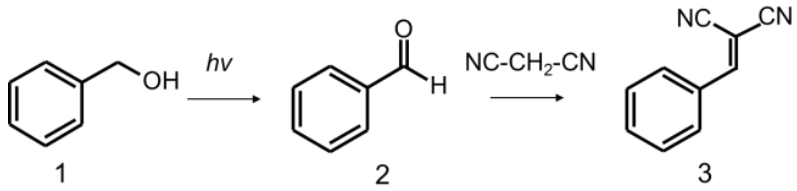

Scheme 3. 2. 1 One-pot sequential photocatalytic oxidation and Knoevenagel condensation reaction over Zr-MOF-NH_2.

3. 2. 2. Experimental

Materials

$ZrCl_4$, 2-aniline-1,4-dicarboxylic acid (H_2BDC-NH_2), 1,4-benzenedicarboxylic acid (H_2BDC), N'N-dimethylformamide (DMF) and 1,4-dioxane were purchased from Nacalai Tesque Inc. Malononitrile, benzyl alcohol, benzaldehyde and benzaldehyde dimethylacetal were purchased from Tokyo Chemical Industry Co., Ltd. p-Xylene was purchased from Kishida Chemicals Co., Ltd.

Catalysts preparation

Zr-MOF-NH_2 was synthesized according to the literature.[25] The mixture of $ZrCl_4$ (0.42 g), H_2BDC-NH_2 (0.30 g) and ion-exchanged water (50 μl) were added in DMF (40 ml) and dispersed by ultrasound for 10 min. The mixture was subject to react under solvothermal conditions in a Teflon-lined stainless steel autoclave at 393 K for 24 h under autogenous pressure. The precipitate was filtrated, washed repeatedly with acetone and dried under vacuum at 473 K for 3 h. For comparison purposes, Zr-MOF was also prepared by using H_2BDC.

General methods

Standard θ–2θ X-ray diffraction (XRD) data were recorded on a Shimadzu X-ray diffracotmeter XRD-6100 using Cu Kα radiation (λ = 1.5406 Å). N_2 adsorption isotherms were collected by using a BEL-SORP mini (BEL Japan, Inc.) after degassing of samples under vacuum at 473 K for 2 h. Diffuse reflectance UV–vis spectra were obtained with a Shimadzu UV–vis recording spectrophotometer 2200A. FT-IR spectra were recorded in transmittance mode by a FT-IR spectrophotometer equipped with a DTGS detector (JASCO FT/IR 660Plus, resolution 4 cm^{-1}). Self-supporting pellets of the samples were loaded in a specially constructed IR cell, which was equipped with CaF_2 windows.

Catalytic reactions

Photocatalytic oxidation: The catalyst (100 mg) and 4 ml of p-xylene containing benzyl alcohol (0.1 mmol) were added to a quartz reaction vessel. Subsequently, the sample was irradiated with the high pressure Hg lamp with stirring at 298 K under air. The progression of the reaction was monitored by a GC (Shimadzu GC-14B with a flame ionization detector) equipped with an InertCap®1 capillary column.

Knoevenagel condensation reaction: The catalyst (100 mg) and 4 ml of p-xylene containing benzaldehyde (0.1 mmol) and malononitrile (3 mmol) were added to a quartz reaction vessel. Subsequently, the mixture was heated to 363 K with stirring under air. The progression of the reaction was monitored by the GC.

One-pot reaction: The catalyst (100 mg) and 4 ml of p-xylene containing benzyl alcohol (0.1 mmol) and malononitrile (3 mmol) or ethyl cyanoacetate were added to a quartz reaction vessel. Subsequently, the sample was irradiated with a high pressure Hg lamp (500 W; Ushio USH-500BY) with stirring at 363 K under air. The progression of the reaction was monitored by the GC.

3. 2. 3. Results and discussion

XRD, N_2 adsorption isotherm, diffuse reflectance UV-Vis and FT-IR measurements were conducted to confirm the formation of Zr-MOF-NH_2. Zr-MOF-NH_2 exhibits a diffraction pattern consistent with the previously reported pattern of the UiO-66 type structure (**Fig. 3. 2. 1**). A specific surface area of Zr-MOF-NH_2 was determined to be 1071 m^2 g^{-1} by using BET (Brunauer-Emmett-Teller) method based calculation on its N_2 adsorption isotherm (**Fig. 3. 2. 2**). This value is similar to that of Zr-MOF which has also the same UiO-66 type structure (1141 m^2 g^{-1}). Diffuse reflectance UV-Vis spectrum also indicates the successful formation of Zr-MOF-NH_2 (**Fig. 3. 2. 3**). In addition, the FT-IR spectrum of Zr-MOF-NH_2 shows bands at 3388 and 3512 cm^{-1} corresponding to the symmetric and asymmetric stretching of primary amines (**Fig. 3. 2. 4**), suggesting that the –NH_2 groups are free without coordination. These results clearly indicate the successful formation of Zr-MOF-NH_2.

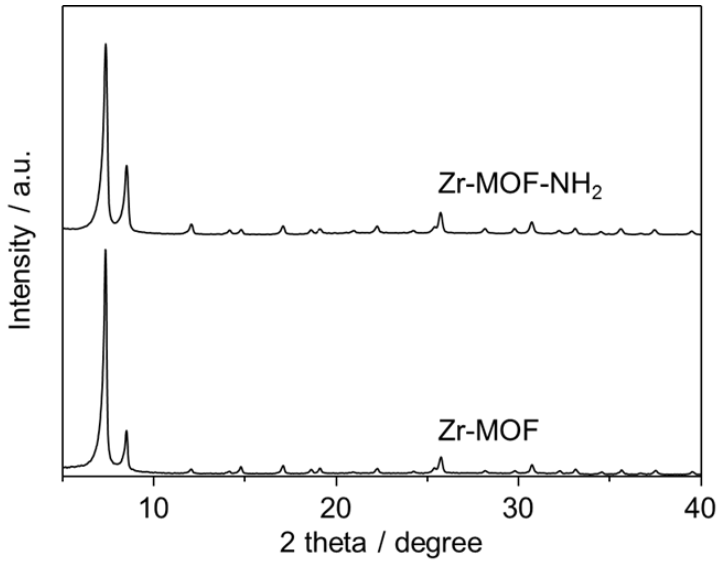

Figure 3. 2. 1. XRD patterns of Zr-MOF and Zr-MOF-NH_2.

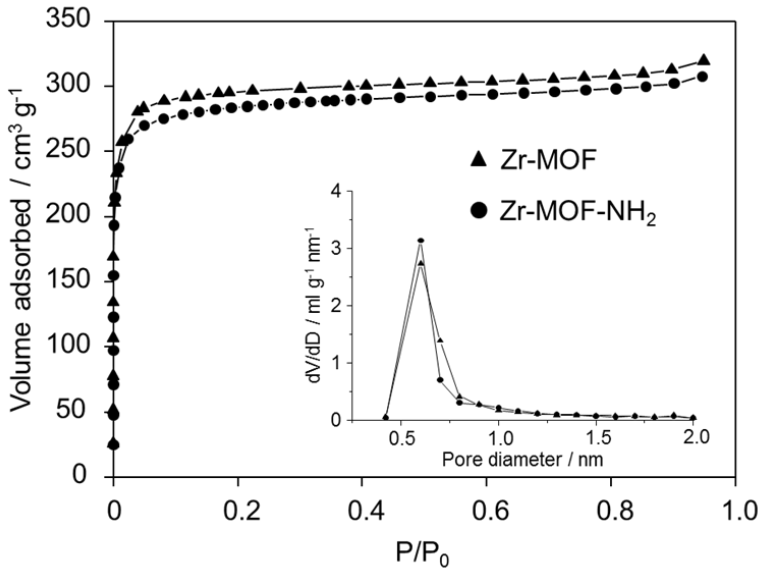

Figure 3. 2. 2. N_2 adsorption isotherms and pore size distribution curves (inset) of Zr-MOF and Zr-MOF-NH_2.

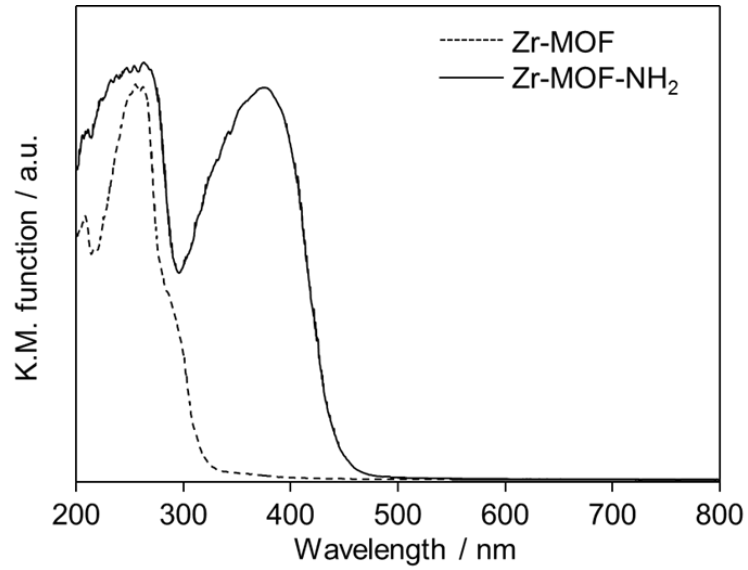

Figure 3. 2. 3. Diffuse reflectance UV-Vis spectra of Zr-MOF and Zr-MOF-NH_2.

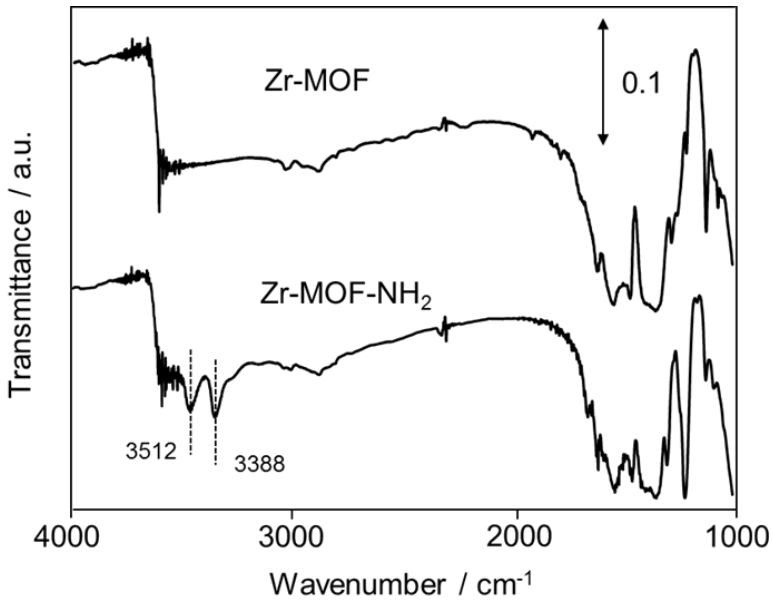

Figure 3. 2. 4. FT-IR spectra of Zr-MOF and Zr-MOF-NH_2.

In an investigation exploring the potential catalytic activity of Zr-MOF-NH_2, photocatalytic oxidation of benzyl alcohol was performed under UV-light irradiation (**Fig. 3. 2. 5**). For comparison of the Zr-MOF-NH_2 catalyst, the reactions were also performed over Zr-MOF without –NH_2 groups and Al-MOF-NH_2 (MIL-53(Al)-NH_2)[27] which does not have

photocatalytic activity. As shown in **Fig. 3. 2. 5**, Zr-MOF-NH_2 and Zr-MOF catalyze the reaction to produce benzaldehyde as the product whereas benzaldehyde is not generated over Al-MOF-NH_2. This result suggests that Zr-oxo clusters within Zr-MOF-NH_2 and Zr-MOF behave as a photocatalyst under UV-light irradiation. Subsequently, the Knoevenagel condensation reaction of benzaldehyde with malononitrile was carried out at 363 K over Zr-MOF-NH_2, Zr-MOF and Al-MOF-NH_2, as shown in **Fig. 3. 2. 6**. The reaction efficiently proceeds over Zr-MOF-NH_2 and Al-MOF-NH_2. It is well-known that the Knoevenagel condensation reaction proceeds through the formation of imine intermediate on the catalysts containing organic amines, followed by the addition of active methylene group. [28] Therefore, the reaction is promoted more efficiently over the catalysts with $–NH_2$ groups than over the catalysts without $–NH_2$ groups. It should be noted that Al-MOF-NH_2 exhibits higher catalytic activity for the reaction than Zr-MOF-NH_2, although both MOFs have $–NH_2$ groups within their structures. This result can be attributed to the large pore size of Al-MOF-NH_2 (0.85 nm)[29] compared to that of Zr-MOF-NH_2 (0.6 nm).[25–26] The large pore size enables facile diffusion of the substrates and products, resulting in the higher catalytic activity. Furthermore, the total basicities of Zr-MOF-NH_2 and Al-MOF-NH_2 were also determined to be 1.25 and 1.58 mmol g^{-1}, respectively by using an acid-base titration method. This basicity difference also accounts for the difference in the activity between Zr-MOF-NH_2 and Al-MOF-NH_2. In addition, interestingly, the reaction is also catalyzed by Zr-MOF that does not contain $–NH_2$ groups. In general, Knoevenagel condensation reactions are promoted by not only base catalysts but also Lewis acid catalysts.[30] It has been widely studied that coordinatively unsaturated metal sites of MOFs can act as Lewis acid catalysts. These facts suggest that coordinatively unsaturated metal sites of MOFs catalyze the Knoevenagel condensation reaction, generating benzylidenemalononitrile as the product. The results emanating from the above effort show that Zr-MOF-NH_2 possesses both photocatalytic activity and basicity that

serve as catalysts for respective photocatalytic oxidation and Knoevenagel condensation reactions.

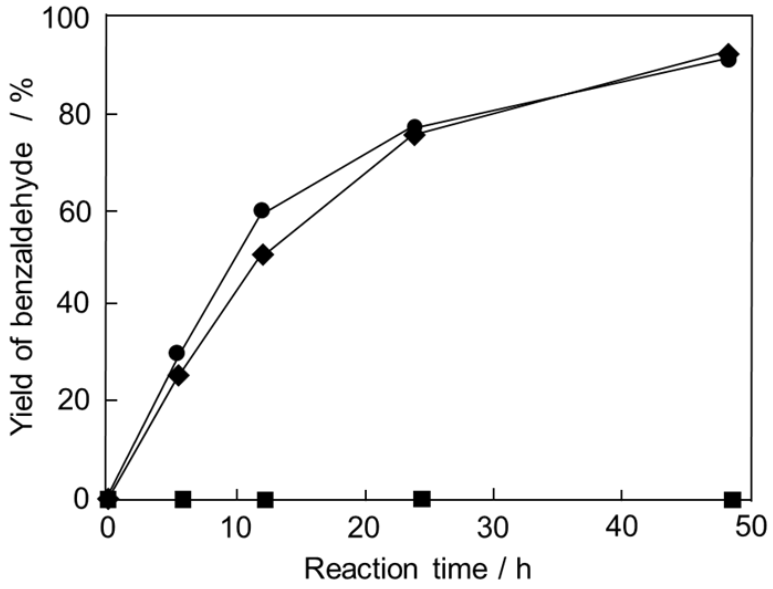

Figure 3. 2. 5. Time course of the photocatalytic oxidation of benzyl alcohol over Zr-MOF-NH_2 (●), Zr-MOF (◆) and Al-MOF-NH_2 (■) under UV-light irradiation at room temperature.

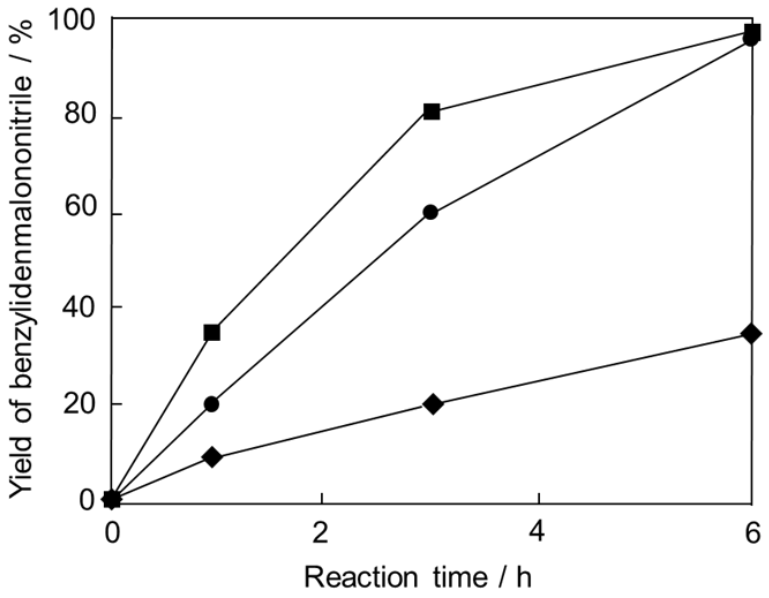

Figure 3. 2. 6. Time course of Knoevenagel condensation of benzaldehyde with malononitrile over Zr-MOF-NH_2 (●), Zr-MOF (◆) and Al-MOF-NH_2 (■) at 363 K.

The potential use of Zr-MOF-NH_2 as a bifunctional catalyst for the one-pot reaction was investigated next. For this purpose, Zr-MOF-NH_2 was employed to promote one-pot synthesis of benzylidenemalononitrile (**3**) from benzyl alcohol and malononitrile that takes place through sequential photocatalytic oxidation and Knoevenagel condensation reactions under UV-light irradiation at 363 K. Inspection of the time course of the process displayed in **Fig. 3. 2. 7** shows that benzylidenemalononitrile is efficiently generated from benzyl alcohol (**1**) via a pathway involving initial formation of benzaldehyde (**2**), and that the yield of **3** reaches 91% after a 48 h reaction time. It is also shown that the reaction does not take place in the absence of a catalyst (entry 11 in **Table 3. 2. 1**). These observations clearly demonstrate that Zr-MOF-NH_2 serves as an effective bifunctional catalyst for this one-pot reaction. However, excess amount of malononitrile (3 mmol) is used for the one-pot reaction compared with benzyl alcohol (0.1 mmol). Curiously, UV-light irradiation decreases the reaction rate of the second step of the reaction (Knoevenagel condensation), as shown in **Fig. 3. 2. 8**.

Therefore, the excess amount of malononitrile is required for the efficient progression of the reaction. A detailed study about the reason why UV-light irradiation decreases the reaction rate is now underway.[31]

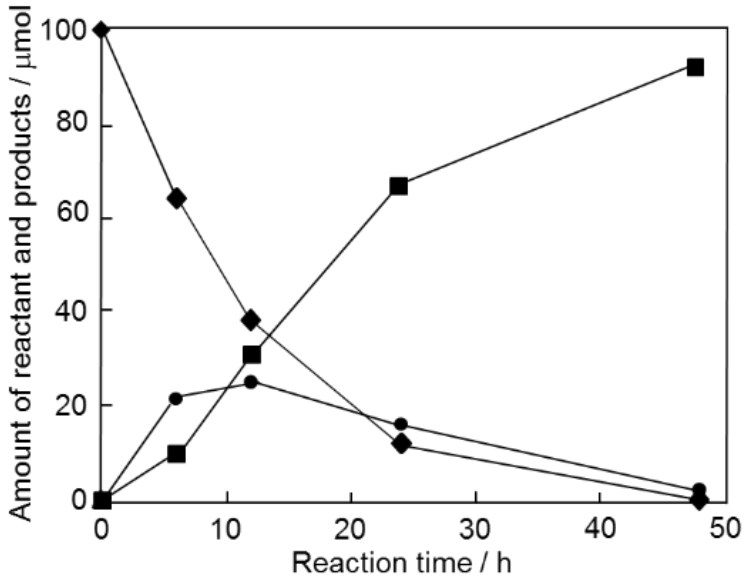

Figure 3. 2. 7. Time course of the one-pot sequential photocatalytic oxidation and Knoevenagel condensation reaction over Zr-MOF-NH_2 under UV-light irradiation at 363 K: benzyl alcohol (◆), benzaldehyde ●), benzylidenemalononitrile (■).

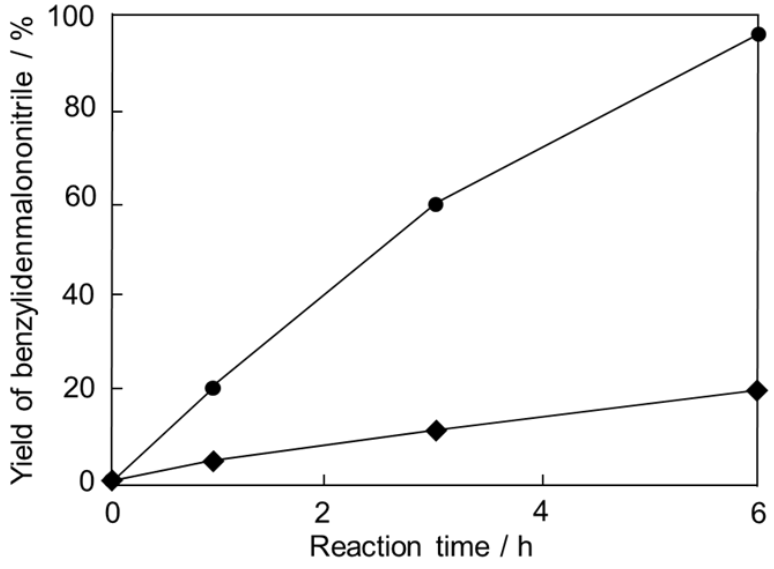

Figure 3. 2. 8. Time course of Knoevenagel condensation of benzaldehyde with malononitrile over Zr-MOF-NH_2 under UV-light irradiation (◆) and without UV-light irradiation (●) at 363 K.

The stability of Zr-MOF-NH_2 was investigated by XRD measurements before and after the reaction, as shown in **Fig. 3. 2. 9**. The diffraction peaks corresponding to the UiO-66 structure is maintained even after the reaction, indicating that Zr-MOF-NH_2 possesses high durability toward the one-pot reaction cascades. Moreover, the reusability test was carried out after the first run. Although the reaction rate is decreased, 89% yield of the final product is achieved after the reaction of 72 h. This result suggests that the catalyst can be reused as a heterogeneous catalyst with slight decrease in the activity.

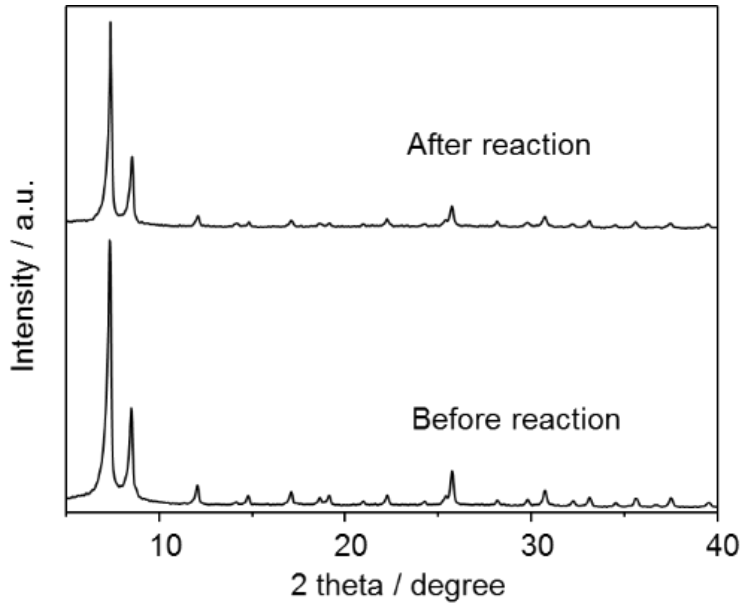

Figure 3. 2. 9. XRD patterns of Zr-MOF-NH_2 before and after the one-pot reaction.

For comparison purposes, some control reactions and the one-pot reactions catalyzed by conventional solid and other MOF catalysts were performed (**Table 3. 2. 1**). When the reaction is performed under UV-light irradiation at 298 K (entry 2), the second step (Knoevenagel condensation of benzaldehyde with malononitrile) does not proceed efficiently whereas the first step of the reaction (photocatalytic oxidation of benzyl alcohol) proceeds to produce benzaldehyde. It was also found that the reaction between benzyl alcohol and

malononitrile does not occur without UV-light irradiation (entry 3), because the first step in the pathway does not take place. From these results, the UV-light irradiation and heating up to 363 K were confirmed to be required to progress the one-pot reaction sequences. In addition, when Zr-MOF or ZrO_2 is employed (entry 4, 5), the second step does not take place efficiently. It is noteworthy that Zr-MOF-NH_2 exhibits higher activity than the mixture of Zr-MOF and amino-functionalized MCM-41 (MCM-41-NH_2)[32–33] or the mixture of ZrO_2 and MCM-41-NH_2, suggesting that the combination of Zr-oxo cluster and BDC-NH_2 unit existing close to each other would be favourable for the one-pot reaction. On the other hand, the reaction hardly occurs over Al-MOF-NH_2 that does not exhibit photocatalytic activity. These results clearly demonstrate that the existence of both photocatalytic activities and basicities, like those found in Zr-MOF-NH_2, are necessary for the promotion of the one-pot benzylidenemalononitrile forming process. Moreover, Zn-MOF-NH_2 (IRMOF-3) and Ti-MOF-NH_2 (MIL-125(Ti)-NH_2) were also prepared and employed for the reaction (entry 9, 10).[34] Since both Zn-MOF-NH_2 and Ti-MOF-NH_2 possess –NH_2 groups and are known to show photocatalytic activities under light irradiation,[35–36] it is expected that the one-pot reaction also proceeds efficiently as well as over Zr-MOF-NH_2. However, their catalytic activities are lower than that of Zr-MOF-NH_2. These facts are rationalized by the stability of the MOF catalysts under the reaction conditions. XRD measurements revealed that the structures of Zn-MOF-NH_2 and Ti-MOF-NH_2 are collapsed during the reaction, whereas the structure of Zr-MOF-NH_2 is maintained under the same conditions. Therefore, Zr-MOF-NH_2 exhibits the higher activity toward one-pot sequential photocatalytic oxidation and Knoevenagel condensation reaction.

Table 3. 2. 1. One-pot sequential photocatalytic oxidation and Knoevenagel condensation reaction using various catalysts.[a]

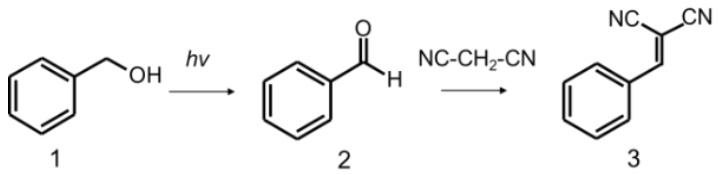

Entry	Catalyst	Conv. (%)	Yield (%)	
			2	3
1	Zr-MOF-NH_2	100	2	91
2[b]	Zr-MOF-NH_2	100	89	1
3[c]	Zr-MOF-NH_2	0	0	0
4	Zr-MOF	96	62	28
5	ZrO_2	100	75	2
6	Zr-MOF + MCM-41-NH_2[d]	71	6	61
7	ZrO_2 + MCM-41-NH_2[e]	77	2	59
8	Al-MOF-NH_2	0	0	0
9	Zn-MOF-NH_2	37	28	7
10	Ti-MOF-NH_2	100	51	32
11	No catalyst	0	0	0

[a] Reaction conditions: Benzyl alcohol (0.1 mmol), malononitrile (3 mmol), p-xylene (4 mL), catalyst (100 mg), 363 K, UV-light irradiation, 48 h. [b] The reaction was performed at 298 K. [c] The reaction was performed without UV-light irradiation. [d] The mixture of Zr-MOF (50 mg) and MCM-41-NH_2 (50 mg) was employed as the catalyst. [e] The mixture of ZrO_2 (50 mg) and MCM-41-NH_2 (50 mg) was employed as the catalyst.

Finally, The Zr-MOF-NH_2 catalyst was applied to another one-pot reaction of benzyl alcohol and ethyl cyanoacetate to produce ethyl α-cyanocinnamate in order to investigate the substrate applicability. The reaction was carried out under the same condition as the one-pot benzylidenemalononitrile forming process except that ethyl cyanoacetate was used in place of malononitrile. Ethyl α-cyanocinnamate as the final product is generated via benzaldehyde as the intermediate product over Zr-MOF-NH_2, and the yield reaches 89% after the reaction time of 96 h. This fact suggests that the developed system can be applied to various one-pot forming processes.

3. 2. 4. Conclusions

In summary, a bifunctional metal–organic framework photocatalyst consisting of Zr-oxo cluster and 2-aniline-1,4-dicarboxylic acid as an organic linker has been synthesized using a solvothermal method (Zr-MOF-NH_2). First, photocatalytic oxidation of benzyl alcohol and Knoevenagel condensation of benzaldehyde with malononitrile were explored as test reactions for the evaluation of photocatalytic and base properties of Zr-MOF-NH_2, respectively. Zr-MOF-NH_2 was found to catalyze the both reactions, indicating that Zr-MOF-NH_2 possesses both photocatalytic-active and base sites. Subsequently, Zr-MOF-NH_2 was applied to the one-pot reaction to produce benzylidenemalononitrile through photocatalytic oxidation and Knoevenagel condensation under UV-light irradiation. Benzylidenemalononitrile as the final product was efficiently generated via benzaldehyde as the intermediate product over Zr-MOF-NH_2. In this process, the Zr-oxo cluster catalyzes the first step of the reaction (photocatalytic oxidation of benzyl alcohol), and subsequently the $–NH_2$ group catalyzes second step (Knoevenagel condensation of benzaldehyde with malononitrile), resulting in the progression of the one-pot reaction. This is the first example of

one-pot reaction systems utilizing photocatalytic and base properties of MOF materials. The observations made in this investigation should offer new insight into the design and manipulation of specifically functioning MOF catalysts.

3. 2. 5. References

1. J. M. Lee, Y. Na, H. Han and S. Chang, *Chem. Soc. Rev.,* 2004, **33**, 302.
2. J. C. Wasilke, S. J. Obrey, R. T. Baker and G. C. Bazan, *Chem. Rev*., 2005, **105**, 1001.
3. H. C. Kolb, M. S. VanNieuwenhze and K. B. Sharpless, *Chem. Rev*., 1994, **94**, 2483.
4. C. Gunanathan, Y. Ben-David and D. Milstein, *Science,* 2007, **317**, 790.
5. V. Cadierno, J. Francos, J. Gimeno and N. Nebra, *Chem. Commun.*, 2007, 2536.
6. T. Zweifel, J.-V. Naubron and H. Grutzmacher, *Angew. Chem., Int. Ed*., 2009, **48**, 559.
7. M. Sasidharan, S. Fujita, M. Ohashi, Y. Goto, K. Nakashima and S. Inagaki, *Chem. Commun.,* 2011, **47**, 10422.
8. A. Corma, T. Rodenas and M. J. Sabater, *J. Catal.,* 2011, **279**, 319.
9. Y. Shiraishi, K. Fujiwara, Y. Sugano, S. Ichikawa and T. Hirai, *ACS catalysis,* 2013, **3**, 312.
10. C. Sanchez, P. Belleville, M. Popall and L. Nicole, *Chem. Soc. Rev.,* 2011, **40**, 696.
11. K. Ariga, A. Vinu, Y. Yamauchi, Q. Ji and J. P. Hill, *Bull. Chem. Soc. Jpn*., 2012, **85**, 1.
12. N. Mizoshita, T. Tani and S. Inagaki, *Chem. Soc. Rev*., 2011, **40**, 789.
13. S. Kitagawa, R. Kitaura and S. Noro, *Angew. Chem*., 2004, **116**, 2388.
14. G. Férey, *Chem. Soc. Rev.*, 2008, **37**, 191.
15. M. O'Keeffe and O. M. Yaghi, *Chem. Rev*., 2012, **112**, 675.
16. Y.-S. Bae and R. Q. Snurr, *Angew. Chem.,* 2011, **123**, 11790; *Angew. Chem. Int. Ed*., 2011, **50**, 11586.
17. M. P. Suh, H. J. Park, T. K. Prasad and D.-W. Lim, *Chem. Rev.,* 2012, **112**, 782
18. J. Li, J. Sculley and H. Zhou, *Chem. Rev*., 2012, **112**, 869
19. M. Yoon, R. Srirambalaji and K. Kim, *Chem. Rev*., 2012, **112**, 1196.

20. A. Corma, H. Garcia and F. X. Llabrés i Xamena, *Chem. Rev.,* 2010, **110**, 4606.
21. B. Li, Y. Zhang, D. Ma, L. Li, G. Li, G. Li, Z. Shi and S. Feng, *Chem. Commun*., 2012, **48**, 6151.
22. R. Srirambalaji, S. Hong, R. Natarajan, M. Yoon, R. Hota, Y. Kim, Y. H. Ko and K. Kim, *Chem. Commun*., 2012, **48**, 11650.
23. J. Park, J. R. Li, Y. P. Chen, J. Yu, A. A. Yakovenko, Z. U. Wang, L. B. Sun, P. B. Balbuena and H. C. Zhou, *Chem. Commun.,* 2012, **48**, 9995.
24. F. G. Cirujano, F. X. Llabrés i Xamena and A. Corma, *Dalton Trans*., 2012, **41**, 4249.
25. J. H. Cavka, S. Jakobsen, U. Olsbye, N. Guillou, C. Lamberti, S. Bordiga and K. P. Lillerud, *J. Am. Chem. Soc*., 2008, **130**, 13850.
26. A. Schaatte, P. Roy, A. Godt, J. Lippke, F. Waltz, M. Wiebcke and P. Behrens, *Chem. Eur. J*., 2011, **17**, 6643.
27. P. S. Crespo, E. V. R. Fernandez, J. Gascon and F. Kapteijin, *Chem. Mater.,* 2011, **23**, 2565.
28. M. Hartmann and M. Fischer, *Micropor. Mesopor. Mater*., 2012, **164**, 38.
29. S. Bourrelly, P. L. Llewellyn, C. Serre, F. Millange, T. Loiseau and G. Férey, *J. Am. Chem. Soc.*, 2005, **127**, 13519.
30. M. J. Climent, A. Corma, S. Iborra and A. Velty, *J. Mol. Catal. A: Chem.,* 2002, **327**, 182.
31. It was at least confirmed that malononitrile is not decomposed by the UV-light irradiation.
32. MCM-41-NH_2 was prepared by post-synthesis grafting of 3-aminopropyltimethoxysilane onto MCM-41 according to the literature; see T. Yokoi, H. Yoshitake and T. Tatsumi, *J. Mater. Chem.,* 2004, **14**, 951.
33. The total basicity of MCM-41-NH_2 was determined to be 1.89 mmol g^{-1} by acid-base titration.

34. Zn-MOF-NH_2 (IRMOF-3) and Ti-MOF-NH_2 (MIL-125(Ti)-NH_2) were synthesized by the recently reported methods; see H. Yim, E. Kang and J. Kim, *Bull. Korean Chem. Soc.,* 2010, **31**, 1041 for Zn-MOF-NH_2, Y. Horiuchi, T. Toyao, M. Saito, K. Mochizuki, M. Iwata, H. Higashimura, M. Anpo and M. Matsuoka, *J. Phys. Chem. C,* 2012, **116**, 20848 and T. Toyao, M. Saito, Y. Horiuchi, K. Mochizuki, M. Iwata, H. Higashimura and M. Matsuoka, *Catal. Sci. Technol*., 2013, **3**, 2092 for Ti-MOF-NH_2.
35. M. Alvaro, E. Carbonell, B. Ferrer, F. X. Llabrés i Xamena and H. Garcia, *Chem. Eur. J.,* 2007, **13**, 5106.
36. M. Dan-Hardi, C. Serre, T. Frot, L. Rozes, G.Maurin, C. Sanchezand and G. Férey, *J. Am. Chem. Soc.,* 2009, **131**, 10857.

3. 3. Zeolitic imidazolate frameworks as heterogeneous catalysts for a one-pot P–C bond formation reaction via Knoevenagel condensation and Phospha-Michael addition

3. 3. 1. Introduction

Over the last several decades, great attention has been paid to green chemistry in order to attain sustainable development in the world. The green chemistry is a concept to produce chemical products with consideration for inherently environmentally and ecologically benign. Most fine chemicals are synthesized through multi-step reactions industrially; therefore, inevitable purification steps produce a large amount of chemical wastes. Moreover, the loss of products during each purification step often reduces the overall efficiency of the synthetic process, dramatically. In this line, one-pot chemical synthesis processes have been recognized as a promising approach to reduce purification steps and improve overall efficiency.[1–3] However, the difficulties in the design of well-controlled isolated catalytic centers which are able to catalyze each reaction step efficiently limit a wide range of general application of one-pot chemical processes.

Metal–organic frameworks (MOFs) are organic–inorganic hybrid porous materials consisting of metal nodes and bridging organic linkers.[4–6] They possess well-defined framework structures and high surface areas derive from ordered pores. Furthermore, the appropriate choice of metal nodes and bridging organic linkers allows for accurate material design.[7–9] These unique features make MOFs a special class of catalyst materials and stimulate research to develop highly functional catalysts.

The present study deals with the potential catalytic performance of zeolitic imidazolate frameworks (ZIFs), which are one of the MOF materials,[10–13] for a one-pot reaction to synthesise organophosphorus compounds. Organophosphorus compounds have

widely been used in the areas of industrial, agricultural and medicinal chemistry because such compounds containing P–C bonds often show attractive biological reactivities.[14–16] Among available methods for the P–C bond formation, phospha-Michel reaction is the most powerful way and holds fundamental position.[17–19] Recently, Hosseini-Sarvari et al. have reported that ZnO nano-rods catalyze a one-pot Knoevenagel condensation and phospha-Michael addition reaction, in which Lewis acid and base sites in ZnO nano-rods are considered to play a significant role in promoting the two step reaction.[20] ZIFs are made up of Zn^{2+} cations as a node and imidazole derivatives as a linker; therefore, it is anticipated to realize a bifunctional effect derive from two isolated active sites, i.e., unsaturated Zn^{2+} cations as Lewis acid sites and unsaturated N atoms in imidazole derivatives as base sites. With these points in mind, ZIF materials have been prepared and applied to a one-pot Knoevenagel condensation and phospha-Michael addition reaction to produce an organophosphorus compound from benzaldehyde, malononitrile and diethyl phosphite (**Scheme 3. 3. 1**). In addition, the substrate scope of the ZIF-catalyzed one-pot three component reaction and recyclability of the ZIF catalyst have been investigated.

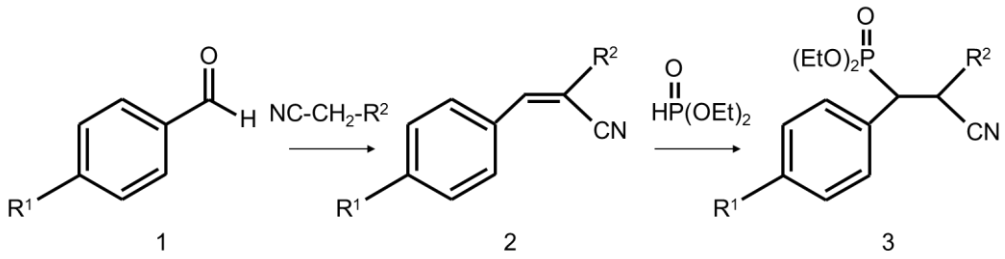

Scheme 3. 3. 1. One-pot sequential Knoevenagel condensation and phospha-Michael addition reaction over Zr-MOF-NH_2.

3. 3. 2. Experimental

Materials

2-Methylimidazole, benzylidenmalononitrile and SiO_2 were purchased from Aldrich Chemical Co. Benzimidazole and $Zn(NO_3)_2 \cdot 4H_2O$ were purchased from Merck. 2-Anilinedicarboxylic acid ($H_2BDC\text{-}NH_2$), methanol, 1, 4-dioxane and aniline were purchased from Nacalai Tesque Inc. Malononitrile, benzaldehyde, diethyl phosphite and 1,2-diphenylethane were purchased from Tokyo Chemical Industry Co., Ltd. ZnO and MgO were purchased from Kishida Chemical Co., Ltd. Al_2O_3 was purchased from Evonik. All materials were used as received without purification.

Catalysts preparation

ZIF-8 was synthesized using the previously-reported method.[1] The mixture of 2-methylimidazole (1.32 g), $Zn(NO_3)_2 \cdot 4H_2O$ (0.60 g) and methanol (44 ml) was vigorously stirred for 24 h at room temperature. The generated precipitate was collected by centrifugation, washed repeatedly with methanol and dried for 12 h at 333 K.

General methods

Standard θ–2θ X-ray diffraction (XRD) data were recorded on a Shimadzu X-ray diffractometer XRD-6100 using Cu Kα radiation (λ = 1.5406 Å). N_2 adsorption isotherms were collected by using a BEL-SORP mini (BEL Japan, Inc.) after degassing of samples under vacuum at 473 K for 2 h. FT-IR spectra were recorded in transmittance mode by a FT-IR spectrophotometer equipped with a DTGS detector (JASCO FT/IR 660Plus, resolution 4 cm^{-1}). Self-supporting pellets of the samples were loaded in a specially constructed IR cell, which was equipped with CaF_2 windows.

Catalytic reactions

Knoevenagel condensation reaction: The reactions were carried out in liquid phase in a 35 ml glass reactor. A solution of benzaldehyde (1 mmol), malononitrile (3 mmol) and 1, 4 dioxane (4 ml) was stirred at 323 K with 50 mg of the catalysts in powder form. The progression of the reaction was monitored by using gas chromatography (Shimadzu GC-14B with a flame ionization detector) equipped with an InertCap ®1 capillary column and ^{1}H-NMR spectroscopy (JEOL ECX-400 spectrometer operating at 400 MHz) with 1, 2-Diphenylethane as an internal standard.

Phospha-Michael addition reaction: The reactions were carried out in liquid phase in a 35 ml glass reactor. A solution of benzylidenmalononitrile (1 mmol), diethyl phosphite (3 mmol) and 1, 4-dioxane (4 ml) was stirred at 323 K with 50 mg of the catalysts in powder form. The progression of the reaction was monitored by using gas chromatography and ^{1}H-NMR spectroscopy (see above).

One-pot Knoevenagel condensation and phospha-Michael addition reaction: The reactions were carried out in liquid phase in a 35 ml glass reactor. A solution of benzaldehyde (1 mmol), malononitrile (3 mmol), diethyl phosphite (3 mmol) and 1, 4 dioxane (4 ml) was stirred at 323 K with 50 mg of the catalysts in powder form. The progression of the reaction was monitored by using gas chromatography and ^{1}H-NMR spectroscopy (see above).

Reusability of the catalyst was studied as follows. After the first run, the catalyst was washed three times with methanol, dried at 333 K in air and reused for the next run. The above procedure was repeated three times.

3. 3. 3. Results and discussion

A ZIF material named ZIF-8 that consists of 2-methylimidazole anions and Zn^{2+}

cations was synthesized using the previously-reported method.[22] The XRD pattern of the synthesized ZIF-8 matched well with the previously-reported one, indicating the successful formation of the ZIF-8 material (**Fig. 3. 3. 1**). Moreover, as shown in **Fig. 3. 3. 2**, the N_2 adsorption-desorption isotherm of ZIF-8 traced the typical type I isotherm with a steep increase in the amount of adsorbed N_2 at very low pressures ($P/P_0 < 0.01$). This finding suggests that ZIF-8 possesses a microporous structure. The BET area of ZIF-8 was determined to be 1716 $m^2\ g^{-1}$ by using a BET-method-based calculation on N_2 adsorption isotherm data. This high BET area is associated with the micropores.

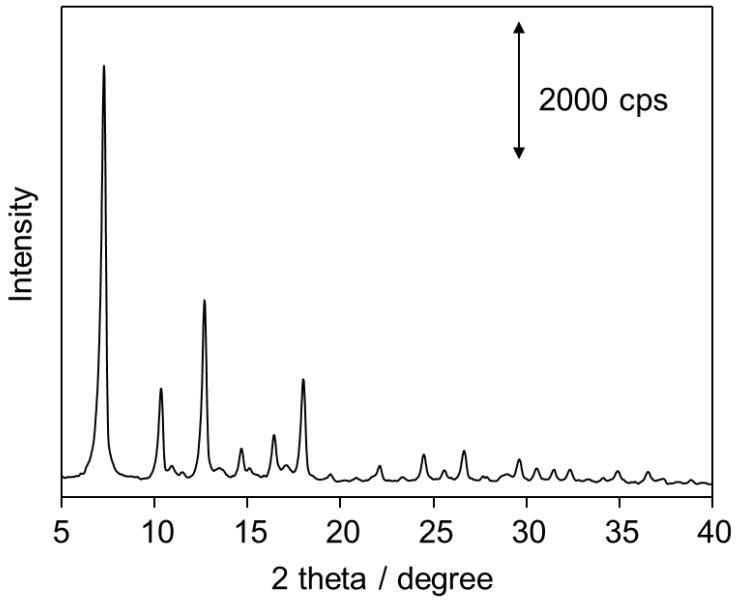

Figure 3. 3. 1. XRD patterns of ZIF-8.

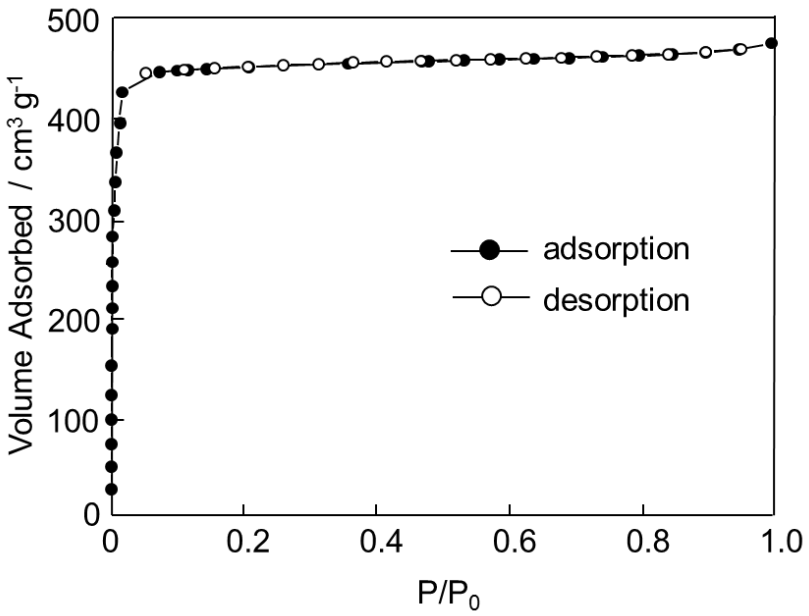

Figure 3. 3. 2. N_2 adsorption isotherms of ZIF-8.

The synthesized ZIF-8 was applied not to the one-pot reaction but to respective catalytic reactions, Knoevenagel condensation and phospha-Michael addition, individually to evaluate its catalytic activities. **Figure 3. 3. 3a** shows the results of Knoevenagel condensation of benzaldehyde with malononitrile over ZIF-8. The reaction efficiently proceeded over ZIF-8 to give benzylidenemalononitrile with complete selectivity. Moreover, it was found from the inspection of the time course for phospha-Michael addition shown in **Fig. 3. 3. 3b** that ZIF-8 also catalyzes the reaction producing the corresponding diethyl (1-phenyl-2,2-dicyanoethyl)phosphonate from benzylidenemalononitrile and diethyl phosphite with high selectivity. These findings indicate that ZIF-8 holds the potential of catalysts for the one-pot reaction to produce organophosphorus compounds via two-step Knoevenagel condensation and phospha-Michael addition.

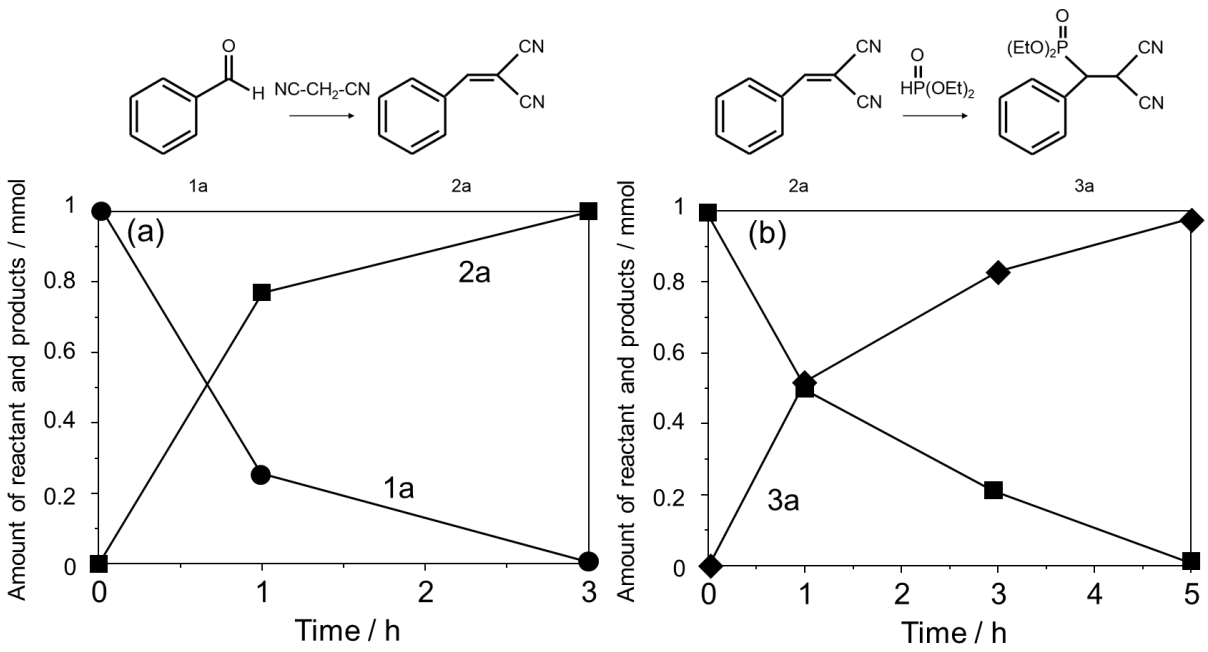

Figure 3. 3. 3. The results of (a) Knoevenagel condensation and (b) phospha-Michael addition using ZIF-8 as a catalyst. Reaction conditions: (a) Catalyst (50 mg), benzaldehyde (1 mmol), malononitrile (3 mmol), 1,4-dioxane (4 mL), 323 K, in air; (b) Catalyst (50 mg), benzylidenemalononitrile (1 mmol), diethyl phosphite (3 mmol), 1,4-dioxane (4 mL), 323 K, in air.

Next, ZIF-8 was applied to one-pot sequential Knoevenagel condensation and phospha-Michael addition. The reaction was carried out at 323 K in the presence of benzaldehyde, malononitrile and diethyl phosphite as reactants and 1,4-dioxane as solvent. As shown in **Fig. 3. 3. 4**, the benzaldehyde (1a) was consumed on ZIF-8, and diethyl (1-phenyl-2,2-dicyanoethyl)phosphonate (3a) was efficiently produced via the formation of intermediate benzylidenemalononitrile (2a). The yield of 3a reached 98% after a 5 h period. Considering that this one-pot reaction does not take place in the absence of catalysts (**Table 3. 3. 1**, entry 11), it was found that ZIF-8 behaves as an effective catalyst to promote the one-pot Knoevenagel condensation and phospha-Michael addition reaction. The catalytic activity of ZIF-8 was then compared to those of conventional solid acid or base catalysts as well as MCM-41-NH_2, which is prepared by a postsynthetic modification of MCM-41 using

3-aminopropyltrimethoxysilane[23] and contains aminopropyl groups that have already been reported to promote the phospha-Michael addition.[24] The results clearly demonstrated the extremely high catalytic activity of ZIF-8 for this one-pot reaction (**Table 3. 3. 1**, entry 2–6). This would be due to a bifunctional effect between Lewis acidity of the unsaturated Zn^{2+} cations and basicity of the unsaturated N atoms of the 2-methylimidazolate units in ZIF-8. The former Knoevenagel condensation reaction is generally catalyzed by base; therefore, the 2-methylimidazolate units in ZIF-8 will contribute the promotion of the reaction as base sites. On the other hand, Lewis acid sites are known to coordinate oxygen of a carbonyl group of aldehydes, and thus, activate the aldehydes in Knoevenagel condensation.[20] For the latter phospha-Michael addition, basic sites and Lewis acidic sites play a role in the deprotonation of the P–H bond in phosphites and activation of a nitrile nitrogen atom of malonates, respectively.[17] The framework structure of ZIF-8 where basic and Lewis acidic sites exist close to each other would enable to activate reactive substrates and facilitate the smooth flow to the following reactions, resulting in the efficient promoting of the one-pot reaction on ZIF-8.

So far, various types of ZIF materials have been developed and reported, such as ZIF-7 formed by bridging benzimidazolate anions and Zn^{2+} cations, ZIF-9 formed by benzimidazolate anions and Co^{2+} cations and ZIF-67 formed by 2-methylimidazolate anions and Co^{2+} cations.[11,13] These three ZIFs were also prepared and used in the one-pot reaction. Among four types of ZIF materials, ZIF-8 gave the best catalytic performance for the one-pot reaction (**Table 3. 3. 1**, entry 7–9). Moreover, the catalytic activity of ZIF-8 was higher than that of IRMOF-3, which consists of 2-amino-1,4-benzenedicarboxylate linkers and Zn-oxo clusters[25] (**Table 3. 3. 1**, entry 10). These results suggest that the combination of 2-methylimidazolate anions and Zn^{2+} cations is beneficial to promoting the one-pot reaction.

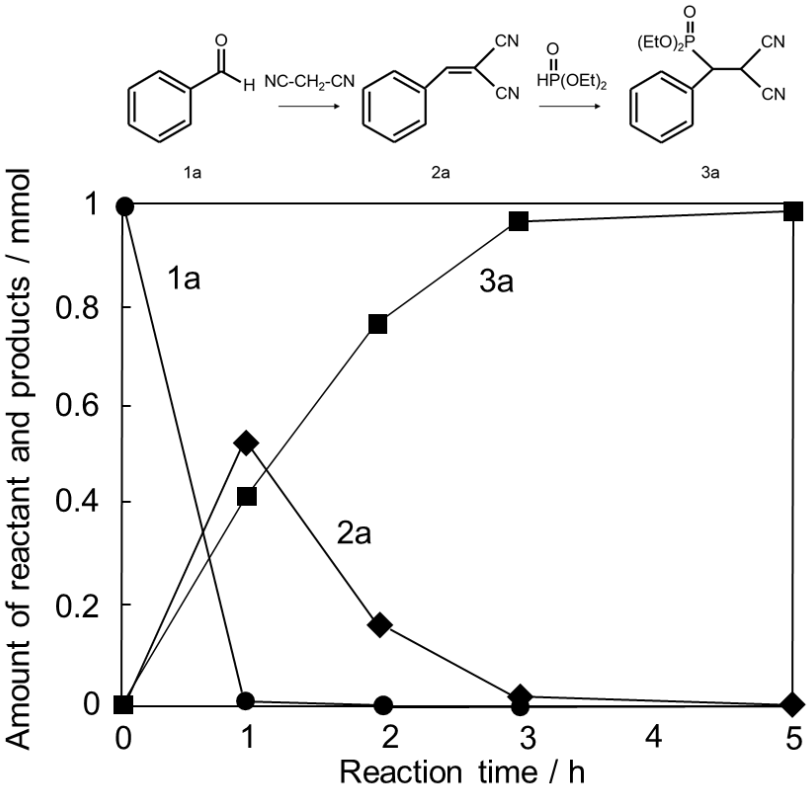

Figure 3. 3. 4. Time course of one-pot sequential Knoevenagel condensation and phospha-Michael addition over ZIF-8. Reaction conditions: Catalyst (50 mg), benzaldehyde (1 mmol), malononitrile (3 mmol), diethyl phosphite (3 mmol), 1,4-dioxane (4 mL), 323 K, in air.

Table 3. 3. 1. One-pot sequential Knoevenagel condensation and phospha-Michael addition using various catalysts.[a]

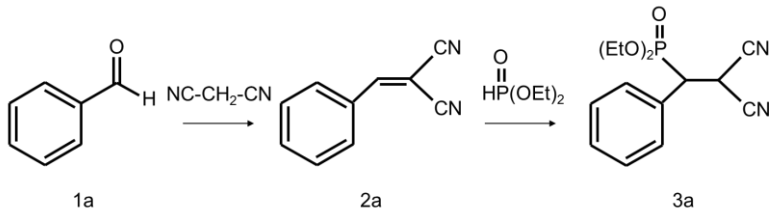

1a 2a 3a

Entry	Catalyst	Conv. (%)	Yield (%)	
			2a	3a
1	ZIF-8	100	2	98
2	ZnO	62	59	2
3	MgO	75	61	14
4	Al_2O_3	88	80	7
5	Hydrotalcite	100	70	26
6	MCM-41-NH_2	81	63	15
7	ZIF-7	88	32	54
8	ZIF-9	81	45	36
9	ZIF-67	100	34	66
10	IRMOF-3	18	11	5
11	No catalyst	0	0	0

[a] Reaction conditions: Catalyst (50 mg), benzaldehyde (1 mmol), malononitrile (3 mmol), diethyl phosphite (3 mmol), 1,4-dioxane (4 mL), 323 K, 5 h, in air. The progression of the reaction was monitored by gas chromatography and ^{1}H-NMR spectroscopy.

Subsequently, the ZIF-8-catalyzed one-pot three component reaction was extended to other substrates. The results are summarized in **Table 3. 3. 2**. In the case using differently-substituted aldehydes (**Table 3. 3. 2**, entry 2–5), the reaction proceeded smoothly on ZIF-8 to give the corresponding organophosphorus compounds (3b–e). Furthermore, ZIF-8 promoted the one-pot reaction in the presence of benzaldehyde, ethyl cyanoacetate and diethyl phosphite and produced 3f in a high yield although the reaction time needed to complete was prolonged because the rate of the former Knoevenagel condensation is generally dominated by pK_a values of the donor molecules.[26]

Finally, the recycling experiments were performed for the evaluation of the recyclability of ZIF-8. The spent catalyst was recovered by filtration after cooling to room temperature, washed several times with methanol, dried at 333 K in air and then reused in the next run. The results shown in **Fig. 3. 3. 5** revealed that ZIF-8 can be recycled at least 3 cycles without significant loss of its reactivity and selectivity. Moreover, almost no change was observed in the XRD pattern of ZIF-8 after the reaction (**Fig. 3. 3. 6**), indicating that ZIF-8 behaves as a heterogeneous catalyst with retaining its framework structure during the reaction.

Table 3. 3. 2. One-pot sequential Knoevenagel condensation and phospha-Michael addition using various catalysts.[a]

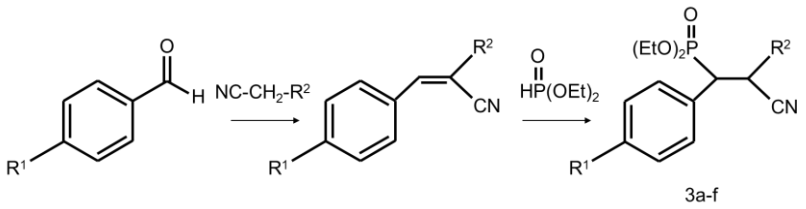

Entry	R^1	R^2	Product	Time (h)	Conv. (%)	Yield (%)
1	H	CN	3a	5	100	98
2	CH_3	CN	3b	5	100	100
3	OH	CN	3c	5	100	99
4	NO_2	CN	3d	5	100	99
5	OCH_3	CN	3e	5	100	99
6	H	$COOC_2H_5$	3f	10	100	99

[a]Reaction conditions: Catalyst (50 mg), aldehyde (1 mmol), active methylene compound (3 mmol), diethyl phosphite (3 mmol), 1,4-dioxane (4 mL), 323 K, in air.

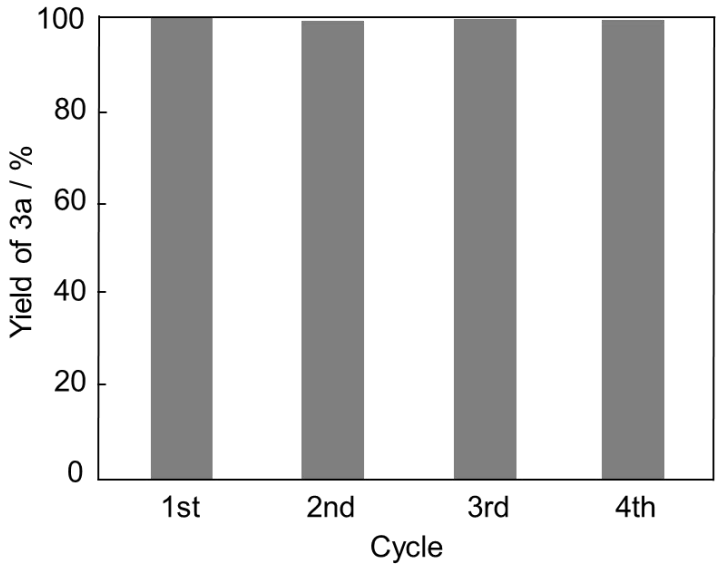

Figure 3. 3. 5. Recycle experiments for one-pot sequential Knoevenagel condensation and phospha-Michael addition using ZIF-8. Reaction conditions: Catalyst (50 mg), benzaldehyde (1 mmol), malononitrile (3 mmol), diethyl phosphite (3 mmol), 1,4-dioxane (4 mL), 323 K, in air.

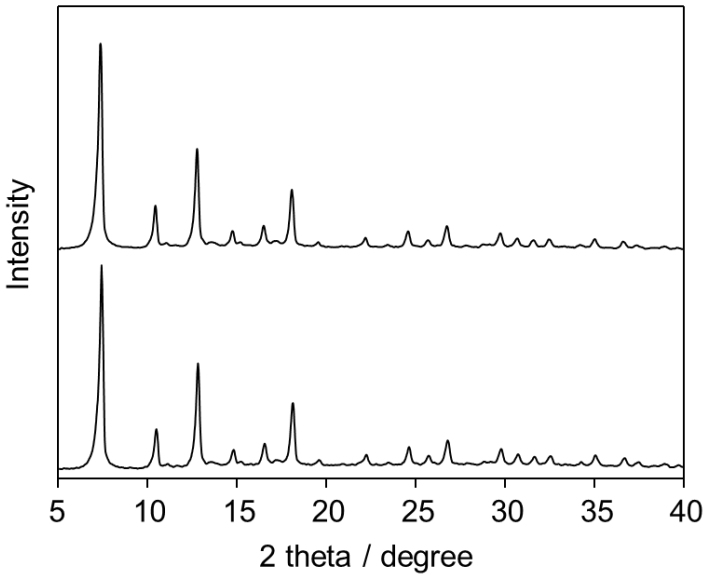

Figure 3. 3. 6. XRD patterns of ZIF-8 before and after the one-pot reaction.

3. 3. 4. Conclusions

In summary, this study described the potential heterogeneous catalytic activity of ZIF-8 for a one-pot P–C bond formation reaction via Knoevenagel condensation and phospha-Michael addition. The one-pot reaction efficiently proceeded on ZIF-8 to give the corresponding organophosphorus compounds from aldehydes, active methylene compounds and diethyl phosphite with extremely high selectivity. The framework structure of ZIF-8, which includes both base sites derive from 2-methylimidazolate anions and Lewis acid sites derive from Zn^{2+} cations, was found to be beneficial to promoting the one-pot reaction. Moreover, ZIF-8 was able to be reused several times without significant loss of its selectivity and reactivity.

3. 3. 5. References

1. N. Hall, *Science*, 1994, **266**, 32.
2. L. F. Tietze, *Chem. Rev.*, 1996, **96**, 115.
3. J.-C. Wasilke, S. J. Obrey, R. T. Baker and G. C. Bazan, *Chem. Rev.*, 2005, **105**, 1001.
4. O. M. Yaghi, M. O'Keeffe, N. W. Ockwig, H. K. Chae, M. Eddaoudi and J. Kim, *Nature*, 2003, **423**, 705.
5. S. Kitagawa, R. Kitaura and S.-i. Noro, *Angew. Chem., Int. Ed*., 2004, **43**, 2334.
6. G. Férey, *Chem. Soc. Rev.*, 2008, **37**, 191.
7. X. Zhao, B. Xiao, A. J. Fletcher, K. Thomas, D. Bradshaw and M. J. Rosseinsky, *Science*, 2004, **306**, 1012.
8. A. Corma, H. Garcia and F. X. Liabres i Xamena, *Chem. Rev*., 2010, **110**, 4606.
9. J. Lee, O. K. Farha, J. Roberts, K. A. Scheidt, S. T. Nguyen and J. T. Hupp, *Chem. Soc. Rev*., 2009, **38**, 1450.
10. X.-C. Huang, Y.-Y. Lin, J.-P. Zhang and X.-M. Chen, *Angew. Chem., Int. Ed*., 2006, **45**, 1557.
11. K. S. Park, Z. Ni, A. P. Côté, J. Y. Choi, R. Huang, F. J. Uribe-Romo, H. K. Chae, M. O'Keeffe and O. M. Yaghi, *Proc. Natl. Acad. Sci. U.S.A.*, 2006, **103**, 10186.
12. H. Wu, W. Zhou and T. Yildirim, *J. Am. Chem. Soc.*, 2007, **129**, 5314.
13. R. Banerjee, A. Phan, B. Wang, C. Knobler, H. Furukawa, M. O'Keeffe and O. M. Yaghi, *Science*, 2008, **319**, 939.
14. L. Tedeschi and D. Enders, *Organic Letters*, 2001, **3**, 3515.
15. S. Sobhani and Z. P. Parizi, *Tetrahedron*, 2011, **67**, 3540.
16. H. Sharghi, S. Ebrahimpourmoghaddam and M. M. Doroodmand, *Tetrahedron*, 2013, **69**, 4708.

17. M. Hosseini-Sarvari and S. Etemad, *Tetrahedron*, 2008, **64**, 5519.

18. S. R. Kolla and Y. R. Lee, *Tetrahedron*, 2012, **68**, 226.

19. S. Sobhani, M. Bazrafshan, A. A. Delluei and Z. P. Parizi, *Appl. Catal., A: Gen.,* 2013, **454**, 145.

20. M. Hosseini-Sarvari and M. Tavakolian, *New J. Chem.*, 2012, **36**, 1014.

21. C. M. Miralda, E. E. Macias, M. Zhu, P. Ratnasamy and M. A. Carreon, *ACS Catal.*, 2012, **2**, 180.

22. T. Yokoi, H. Yoshitake and T. Tatsumi, *J. Mater. Chem.*, 2004, **14**, 951.

23. S. Sobhani, Z. P. Parizi and S. Rezazadeh, *J. Organomet. Chem.*, 2011, **696**, 813.

24. M. Eddaoudi, J. Kim, N. Rosi, D. Vodak, J. Wachter, M. O'Keeffe and O. M. Yaghi, *Science*, 2002, **295**, 469.

25. A. Dhakshinamoorthy, M. Opanasenko, J. Čejka and H. Garcia, *Catal. Sci. Technol.*, 2013, **3**, 2509.

Chapter 4

Development of metal nanoparticles encapsulated within metal−organic frameworks as heterogeneous hydrogenation catalysts

4. 1. Encapsulation of metal nanoparticles within a Zr-based metal−organic framework for highly efficient, reusable hydrogenation catalysts

4. 1. 1. Introduction

Recently, metal nanoparticles have been the focus of much attention due to their unique catalytic, electrocatalytic, electronic, magnetic and optical features, which are not provided by bulk materials.[1-7] However, most colloidal metal nanoparticles used as catalysts are homogeneously dispersed in solvent and result in limitations of recyclability. With these facts in mind, much effort has been devoted to the immobilization of metal nanoparticles onto solid supports to design highly active and recyclable heterogeneous catalysts.

Metal–organic frameworks (MOFs) also called porous coordination polymers (PCPs) have emerged as promising platform for supported catalysts owing to their highly ordered porous structures and well-controlled surface functionalities.[8, 9] These unique features come from various combinations of metal nodes and bridging organic linkers that constitute MOF/PCPs. In general, metal nanoparticles are immobilized onto MOF/PCPs through impregnation and precipitation methods after the synthesis of MOF/PCPs. These methodologies are essentially hard to realize the uniform-sized nanoparticle synthesis and the leaching prohibition. The most desirable is the confinement of size-controlled colloidal metal nanoparticles preliminarily prepared within the framework of MOF/PCPs during the synthesis of MOF/PCPs. Additionally, in the synthetic process of colloidal metal nanoparticles, the formation of alloy nanoparticles is also easily attained. Alloying provides geometric structure change and systematic and precise control of electronic states, leading to the improvement of catalytic performances.[10-13]

In this study, the potential heterogeneous catalytic performance of Pd nanoparticles

encapsulated into a Zr-based MOF (Pd@Zr-MOF) has been investigated. Pd nanoparticles have been subjected to extensive research in the fields of catalytic chemistry owing to their efficient catalytic activities for various useful reactions. In particular, they are known to be the most common hydrogenation catalysts.[14-16] On the other hand, Zr-MOF that behaves as a cage for Pd nanoparticles possesses relatively high stability among every MOF materials in addition to the highly ordered structure with uniform micropores.[17-19] These characteristics should make Pd@Zr-MOF effective recyclable catalysts. Moreover, the feasibility of a promotional effect by alloying Pd with Au in this catalyst synthetic concept have also been investigated.

4. 1. 2. Experimental

Materials

Palladium chloride ($PdCl_2$), polyvinylpyrrolidone (PVP) K30, sodium borohydride ($NaBH_4$), zirconium chloride ($ZrCl_4$), N'N-dimethylformanide (DMF) and acetone were purchased from Nacalai Tesque Inc. Tetrachloroauric acid ($HAuCl_4$), terephthalic acid (TPA) and phosphoric acid (H_3PO_4) were purchased from Kishida Chemicals Co., Ltd. Solvents were purified by standard procedures.

Catalysts preparation

Synthesis of colloidal Pd nanoparticles dispersed in DMF

The colloidal Pd nanoparticles were prepared by the previously-reported procedure with a slight modification.[20] Typically, 20 mg of $PdCl_2$ (Pd: 1.12×10^{-4} mol), 834 mg of PVP, and 20 mL of H_2O were mixed and stirred at 273 K in an ice bath. A mixture of 30 mg of $NaBH_4$ and 0.5 mL of H_2O were then added in the above solution, which was stirred for 30

min. The resulting colloidal solution was evaporated almost to dryness and then redispersed in 10 mL of DMF through ultrasonic irradiation.

Synthesis of colloidal Pd−Au nanoparticles dispersed in DMF

The colloidal Pd−Au bimetallic or pure Au nanoparticles were prepared by the same method as the case with the Pd nanoparticles, excepting for using precursor solutions containing appropriate ratios of $PdCl_2$ and $HAuCl_4$.[20] The Pd/Au molar ratio of 3/1, 1/1, 1/3 and 0 was employed for the precursor solutions (Au + Pd: 1.12×10^{-4} mol).

Synthesis of Pd@Zr-MOF, PdAu@Zr-MOF and Au@Zr-MOF

Pd@Zr-MOF was prepared by a solvothermal method based on the preparation procedure of Zr-MOF.[17] Firstly, 424 mg of $ZrCl_4$, 272 mg of TPA and 6.7 mL of colloidal Pd nanoparticles dispersed in DMF was added in 40 mL of DMF. The obtained mixture was then loaded into a Teflon-lined stainless-steel and subjected to solvothermal conditions for 24 h at 393 K under autogenous pressure. The formed precipitate was separated by filtration, washed repeatedly with acetone and dried at 473 K for 2 h. In the synthesis of PdAu@Zr-MOF and Au@Zr-MOF, the precursor solutions containing 6.7 mL of colloidal Pd−Au alloy nanoparticles with different Pd/Au ratio of Pd/Au = 1/3, Pd/Au = 1 and Pd/Au = 3 or pure Au nanoparticles dispersed in DMF were employed in place of colloidal Pd nanoparticles.

General methods

Standard θ–2θ X-ray diffraction (XRD) data were recorded on a Shimadzu X-ray diffractometer XRD-6100 using Cu Kα radiation (λ = 1.5406 Å). Specific surface areas were estimated from the amount of N_2 adsorption at 77 K using the BET (Brunauer-Emmett-Teller) equilibrium equation. Diffuse reflectance UV–vis spectra were obtained with a Shimadzu UV–vis recording spectrophotometer 2200A. Transmission electronic microscope (TEM) images were taken with JEM-2000FX operating under 200 kV accelerating voltage. Electron

spin resonance (ESR) spectra were recorded with a JEOL JES-RE-2X at 77 K.

Catalytic reaction

The hydrogenation of nitrobenzene to produce aniline was performed to evaluate the catalytic activity of the synthesized catalysts. The powdered catalysts (metal content: 1.0×10^{-5} mol), nitrobenzene (1.25 mmol for Pd@Zr-MOF or 10 mmol for PdAu@Zr-MOF) and methanol (10 mL) were introduced into a glass reaction vessel with a reflux condenser. The resulting mixture was bubbled with hydrogen for 15 min and then stirred at 313 K under hydrogen bubbling (10 mL min^{-1}). The progress of the reaction was monitored by gas chromatography (GC) analysis using an internal standard technique (*n*-dodecane). Analytical GC was performed using a Shimadzu GC-14B with a flame ionization detector equipped with Inertcap® 1 column.

The recycling experiments were performed by the following procedure. The catalyst samples after reaction were recovered by centrifugation and decantation and washed with methanol thoroughly three times, followed by natural drying at 373 K for 3 h. The resulting powdered samples were used in another catalytic cycle.

4. 1. 3. Results and discussion

Figure 4. 1. 1 displays XRD patterns of Pd@Zr-MOF and Zr-MOF. The diffraction pattern of Pd@Zr-MOF is coincident with that of Zr-MOF, suggesting that the UiO-66 type structure was formed even using a precursor solution containing colloidal Pd nanoparticles.[17] In addition, N_2 adsorption−desorption measurements reveal the formation of angstrom-sized pores. Both of the N_2 adsorption−desorption isotherms of Pd@Zr-MOF and Zr-MOF shown in **Fig. 4. 1. 2** exhibited the typical type I isotherm with a steep increase in the amount of adsorbed N_2 at very low pressures ($P/P_0 < 0.01$), indicating the formation of a rigid

microporous structure. The BET specific surface area (S_{BET}) and micropore volume (V_{micro}) of Pd@Zr-MOF are determined to be 944 m^2 g^{-1} and 0.42 cm^3 g^{-1}, respectively, which are almost similar values to those of Zr-MOF (S_{BET} = 1171 m^2 g^{-1} and V_{micro} = 0.50 cm^3 g^{-1}). Slight decreases in the specific surface and pore volume of Pd@Zr-MOF will be caused by a pore blockage due to the presence of Pd nanoparticles.

To gain an insight into the size and location of the immobilized Pd nanoparticles, TEM observations were performed. **Figure 4. 1. 3** shows TEM images of Pd@Zr-MOF. In this TEM image, highly dispersed Pd nanoparticles with a mean size of ca. 5 nm were observed. Moreover, these images seem to demonstrate that Pd nanoparticles were located mainly on the inside of the Zr-MOF particles.

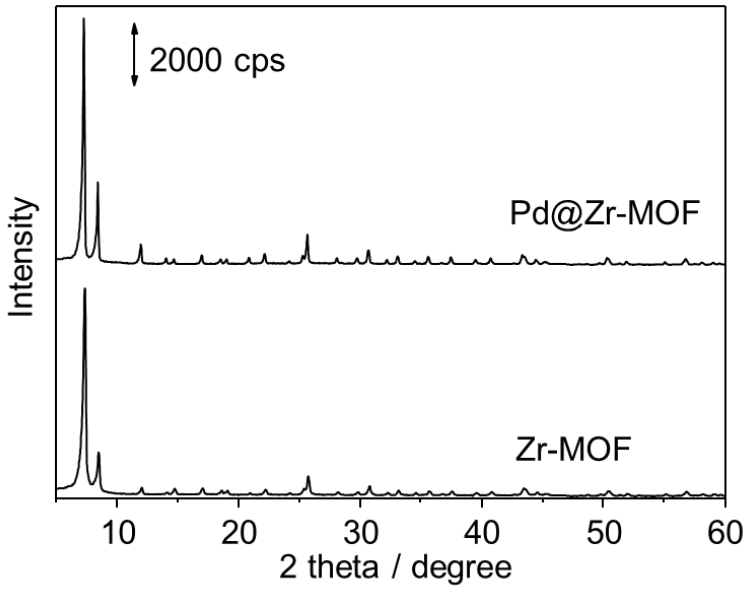

Figure 4. 1. 1. XRD patterns of Zr-MOF and Pd@Zr-MOF.

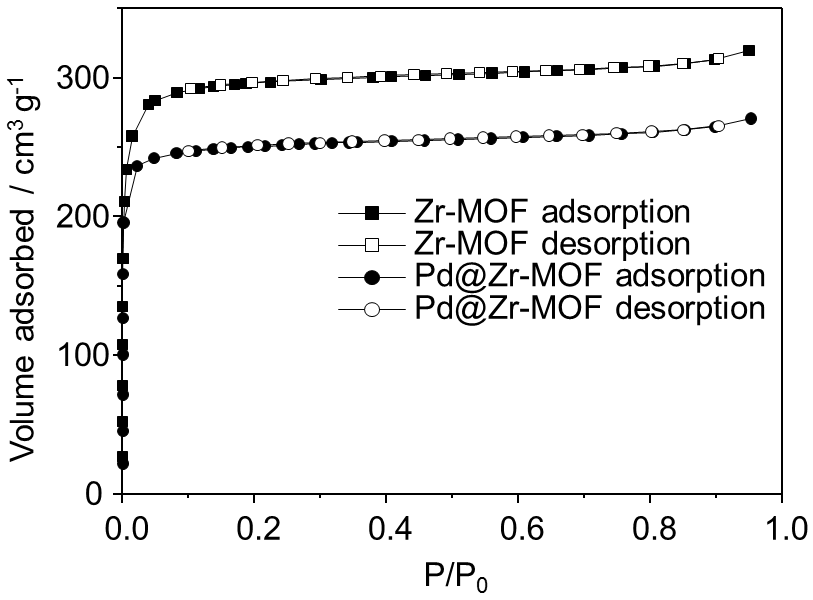

Figure 4. 1. 2. N_2 adsorption–desorption isotherms of Zr-MOF and Pd@Zr-MOF.

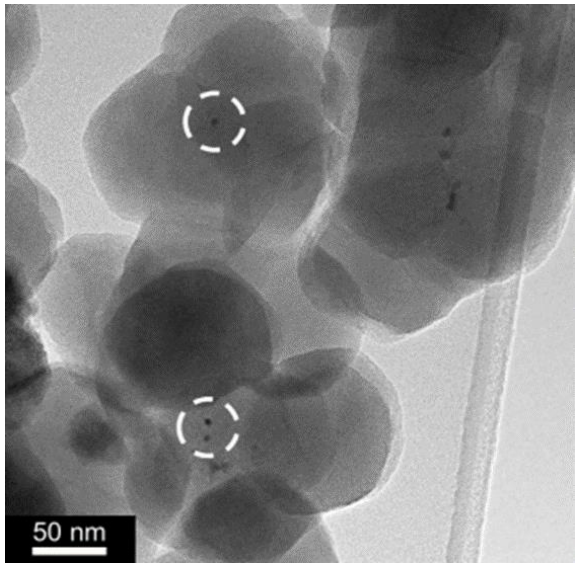

Figure 4. 1. 3. TEM image of Pd@Zr-MOF.

The hydrogenation of nitrobenzene to aniline was then performed over Pd@Zr-MOF. For comparison purposes, Pd nanoparticles deposited on Zr-MOF (Pd/Zr-MOF) were prepared by a post-synthetic impregnation method (details are given in the supporting information) and were used in the same catalytic reaction. The time courses of the

hydrogenation of nitrobenzene to aniline by using Pd@Zr-MOF, Pd/Zr-MOF and Zr-MOF are shown in **Fig. 4. 1. 4**. The reaction proceeded efficiently over Pd@Zr-MOF and Pd/Zr-MOF, while no reaction occurred when using Zr-MOF. These results indicate that Pd nanoparticles act as effective catalysts for this hydrogenation reaction and that Zr-MOF does not have active center. The reaction rates over Pd@Zr-MOF and Pd/Zr-MOF show not so much difference, and nearly 100% conversion of nitrobenzene was achieved within only 2 h. In addition, there were negligible by-products (e.g., nitrosobenzene) in the reaction products.

On the other hand, recycling experiments demonstrate clear differences of the catalyst stability between Pd@Zr-MOF and Pd/Zr-MOF. The results of recycling experiments are summarized in **Fig. 4. 1. 5**. Pd@Zr-MOF exhibited reusability at least 4 times without significant loss of its catalytic activity. In contrast, the catalytic activity of Pd/Zr-MOF was gradually decreased when being repeatedly employed for the reaction. These results indicate that Pd nanoparticles in Pd@Zr-MOF are encapsulated within Zr-MOF and immobilized strongly enough to prohibit from leaching during the reaction.

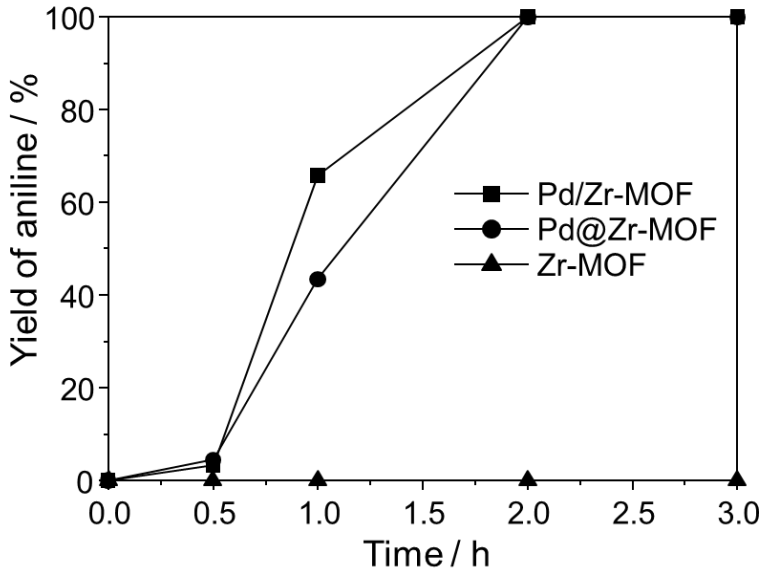

Figure 4. 1. 4. Time course of hydrogenation of nitrobenzene over Pd@Zr-MOF, Pd/Zr-MOF and Zr-MOF.

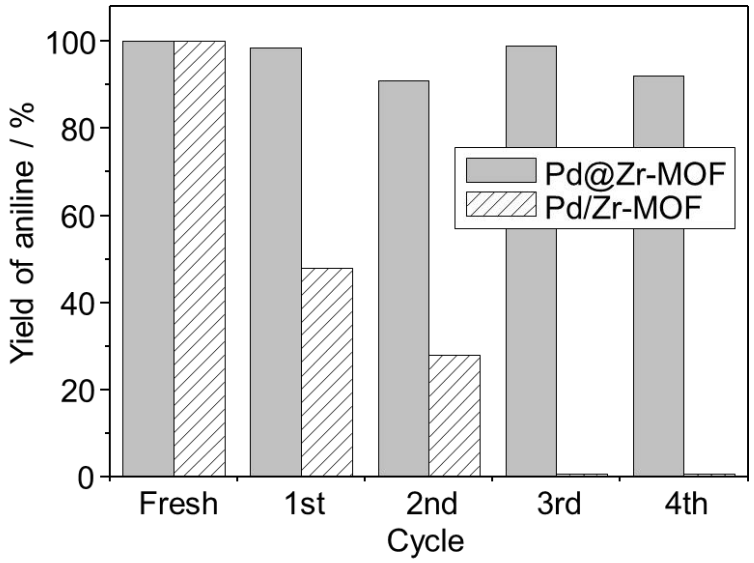

Figure 4. 1. 5. Recycling experiments for Pd@Zr-MOF and Pd/Zr-MOF.

In the encapsulation procedure developed here, the types and compositions of catalytically active metal nanoparticles can be readily varied during the process of the metal nanoparticle synthesis. Pd−Au bimetallic nanoparticles were also tried to be encapsulated in Zr-MOF (PdAu@Zr-MOF) for further improvement of catalytic activity. Firstly, colloidal Pd−Au bimetallic nanoparticles were prepared and characterized by using UV−vis absorption measurements. **Figure 4. 1. 6** shows UV−vis absorption spectra of colloidal Pd−Au bimetallic nanoparticles with different Pd/Au ratio. Colloidal pure Au nanoparticles (Pd/Au = 0) exhibited clear absorption band at around 540 nm which originates from localized surface plasmon resonance of Au nanoparticles. As contrasted to the pure Au sample, all colloidal bimetallic samples did not show absorption bands derive from localized surface plasmon resonance. This finding suggests that Au and Pd nanoparticles exist not independently of each other but as alloy particles.[21] Following the successful formation of colloidal Pd−Au bimetallic nanoparticles, PdAu@Zr-MOF was synthesized by the same solvothermal method as one used for the synthesis of Pd@Zr-MOF except for using different precursor solutions. As shown in **Fig. 4. 1. 7**, PdAu@Zr-MOF and Au@Zr-MOF exhibited almost the same

diffraction patterns as that of Zr-MOF, indicating the formation of the UiO-66-type framework structure.

The effect of alloying with Au on the catalytic activity was then investigated through the same hydrogenation reaction. **Figure 4. 1. 8** presents the results of the hydrogenation of nitrobenzene to aniline catalyzed by various metal nanoparticles encapsulated in Zr-MOF. The alloying with Au led to the enhancement of the catalytic activity, and the optimal mixing ratio was found to be Pd/Au = 3. On the other hand, Au@Zr-MOF hardly promoted the hydrogenation reaction under the same reaction conditions. This gives an indication that a synergic effect exists between Pd and Au atoms for Pd−Au bimetallic nanoparticles within PdAu@Zr-MOF. Recently, some researchers reported the enhanced catalytic activity for hydrogenation reactions when using bimetallic Pd−Au nanoparticle catalysts, where the decrease in electron density of Pd atoms due to electronic interaction between Pd and Au atoms was explained to be responsible for the catalytic activity improvement.[10,21,22] Similar electronic enhancement effects would take place in the bimetallic catalysts developed here. By contrast, the enhancement effect was almost negligible when the physical mixture of Pd@Zr-MOF and Au@Zr-MOF was employed for the catalyst. This finding suggests that the mixing at atomic level is absolutely imperative in order to achieve the catalytic enhancement by Au addition.

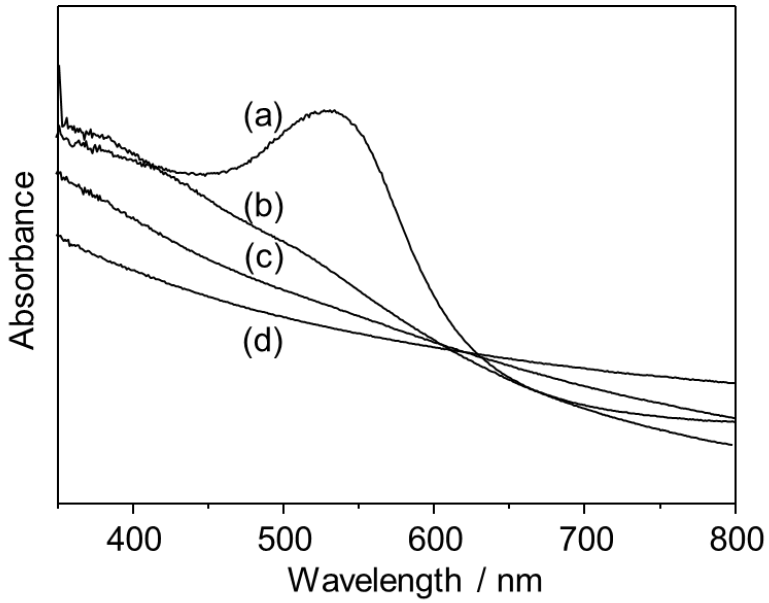

Figure 4. 1. 6. UV–vis absorption spectra of colloidal Pd−Au bimetallic nanoparticles with different Pd/Au ratio of (a) pure Au, (b) Pd/Au = 1/3, (c) Pd/Au = 1 and (d) Pd/Au = 3.

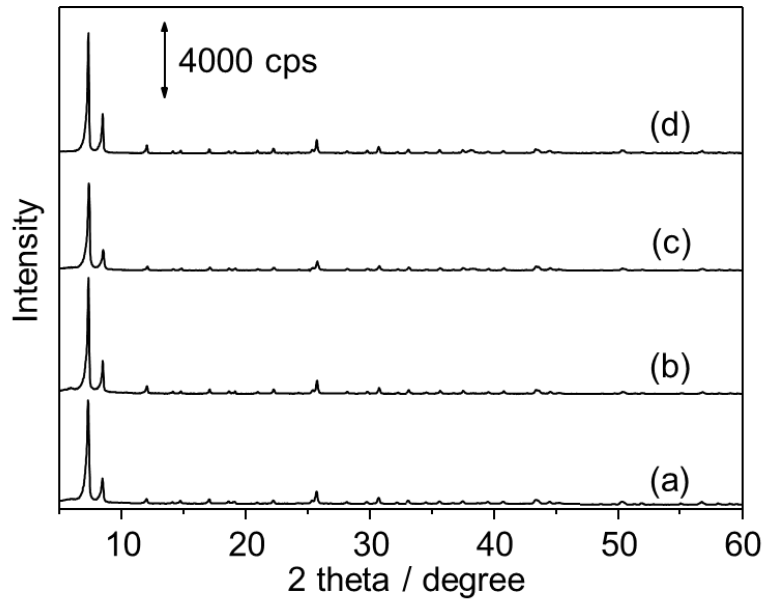

Figure 4. 1. 7. XRD patterns of (a) Au@Zr-MOF and (b–d) PdAu@Zr-MOF with different Pd/Au ratio of (b) Pd/Au = 1/3, (c) Pd/Au = 1 and (d) Pd/Au = 3.

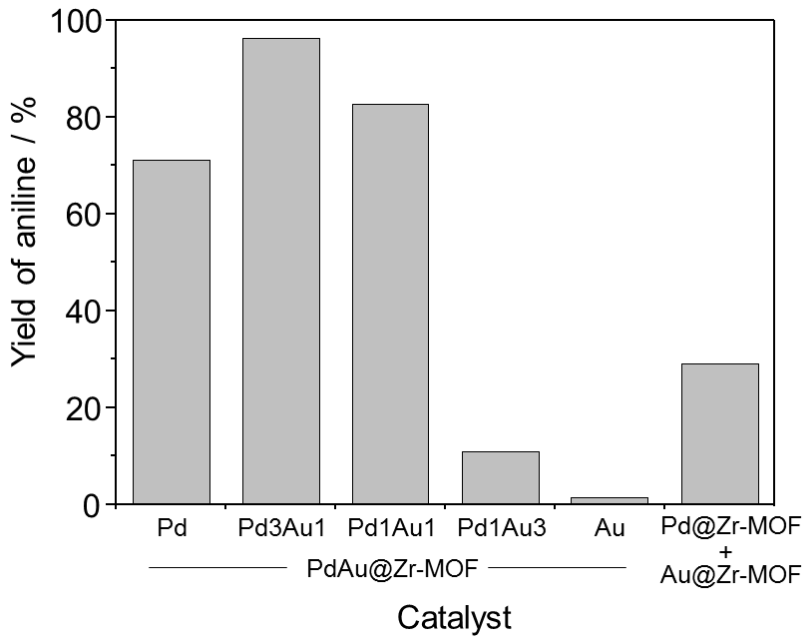

Figure 4. 1. 8. Hydrogenation of nitrobenzene over various metal nanoparticles-encapsulated Zr-MOF catalysts.

4. 1. 4. Conclusions

Pd nanoparticles have been shown to be successfully encapsulated within Zr-MOF during the synthesis of the framework structure of Zr-MOF. The resulting material exhibited an efficient catalytic activity for hydrogenation of nitrobenzene to give aniline in a good yield. The encapsulation of Pd nanoparticles within Zr-MOF was found to provide high recyclability of the catalyst. Moreover, the improvement of catalytic activity was easily attained by alloying of Pd nanoparticles with Au before encapsulation of the metal nanoparticles.

4. 1. 5. References

1. S. Link and M. A. El-Sayed, *J. Phys. Chem. B*, 1999, **103**, 8410.
2. A. Roucoux, J. Schulz and H. Patin, *Chem. Rev.*, 2002, **102**, 3757.
3. K. L. Kelly, E. Coronado, L. L. Zhao and G. C. Schatz, *J. Phys. Chem. B*, 2002, **107**, 668.
4. S. A. Maier, P. G. Kik, H. A. Atwater, S. Meltzer, E. Harel, B. E. Koel and A. A. G. Requicha, *Nat. Mater.*, 2003, **2**, 229.
5. M. Haruta, *Chem. Rec.*, 2003, **3**, 75.
6. A. Corma and P. Serna, *Science*, 2006, **313**, 332.
7. J. N. Anker, W. P. Hall, O. Lyandres, N. C. Shah, J. Zhao and R. P. Van Duyne, *Nat. Mater.*, 2008, **7**, 442.
8. O. M. Yaghi, M. O'Keeffe, N. W. Ockwig, H. K. Chae, M. Eddaoudi and J. Kim, *Nature*, 2003, **423**, 705.
9. S. Kitagawa, R. Kitaura and S. Noro, *Angew. Chem., Int. Ed.*, 2004, **43**, 2334.
10. N. Toshima, M. Harada, Y. Yamazaki and K. Asakura, *J. Phys. Chem.*, 1992, **96**, 9927.
11. N. Toshima and T. Yonezawa, *New J. Chem.*, 1998, **22**, 1179.
12. B. Coq and F. Figueras, *J. Mol. Catal. A: Chem.*, 2001, **173**, 117.
13. R. Ferrando, J. Jellinek and R. L. Johnston, *Chem. Rev.*, 2008, **108**, 845.
14. M. Zhao and R. M. Crooks, *Angew. Chem., Int. Ed.*, 1999, **38**, 364.
15. K. Esumi, R. Isono and T. Yoshimura, *Langmuir*, 2003, **20**, 237.
16. S. Mandal, D. Roy, R. V. Chaudhari and M. Sastry, *Chem. Mater.*, 2004, **16**, 3714.
17. J. H. Cavka, S. Jakobsen, U. Olsbye, N. Guillou, C. Lamberti, S. Bordiga and K. P. Lillerud, *J. Am. Chem. Soc.*, 2008, **130**, 13850.

18. J. Long, S. Wang, Z. Ding, S. Wang, Y. Zhou, L. Huang and X. Wang, *Chem. Commun.*, 2012, **48**, 11656.

19. M. Pintado-Sierra, A. M. Rasero-Almansa, A. Corma, M. Iglesias and F. Sánchez, *J. Catal.*, 2013, **299**, 137.

20. W. Hou, N. A. Dehm and R. W. J. Scott, *J. Catal.*, 2008, **253**, 22.

21. R. W. J. Scott, O. M. Wilson, S.-K. Oh, E. A. Kenik and R. M. Crooks, *J. Am. Chem. Soc.*, 2004, **126**, 15583.

22. Y. Mizukoshi, T. Fujimoto, Y. Nagata, R. Oshima and Y. Maeda, *J. Phys. Chem. B*, 2000, **104**, 6028.

4. 2. Yolk-shell Pd nanoparticles@ZIF nanostructures for size-selective hydrogenation reactions

4. 2. 1. Introduction

Metal–organic frameworks (MOFs) also called porous coordination polymers (PCPs) are new crystalline hybrid materials prepared via well-established principles of coordination chemistry using self-assembly of metal ions or metal clusters with organic linkers.[1–6] Unlike traditional inorganic porous materials, unlimited possible combination of such an assembly enables to access the reticular structures with tunable porosity and attractive functions. In addition, new synergetic properties have been realized by incorporating functional species into MOFs to form composite materials in order to further expand the functionalization of MOFs.[7–10] There have been a large number of reports describing the incorporation of functional components into MOFs.[11–15] Among them, encapsulation of nanoparticles is widely investigated to demonstrate specific functional properties that cannot be obtained from the parent MOFs.[16–18]

Specifically, yolk-shell nanostructures have gained recent research interest due to their potential applications in heterogeneous catalysis.[19–20] Integrating the functions of the nanocrystal core, the nanostructured shell, and the cavity in between provides a tool for optimizing the performance of a nanomaterial. In a yolk-shell catalyst, the metal core provides a catalytically active surface for the reaction and the porous shell serves as a barrier layer to prevent aggregation of the active surface with neighboring metal cores during the reaction.[21–22] Compared with the core-shell nanostructure, in which the shell is directly on the metal surface, the yolk-shell structure is characteristic of a free noble metal core inside a hollow shell with a relatively homogeneous surrounding environment, allowing for exposure

of all the active sites to contact with the reactants during the catalytic process.[23] It has been proposed that the shell in the yolk-shell structure could introduce multiple functions into the catalyst, such as regulation of diffusion and control of molecular-size selectivity.[24–25] However, in most of the yolk-shell catalysts, the shell has served only one function, acting as a protective layer to prevent aggregation between particles during the reaction.[26] This is mainly because the shell materials were limited to nonordered porous materials, restricting the functions of the shells.

Herein a general synthetic strategy for yolk-shell structures is proposed with zeolitic imidazolate frameworks (ZIFs), which are one of the MOF materials.[27] The synthetic strategy involves the deposition of Pd nanoparticles on carboxylate-terminated polystyrene (PS), followed by coatings with ZIF-8.[28] Subsequently, PS was extracted by washing with dimethylformamide (DMF) solution to obtain Pd@ZIF-8 having the yolk-shell structure, as shown in **Scheme 4. 2. 1**. Size-selective hydrogenation reactions have been realized over Pd@ZIF-8 by taking advantage of the uniform and microporous structure of the ZIF-8 shell. The method proposed here can offer a simple approach to design MOF catalysts having yolk-shell structures with the size selectivity. Indeed, the present results demonstrate that MOFs can be used as interesting platforms to create multifunctional catalysts.

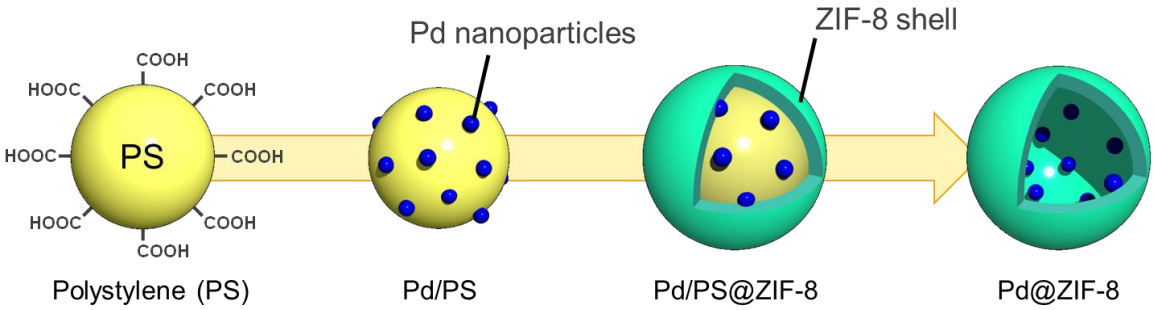

Scheme 4. 2. 1. Schematic illustration of synthesis of yolk-shell Pd@ZIF-8.

4. 2. 2. Experimental

Materials

Styrene, methacrylic acid, dimethylformamide (DMF), peroxydisulfuric acid, methanol, palladium chloride ($PdCl_2$), sodium borohydride ($NaBH_4$), n-octane, 2-octane, cyclohexene, cyclohexane, cyclooctene, n-decane and n-hexane were purchased from Nacalai Tesque Inc. Sodium hydroxide and sodium carbonate were purchased from Kishida Chemicals Co., Ltd. 2-Methylimidazole, 1-octene, 1-octyne, 2-octane and cyclooctane were purchased from Tokyo Chemical Industry Co. Ltd. $Zn(NO_3)_2 \cdot 4H_2O$ was purchased from Merck. Solvents were purified by standard procedures.

Catalysts preparation

Synthesis of polystyrene colloidal templates (PS)

Non-crosslinked, monodisperse polystyrene spheres with carboxylic acid terminated surfaces were synthesized using an emulsifier-free emulsion polymerization technique.[29] In a typical synthesis, a three-necked, 200 ml round-bottomed flask was filled with water (80 ml) and heated to 348 K before styrene (7.0 g) and methacrylic acid (0.35 g) were added under intensive stirring. Nitrogen was bubbled to deaerate the mixture for 30 min. In a separate 25 ml polyethylene bottle, sodium hydroxide (24 mg) and sodium carbonate (24 mg) was dissolved in water (5 ml), and the solution was added to the former solution which was reheated to 348 K. Potassium persulfate initiator (30 mg) was added to water (5 ml) and the solution was deaerated for 10 min. After the initiator was added to the total solution, nitrogen was passed through the flask for 10 min. The temperature was kept at 348 K for 12 h. After alternating centrifugation and dispersion using water several times to expunge residues, monodisperse carboxylate-terminated polystyrene particles (330 nm) were obtained and fully

dispersed in methanol.

Synthesis of Pd supported PS (Pd/PS)

PS (500 mg) and $PdCl_2$ (8.3 mg) were dissolved in methanol (3.6 mL) and the solution was stirred for 2 h at room temperature. Methanol (1.9 ml) containing sodium boron hydride (11.1 mg) was slowly added to the mixed solution. After the solution was kept stirring for 30 min, Pd supported PS (Pd/PS) was washed with methanol 3 times and redisposed in methanol.

Synthesis of Pd/PS encapsulated ZIF-8 (Pd/PS@ZIF-8)

Methanol containing Pd/PS (1.2 ml), 2-methylimidazole (830 mg), $Zn(NO_3)_2 \cdot 4H_2O$ (264 mg) and methanol (40 ml) were mixed in a 200 ml glass vessel. The mixed solution was stirred for 10 min. at 343 K. The resulting Pd/PS encapsulated ZIF-8 (Pd/PS@ZIF-8) was washed with methanol 3 times and collected by centrifugation.

Synthesis of Pd encapsulated ZIF-8 (Pd@ZIF-8)

Pd/PS@ZIF-8 was added in DMF (50 ml) and kept for 12 h. the resulting solid was washed with DMF and methanol, and then dried in air at 343 K (Pd@ZIF-8).

General methods

Standard θ–2θ X-ray diffraction (XRD) data were recorded on a Shimadzu X-ray diffractometer XRD-6100 using Cu Kα radiation (λ = 1.5406 Å). Specific surface areas were estimated from the amount of N_2 adsorption at 77 K using the BET (Brunauer-Emmett-Teller) equilibrium equation. Diffuse reflectance UV–vis spectra were obtained with a Shimadzu UV–vis recording spectrophotometer 2200A. Transmission electronic microscope (TEM) images were taken with JEM-2000FX operating under 200 kV accelerating voltage. Electron spin resonance (ESR) spectra were recorded with a JEOL JES-RE-2X at 77 K. X-ray absorption fine structure (XAFS) spectra were recorded at the BL-01B1 facility of the Photon

Factory at Spring-8 at the Japan Synchrotron Radiation Research Institute (JASRI). The Pd K-edge XAFS spectra were measured in the fluorescence mode, with a Si(111) double-crystal monochromator at room temperature.

Catalytic reaction

The hydrogenation reactions were performed to evaluate the catalytic activity of the prepared catalysts. Typically, the catalysts (Pd = 5 μmol), 1-octene (5 mmol) and methanol (10 mL) were introduced into a glass reaction vessel with a reflux condenser. The resulting mixture was bubbled with hydrogen for 15 min and then stirred at 313 K under hydrogen bubbling (10 mL min^{-1}). The progress of the reaction was monitored by gas chromatography analysis using an internal standard technique (*n*-decane).

The recycling experiments were performed by the following procedure. The catalyst samples after reaction were recovered by centrifugation and decantation and washed with methanol thoroughly three times, followed by natural drying at 373 K for 3 h. The resulting powdered samples were used in another catalytic cycle.

4. 2. 3. Results and discussion

Pd@ZIF-8 with yolk-shell nanostructure was synthesized by utilizing carboxylate-terminated polystyrene (PS) as a template. **Figure 4. 2. 1** and **4. 2. 2** display the successful formation of the yolk-shell nanostructure through this template method. Pd nanoparticles with the size of 10-20 nm can be seen inside of the ZIF-8 shells. Powder X-ray diffraction (XRD) measurements were carried out in order to confirm the formation of ZIF-8 structures, as shown in **Fig. 4. 2. 3**. It was found that the observed diffraction patterns for Pd@ZIF-8 are in good agreement with the previously-reported diffraction pattern of a ZIF-8-type structure.[30] No diffraction peaks corresponding to residual precursors or oxide

species were observed in the patterns. N_2 adsorption isotherms are shown in **Fig. 4. 2. 4**. Using the BET (Brunauer-Emmett-Teller) method, the specific surface area of Pd@ZIF-8 was measured to be 1231 m^2g^{-1}. This high surface area indicates the successful formation of the ZIF-8 structure. The local structure of Pd species in Pd@ZIF-8 was investigated by XAFS measurements (**Fig. 4. 2. 5**). The edge position as well as the shape of the XANES spectrum of Pd@ZIF-8 corresponds well to those of Pd foil used as a reference. Fourier transform of the EXAFS (FT-EXAFS) spectrum (without phase-shift corrections) of Pd@ZIF-8 exhibits one strong peak corresponding to neighboring Pd atoms (2.0–3.0 Å). Other peaks arising from oxides were not observed in the spectrum. These facts indicate that Pd species in Pd@ZIF-8 mainly exist in a metal state without change during the preparation process.

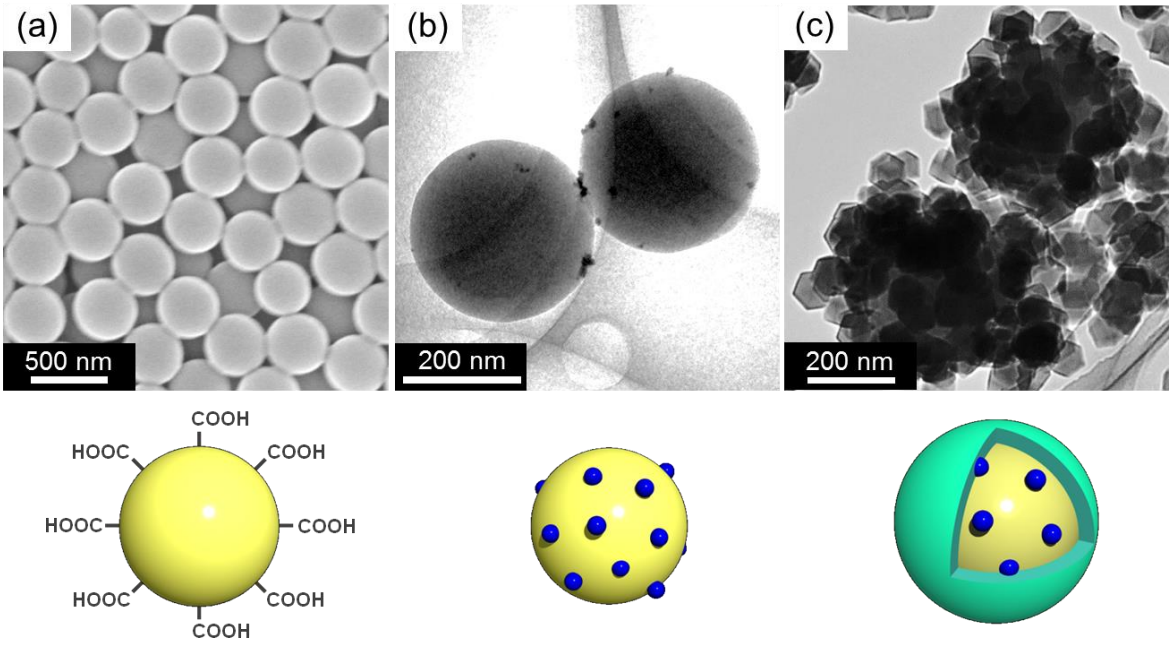

Figure 4. 2. 1. SEM image of (a) carboxylate-terminated PS and TEM images of (b) Pd/PS and (c) Pd/PS@ZIF-8 with schematic illustrations.

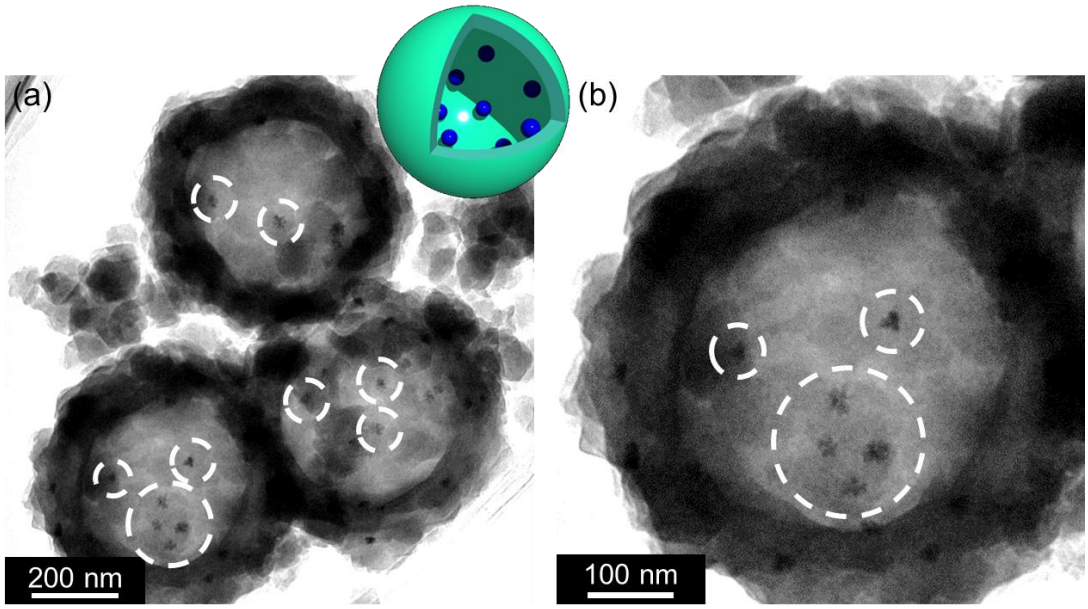

Figure 4. 2. 2. TEM images of Pd@ZIF-8 with schematic illustration.

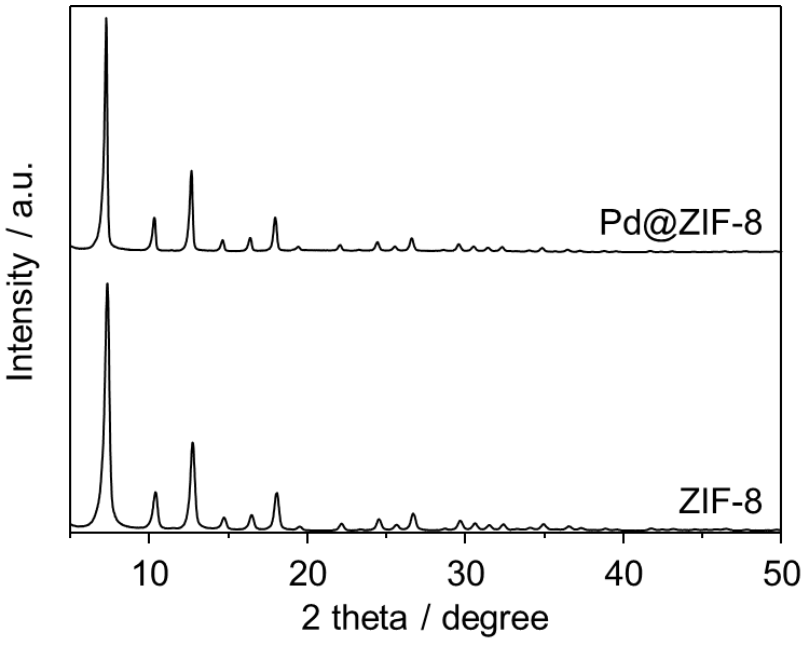

Figure 4. 2. 3. XRD patterns of Pd@ZIF-8 and ZIF-8.

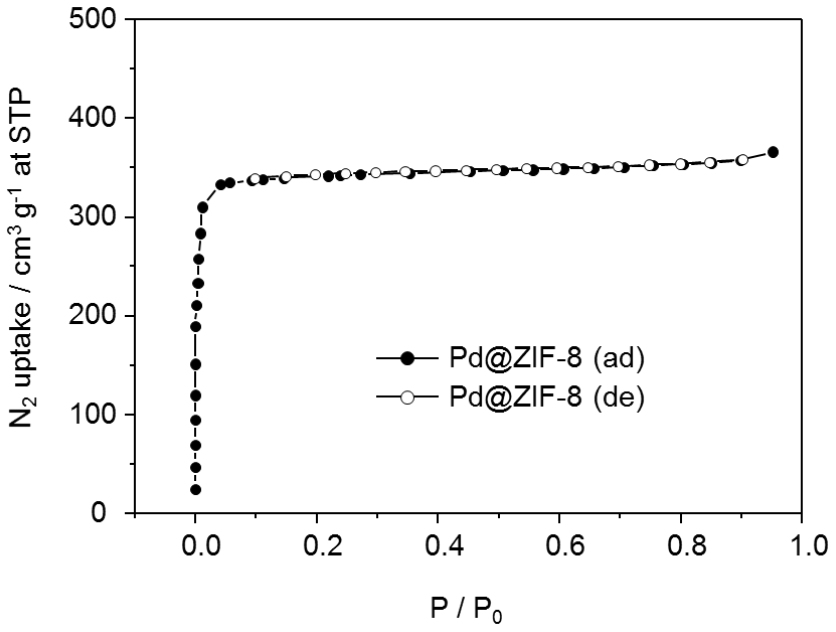

Figure 4. 2. 4. N_2 adsorption-desorption isotherm of Pd@ZIF-8.

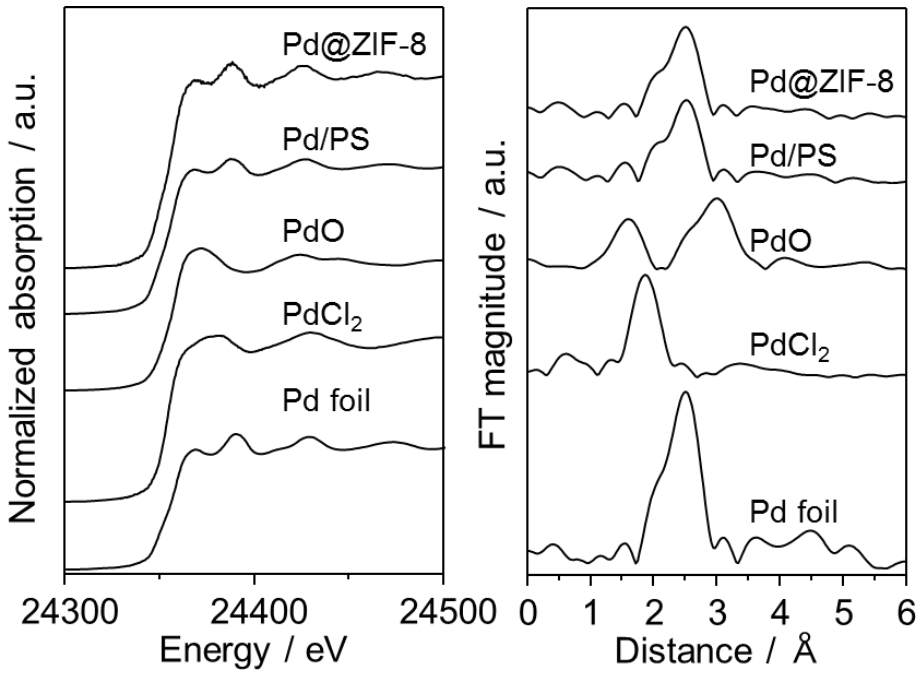

Figure 4. 2. 5. XANES and EXAFS spectra of Pd@ZIF-8, Pd/PS, PdO, $PdCl_2$ and Pd foil.

The prepared Pd@ZIF-8 catalyst has been utilized for a competitive hydrogenation of olefins in the liquid phase. **Figure 4. 2. 6** shows time course of 1-octene and cyclooctene

conversion in the competitive hydrogenation reaction over Pd@ZIF-8. Pd@ZIF-8 catalyzed the hydrogenation of 1-octene, while the hydrogenation of cyclooctene was not efficiently promoted. This result can be attributed to size selective property of Pd@ZIF-8 derived from uniform and microporous structure nature of ZIF-8 shell. 1-Octene molecules (1.7 Å)[31] were small enough to diffuse through the pore apertures of the ZIF-8 shells (3.4 Å)[30] without serious hindrance. In contrast, the cyclooctene molecules (5.5 Å)[31] were much bigger than the pore apertures. As a result, hydrogenation reaction of 1-octene was preferentially promoted over Pd@ZIF-8. It was also found that Pd@ZIF-8 could be reused at least three times without significant loss in the catalytic activity and selectivity, as shown in **Fig. 4. 2. 7**. In order to check the durability of the catalyst, TEM, XRD and XAFS measurements were carried out. The yolk shell structure was found to be retained even after the catalytic reaction, as shown in **Fig. 4. 2. 8**. The results of XRD measurements (**Fig. 4. 2. 9**) revealed that the diffraction peaks corresponding to the ZIF-8 structure was maintained even after the reaction. In addition, no significant change was observed for Pd nanoparticles encapsulated in the ZIF-8 shell after the hydrogenation reaction. These results clearly indicate that Pd@ZIF-8 possesses high durability toward the competitive hydrogenation reaction of olefins.

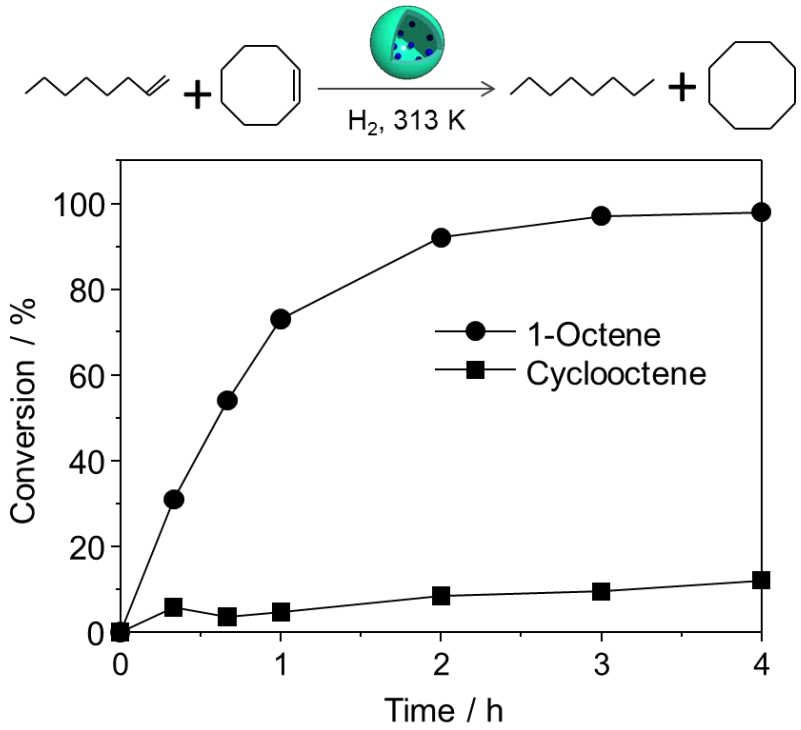

Figure 4. 2. 6. Time course of 1-octene and cyclooctene conversion in the competitive hydrogenation reaction over Pd@ZIF-8. Reaction conditions: 1-octene (5.0 mmol), cyclooctene (5.0 mmol), methanol (10 mL), n-decane (10 μL) and catalyst (Pd = 5.0 μmol), T = 313 K, t = 4 h.

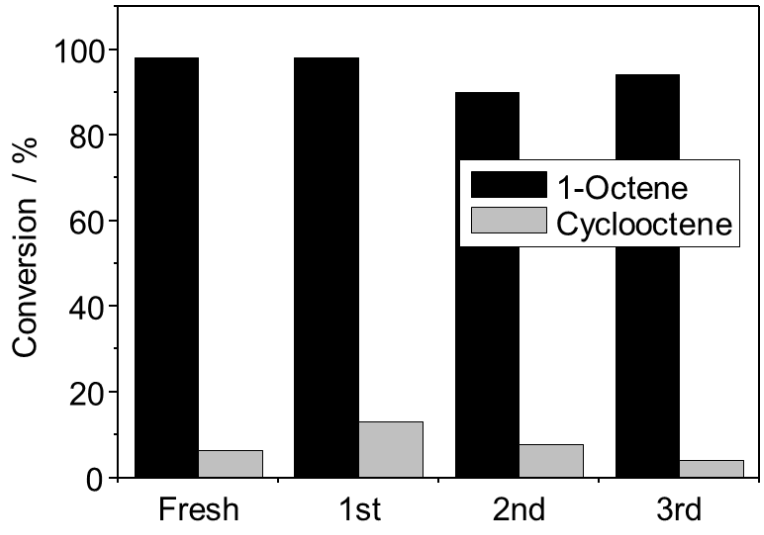

Figure 4. 2. 7. Recycling experiment of 1-octene and cyclooctene conversion in the competitive hydrogenation reaction over Pd@ZIF-8. Reaction conditions: 1-octene (5.0 mmol), methanol (10 mL), n-decane (10 μL) and Pd@ZIF-8 (Pd = 5.0 μmol), T = 313 K, t = 4 h.

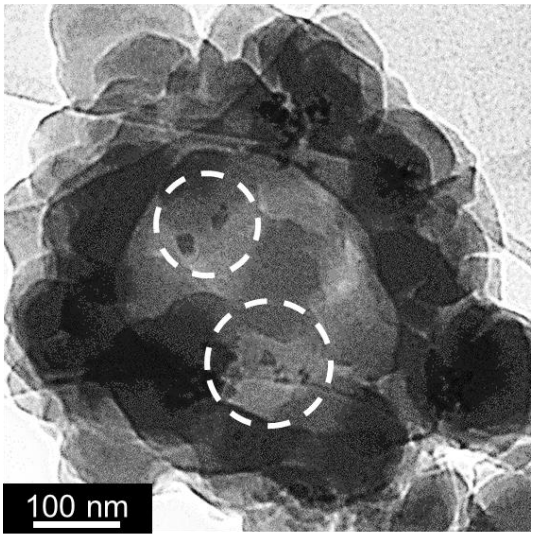

Figure 4. 2. 8. TEM image of Pd@ZIF-8 after the catalytic reaction.

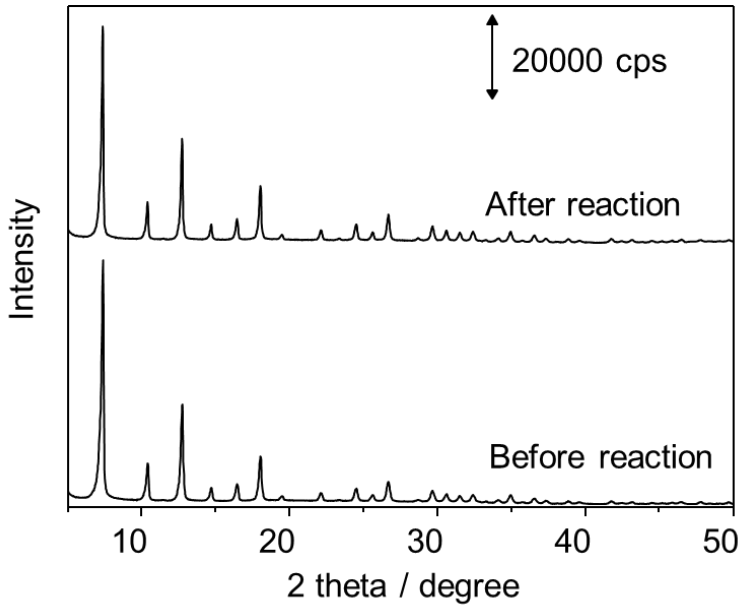

Figure 4. 2. 9. XRD patterns of Pd@ZIF-8 before and after the catalytic reaction.

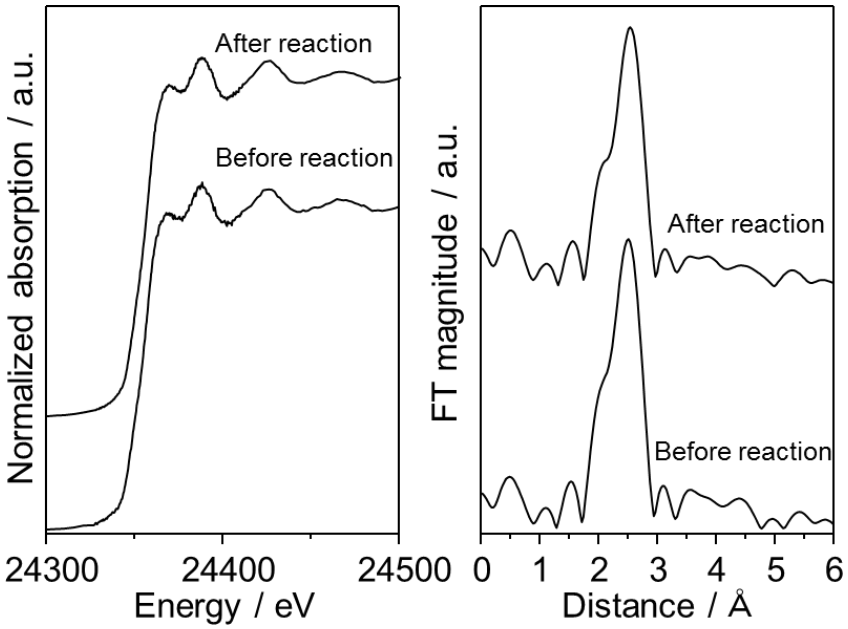

Figure 4. 2. 10. XANES and EXAFS spectra of Pd@ZIF-8 before and after the catalytic reaction.

4. 2. 4. Conclusions

Pd nanoparticles have been incorporated within a ZIF-8 shell through templating method using carboxylate-terminated polystyrene spheres to construct yolk-shell structures. The prepared catalyst, Pd@ZIF-8, was successfully applied to a competitive hydrogenation of olefins in the liquid phase. Hydrogenation of 1-octene proceeded smoothly over Pd@ZIF-8, while hydrogenation of cyclooctene was not efficiently promoted. This result is attributable to size selective property of Pd@ZIF-8 as a consequence of uniform and microporous structure nature of ZIF-8 shell. Pd@ZIF-8 could be reused at least three times without significant loss in the catalytic activity and selectivity. Moreover, the yolk shell structure was found to be retained even after the catalytic reaction, indicating the high stability of Pd@ZIF-8. These findings suggest new possibilities to design highly functional size-selective catalysts by using MOFs as interesting platforms.

4. 2. 5. References

1. S. Furukawa, J. Reboul, S. Diring, K. Sumida and S. Kitagawa, *Chem. Soc. Rev*., 2014, **43**, 5700.
2. H. Furukawa, K. E. Cordova, M. O'Keeffe and O. M. Yaghi, *Science*, 2013, **341**, 1230444.
3. G. Férey, *Chem. Soc. Rev.*, 2008, **37**, 191.
4. J. D. Evans, C. J. Sumby and C. J. Doonan, *Chem. Soc. Rev*., 2014, **43**, 5933.
5. S. Ou and C. D. Wu, *Inorg. Chem. Front.*, 2014, **1**, 721.
6. S.-L. Li and Q. Xu, *Energy Environ. Sci.*, 2013, **6**, 1656.
7. D. Bradshaw, A. Garai and J. Huo, *Chem. Soc. Rev.*, 2012, **41**, 2344.
8. A. Aijaz, A. Karkamkar, Y. J. Choi, N. Tsumori, E. Ronnebro, T. Autrey, H. Shioyama and Q. Xu, *J. Am. Chem. Soc.*, 2012, **134**, 13926.
9. J. Lee, O. K. Farha, J. Roberts, K. A. Scheidt, S. T. Nguyen and J. T. Hupp, *Chem. Soc. Rev*., 2009, **38**, 1450.
10. P. Falcaro, R. Ricco, C. M. Doherty, K. Liang, A. J. Hill and M. J. Styles, *Chem. Soc. Rev*., 2014, **43**, 5513.
11. M. Kim, J. F. Cahill, Y. Su, K. A. Prather and S. M. Cohen, *Chem. Sci.*, 2012, **3**, 126.
12. P. Falcaro and S. Furukawa, *Angew. Chemie-Int. Ed.*, 2012, **51**, 8431.
13. C. J. Doonan, W. Morris, H. Furukawa and O. M. Yaghi, *J. Am. Chem. Soc.*, 2009, **131**, 9492.
14. Y. Liu and Z. Tang, *Adv. Mater.*, 2013, **25**, 5819.
15. W. Zhang, G. Lu, S. Li, Y. Liu, H. Xu, C. Cui, W. Yan, Y. Yang and F. Huo, *Chem. Commun.*, 2014, **50**, 4296.

16. H. Zhang, S. Qi, X. Niu, J. Hu, C. Ren, H. Chen and X. Chen, *Catal. Sci. Technol.*, 2014, **4**, 3013.
17. R. Ricco, L. Malfatti, M. Takahashi, A. J. Hill and P. Falcaro, *J. Mater. Chem. A*, 2013, **1**, 13033.
18. P. Falcaro, F. Normandin, M. Takahashi, P. Scopece, H. Amenitsch, S. Costacurta, C. M. Doherty, J. S. Laird, M. D. H. Lay, F. Lisi, A. J. Hill and D. Buso, *Adv. Mater.*, 2011, **23**, 3901.
19. S. Ikeda, S. Ishino, T. Harada, N. Okamoto, T. Sakata, H. Mori, S. Kuwabata, T. Torimoto, M. Matsumura, *Angew. Chem., Int. Ed.,* 2006, **45**, 7063.
20. I. Lee, J. B. Joo, Y. D. Yin, F. Zaera, *Angew. Chem., Int. Ed*., 2011, **50**, 10208.
21. C. H. Kuo, M. H. Huang, *J. Am. Chem. Soc.,* 2008, **130**, 12815.
22. X. J. Wu, D. S. Xu, *J. Am. Chem. Soc*., 2009, **131**, 2774.
23. Y. D. Yin, R. M. Rioux, C. K. Erdonmez, S. Hughes, G. A. Somorjai, A. P. Alivisatos, *Science*, 2004, **304**, 711.
24. X. J. Wu, D. S. Xu, *Adv. Mater.,* 2010, **22**, 1516.
25. R. Guttel, M. Paul, F. Schuth, *Catal. Sci. Technol.*, 2011, **1**, 65.
26. Y. Yang, J. Liu, X. Li, X. Liu, Q. Yang, *Chem. Mater.,* 2011, **23**, 3676.
27. K. S. Park, Z. Ni, A. P. Côté, J. Y. Choi, R. Huang, F. J. Uribe-Romo, H. K. Chae, M. O'Keeffe and O. M. Yaghi, *Proc. Natl. Acad. Sci. U. S. A.*, 2006, **103**, 10186.
28. N. L. Torad, M. Hu, Y. Kamachi, K. Takai, M. Imura, M. Naito and Y. Yamauchi, *Chem. Commun.*, 2013, **49**, 2521.
29. F. Li, Y. N. Wu, W. Zhu, J. Cui, C. A. Tao, C. Lin, P. M. Hannam and G. Li, *Angew. Chem., Int. Ed*., 2011, **50**, 12518.
30. C. Chizallet and N. Bats, *J. Phys. Chem. Lett.*, 2010, **1**, 349.

31. C. Kuo, Y. Tang, L. Chou, B. T. Sneed, C. N. Brodsky and Z. Zhao, *J. Am. Chem. Soc*., 2012, **134**, 14345.

Chapter 5

General conclusions

General conclusions

In this thesis, metal−organic frameworks (MOFs) have been utilized as highly functional heterogeneous catalysts. The results obtained in this study indicate that MOFs serve as multifunctional platforms for a variety of catalytic applications including photocatalytic reactions, one-pot sequential reactions and hydrogenation reactions. MOF-based catalysts developed here have been demonstrated to exhibit superior catalytic performance to the conventional solid catalysts explored in this study. In addition, the reaction mechanisms have been also investigated and discussed by using various characterization techniques. The main results obtained have been summarized below.

Summary of Chapter 2

Chapter 2 deals with developments of novel visible-light-responsive MOF photocatalysts through design of visible-light-active organic linkers acting as a light harvesting unit. An amino-functionalized Ti-based MOF was synthesized by using a 2-anilinedicarboxylic acid organic linker (Ti-MOF-NH_2). Ti-MOF-NH_2 efficiently promoted hydrogen production reaction in an aqueous solution containing triethanolamine (TEOA) as a sacrificial electron donor under visible-light irradiation conditions. In this process, the organic linker absorbs visible light and its excited state transfers an electron to the photocatalytically active titanium-oxo cluster. Ti-MOF-NH_2 was also fond to catalyze photocatalytic reduction of nitrobenzene under visible-light irradiation. Furthermore, utilizable range of wavelength and sacrificial reagents of MOF photocatalyst-catalyzed systems were successfully expanded up to 620 nm by employing a bis(4'-(4-carboxyphenyl)-terpyridine)Ru(II) complex ($Ru(tpy)_2$)

as an organic linker.

Summary of Chapter 3

In Chapter 3, various one-pot reactions have been developed using multifunctional MOF catalysts. The multifunctional MOFs have been designed by modifying or varying the core metal-oxo clusters and bridging organic linkers. An amino-functionalized Al-based MOF, MIL-101(Al)-NH_2, was found to serve as a bifunctional acid-base catalyst to promote a one-pot reaction producing benzylidenemalononitrile via sequential deacetalization and Knoevenagel condensation. Observations made in this effort show that activity of MIL-101(Al)-NH_2 as acid-base bifunctional catalysts is superior to those of conventional heterogeneous, homogeneous as well as other functionalized metal-organic framework catalysts. Moreover, a bifunctional MOF photocatalyst consisting of Zr-oxo cluster and 2-aniline-1,4-dicarboxylic acid as an organic linker (Zr-MOF-NH_2) has been synthesized and employed for a one-pot reaction to produce benzylidenemalononitrile through photocatalytic oxidation and Knoevenagel condensation under UV-light irradiation. In this process, the Zr-oxo cluster catalyzes the first step of the reaction (photocatalytic oxidation of benzyl alcohol), and subsequently the $–NH_2$ group catalyzes second step (Knoevenagel condensation of benzaldehyde with malononitrile), resulting in the progression of the one-pot reaction. Furthermore, a sequential one-pot reaction to produce organophosphorus compounds via Knoevenagel condensation and phospha-Michael addition has been realized by utilizing a zeolitic imidazolate framework (ZIF-8) as a heterogeneous catalyst. The combination of 2-methylimidazolate anions as a Lewis base sites and Zn^{2+} ions as a Lewis acid sites in ZIF-8 was revealed to be effective for the efficient promotion of the one-pot reaction.

Summary of Chapter 4

Metal nanoparticles as catalytically active components have been encapsulated in MOF materials and utilized for hydrogenation reactions as highly efficient and reusable catalysts in Chapter 4. Colloidal Pd nanoparticles preliminarily prepared were confined within the framework of Zr-MOF during MOF synthesis process. The resulting Pd@Zr-MOF catalyst exhibited an efficient catalytic activity for hydrogenation of nitrobenzene and high recyclability due to the encapsulation of Pf nanoparticles. In addition, this catalyst design methodology could be applied to Pd–Au bimetallic nanoparticles; as a consequence, an improved catalytic activity based on alloying was attained. In addition, yolk-shell nanostructures were designed with Pd nanoparticles and ZIF-8 shell for size-selective hydrogenation reactions (Pd@ZIF-8). The synthetic strategy involved the deposition of Pd nanoparticles on carboxylate-terminated polystyrene (PS), followed by coatings with ZIF-8. Subsequently, PS was extracted by washing with dimethylformamide (DMF) solution to obtain Pd@ZIF-8 having the yolk-shell structure. The size selectivity was realized by taking advantage of the uniform and microporous structure nature of ZIF-8. Size selective property of the Pd@ZIF-8 catalyst was evaluated through a competitive hydrogenation of olefins. Pd@ZIF-8 efficiently catalyzed the hydrogenation of 1-octene, while the hydrogenation of cyclooctene hardly proceeded. It was also found that Pd@ZIF-8 could be reused at least three times without significant loss in the catalytic activity and selectivity.

Acknowledgement

The author, Takashi Toyao, would like to express his sincere gratitude to Prof. Masaya Matsuoka of the Department of Applied Chemistry, Graduate School of Engineering, Osaka Prefecture University, for his warm encouragement and invaluable instruction during the course of this study.

Sincere thanks are also extended to Prof. Masahiro Tatsumisago and Prof. Hiroshi Inoue of Osaka Prefecture University for their critical reading of the thesis and for their many useful suggestions for its improvement.

The author also wishes to thank Associate Prof. Masato Takeuchi and Assistant Prof. Yu Horiuchi of Osaka Prefecture University for their helpful suggestions and stimulating discussions throughout the present research. Also, sincere thanks are extended to Prof. Masahide Takahashi for his helpful assistance and advice.

Deep thanks are also extended to the author's colleagues, Masakazu Saito, Kozo Ueda, Kenji Nishikawa, Mika Fujiwaki, Kenta Miyahara, Hayato Yuki, Akira Sakiyama and Nana Ueno for their help and experimental assistance.

Heartfelt thanks are extended to Dr. Paolo Falcaro, Prof. Roland A Fischer, Prof. Srinivasan Natarajan and Dr. Catherine Louis of for their numerous helpful and valuable advices.

Finally, the author would like to express his sincere gratitude to his family who have always prayed for his well-being and to complete his studies.

Takashi Toyao

Sakai, Osaka,

July, 2015

List of publications

1. Visible-Light-Promoted Photocatalytic Hydrogen Production by Using an Amino-Functionalized Ti(IV) Metal-Organic Framework
Y. Horiuchi, T. Toyao, M. Saito, K. Mochizuki, M. Iwata, H. Higashimura, M. Anpo, M. Matsuoka
The Journal of Physical Chemistry C, 2012, **116**, 20848-20853.

2. Efficient Hydrogen Production and Photocatalytic Reduction of Nitrobenzene over Visible-Light-Responsive Metal-Organic Framework Photocatalyst
T. Toyao, M. Saito, Y. Horiuchi, K. Mochizuki, M. Iwata, H. Higashimura, M. Matsuoka
Catalysis Science & Technology, 2013, **3**, 2092-2097.

3. Development of Ru Complex-Incorporated MOF Photocatalyst for Hydrogen Production under Visible-Light Irradiation
T. Toyao, M. Saito, S. Dohshi, K. Mochizuki, M. Iwata, H. Higashimura, Y. Horiuchi, M. Matsuoka
Chemical Communications, 2014, **50 (51)**, 6779-6781.

4. Recent Advances in Visible-Light-Responsive Photocatalysts for Hydrogen Production and Solar Energy Conversion – from Semiconducting TiO_2 to MOF/PCP Photocatalysts
Y. Horiuchi, T. Toyao, M. Takeuchi, M. Matsuoka, M. Anpo
Physycal Chemistry Chemical Physics, 2013, **15**, 13243-13253.

5. Application of an Amino-Functionalised Metal-Organic Framework: An Approach to a One-Pot Acid-Base Reaction
T. Toyao, M. Fujiwaki, Y. Horiuchi, M. Matsuoka
RSC Advances, 2013, **3**, 21582-21587.

6. Development of a Novel One-pot Reaction System Utilizing a Bifunctional Zr-based Metal-Organic Framework
T. Toyao, M. Saito, Y. Horiuchi, M. Matsuoka
Catalysis Science & Technology, 2014, **4**, 625-628.

7. Zeolitic Imidazolate Frameworks as Heterogeneous Catalysts for a One-Pot P–C Bond Formation Reaction via Knoevenagel Condensation and Phospha-Michael Addition
Y. Horiuchi, T. Toyao, M. Fujiwaki, S. Dohshi, T. H. Kim, M. Matsuoka
RSC advances, 2015, **5**, 24687-24690.

8. Encapsulation of Metal Nanoparticles within a Zr-based Metal−Organic Framework for Highly Efficient, Reusable Hydrogenation Catalysts
Y. Horiuchi, T. Toyao, K. Nishikawa S. Dohshi, T. H. Kim, M. Matsuoka
Submitted to *Applied Catalysis A: General*

9. Yolk-shell Pd Nanoparticles@MOF Nanostructures for Size-Selective Hydrogenation Reactions
Y. Horiuchi, T. Toyao, K. Nishikawa S. Dohshi, T. H. Kim, M. Matsuoka
Submitted to *Journal of Materials Chemistry A*